TECHNISCHE UNIVERSITÄT MÜNCHEN

Lehrstuhl für Biotechnologie der Nutztiere

Functions of snail homolog 1 (Snail) in pancreatic cancer

Mariel Cathérine Paul

Vollständiger Abdruck der von der Fakultät Wissenschaftszentrum Weihenstephan für Ernährung, Landnutzung und Umwelt der Technischen Universität München zur Erlangung des akademischen Grades eines

Doktors der Naturwissenschaften

genehmigten Dissertation.

Vorsitzender:	Univ.-Prof. Dr. M. Schemann
Prüfer der Dissertation:	1. Univ.-Prof. A. Schnieke, Ph.D.
	2. Priv.-Doz. Dr. D. Saur

Die Dissertation wurde am 20.02.2013 bei der Technischen Universität München eingereicht und durch die Fakultät Wissenschaftszentrum Weihenstephan für Ernährung, Landnutzung und Umwelt am 18.07.2013 angenommen.

Table of contents

List of tables

List of figures

Abbreviations

°C	degree Celsius
A	adenine
ACC	acinar cell carcinoma
ADM	acinar-to-ductal metaplasia
Amy1	alpha amylase 1
APC	adenomatous polyposis coli
APS	ammonium persulfate
BID	BH3 interacting-domain death agonist
Bmp	bone morphogenetic protein
bp	base pairs
BSA	bovine serum albumin
βTrCP	beta-transducin repeat containing protein
C	cytosine
Cdh1	E-cadherin
CDK	cyclin-dependent kinase
Cdkn1a ($p21^{CIP1}$)	cyclin-dependent kinase inhibitor 1A
cDNA	complementary deoxyribonucleic acid
Cel	carboxyl ester lipase
Cela1	chymotrypsin-like elastase family, member 1
CGH	comparative genomic hybridization
ChIP-seq	chromatin immunoprecipitation sequencing
cm	centimeter
CMV	cytomegalovirus
ConTra	conserved transcription factor binding sites
Cpa1	carboxypeptidase A1
Crb	crumbs homolog
CypA	cyclophilin
D-MEM	Dulbecco's modified eagle medium
d.p.c.	days post coitum
DDR	DNA damage repair
DFF	DNA fragmentation factor
DMSO	dimethylsulfoxide
DNA	deoxyribonucleic acid
DPC4	deleted in pancreatic cancer locus 4
DTT	dithiothreitol
Dusp26	dual specificity phosphatase 26
dUTP	2´-deoxyuridine, 5´-triphosphate

E	embryonic development day
ECM	extracellular matrix
EDTA	ethylenediaminetetraacetic acid
Egf	epidermal growth factor
eGFP	enhanced green fluorescent protein
Egfr	epidermal growth factor receptor
Egr1	early growth response 1
EGTA	ethylene glycol tetraacetic acid
EMT	epithelial-mesenchymal transition
ER	estrogen receptor
Erk	mitogen-activated protein kinase kinase kinase 1
ES	embryonic stem
et al.	et alii
FCS	fetal calf serum
FDR	False discovery rate
FGF	fibroblast growth factor
fM	femtomol / femtomolar
g	gram
G	guanine
GEM	genetically engineered mouse model
Gfi	growth factor independence
GSEA	gene set enrichment analysis
GSK3β	glycogen synthase kinase 3 beta
h	hours
H&E	hematoxylin and eosin
HDAC	histone deacetylase
HEK	human embryonic kidney
HEPES	4-(2-hydroxyethyl)-1-piperazineethanesulfonic acid
HGF	hepatocyte growth factor
HNF4α	hepatic nuclear factor 4α
ILK	integrin linked kinase
kb	kilobase pairs
Kras	v-Ki-ras2 Kirsten rat sarcoma viral oncogene homolog
Krt	cytokeratin
l	liter
LIF	leukemia inhibitory factor
LOH	loss of heterozygosity
LSL	loxP-stop-loxP
M	mol / molar
MAPK	mitogen-activated protein kinase

mbar	millibar
MDCK	Madin-Darby canine kidney
Mdm2	transformed mouse 3T3 cell double minute 2
MEF	mouse embryonic fibroblast
mg	milligram
min	minutes
ml	milliliter
mm	millimeter
mM	millimol / millimolar
MTA3	metastasis-associated protein 3
mut	mutated
NES	nuclear export signal
ng	nanogram
nm	nanometer
nM	nanomol / nanomolar
NOM	nominal
OD	optical density
OIS	oncogene-induced senescence
p	phospho
PAK1	p21 protein-activated kinase 1
PanIN	pancreatic intraepithelial neoplasia
PBS	phosphate buffered saline
PCR	polymerase chain reaction
PDAC	pancreatic ductal adenocarcinoma
Pdx1	pancreatic and duodenal homeobox 1
PI3K	phosphoinositide 3-kinase
Prc2	polycomb repressive complex 2
PTEN	phosphatase and tensin homolog
Ptf1a	pancreas transcription factor subunit alpha
R26	Rosa26
Rb	retinoblastoma
Rbpj	recombination signal binding protein for immunoglobulin kappa J region
Rbpjl	recombination signal binding protein for immunoglobulin kappa J region-like
RCAS	replication-competent avian sarcoma-leukosis virus long terminal repeat with a splice acceptor
RMA	robust multi-array average
RNA	ribonucleic acid
rpm	rounds per minute
RT	room temperature
SA β-gal	senescence-associated β-galactosidase

SDS	sodium dodecyl sulfate
sec	seconds
SMAD4	mothers against decapentaplegic homolog 4
SNAG	Snail/Gfi
Snail	snail homolog 1
T	thymine
TAE	tris acetate EDTA
TBS	tris buffered saline
TEMED	N,N,N',N'-tetramethylethylenediamine, 1,2-bis(dimethylamino)-ethane
TFT	transcription factor target
TGFβ	transforming growth factor β
TP53 / Trp53	transformation related protein 53
Tris	tris-(hydroxymethyl)-aminomethan
TSB	tryptic soy broth
TUNEL	Terminal deoxynucleotidyl transferase dUTP nick end labeling
U	units
V	volt
VDR	vitamin D receptor
w	weeks
Wnk2	with no lysine (K)
wt	wild type
yr	years
α-SMA	alpha smooth muscle actin
µF	microfarad
µg	microgram
µl	microliter
µm	micrometer
µM	micromol / micromolar

1 Introduction

1.1 Pancreatic cancer

Pancreatic cancer is the fourth leading cause of cancer-related death in the Western world. Whereas the overall incidence is only 3%, estimating 44000 new cases in the United States in 2011, 38000 estimated deaths reflect the extremely high mortality of this disease (Siegel *et al.*, 2011). Besides ductal adenocarcinomas, which build the vast majority of exocrine pancreatic neoplasms, further less common tumors with acinar, mixed, or undetermined differentiation exist.

1.1.1 Pancreatic ductal adenocarcinoma

Accounting for more than 85% of cases, pancreatic ductal adenocarcinoma (PDAC) is the most common malignant neoplasm of the pancreas. Besides inherited predisposition in 10% of patients, main risk factors are chronic pancreatitis, advanced age, obesity, and smoking (Hezel *et al.*, 2006). Unspecific early symptoms, aggressive biological behavior, rapid dissemination, as well as lack of sufficient diagnostic tools and effective therapeutic concepts, result in 5-year survival rates below 6% (Bardeesy and DePinho, 2002; Schneider *et al.*, 2005; Siegel *et al.*, 2011). Typically, PDAC shows very early infiltration into adjacent tissue including blood vessels, and mainly metastasizes into peritoneal cavity, lymphatics, liver, and lungs. A further characteristic feature of PDAC is the abundance of stroma consisting of fibroblasts and inflammatory cells, named desmoplasia (Hezel *et al.*, 2006). In

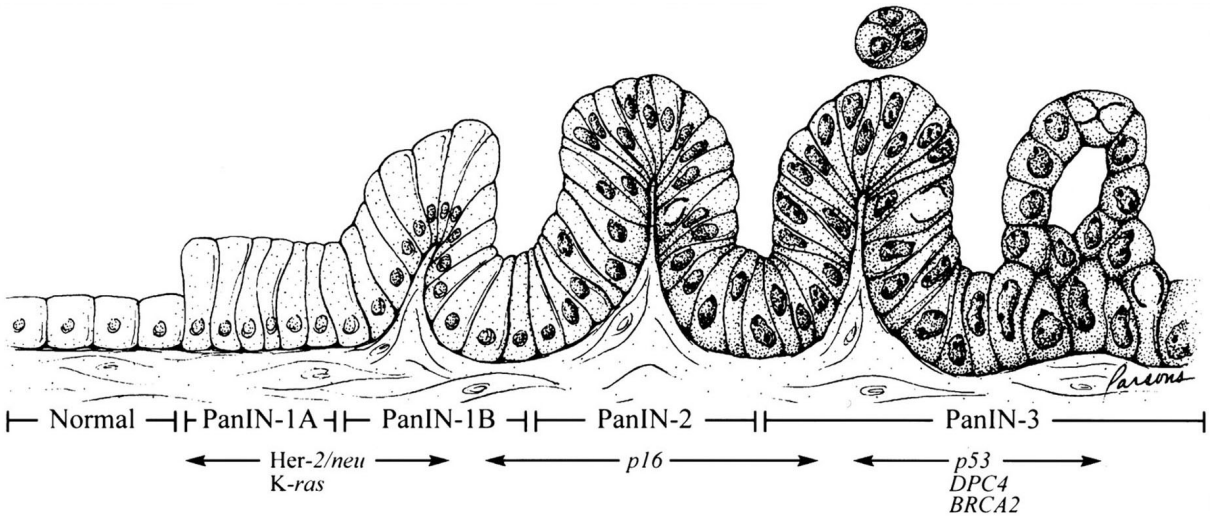

Figure 1-1: Progression model for pancreatic ductal adenocarcinoma.
The progression of normal ductal epithelium to invasive pancreatic cancer occurs through different stages of pancreatic intraepithelial neoplasias (PanINs). Overexpression of HER2/neu (ERBB2) and point mutations of KRAS happen early during this progression, followed by later inactivation of $p16^{INK4A}$, TP53, DPC4 (SMAD4), and BRCA2. Reprinted by permission from the American Association for Cancer Research (Hruban *et al.*, 2000).

spite of tremendous efforts to unravel underlying molecular pathways, PDAC is one of the cancer types for which survival rates have shown the least improvements during the last decades (Siegel *et al.*, 2011). Currently, surgical resection of localized tumors at early stages remains the only possibility of curation. Unfortunately, 85%–90% of the patients already have disseminated tumors at time of diagnosis, shrinking the number of resectable tumors to approximately 10%. Even among these operated patients, only 20% survive longer than 5 years (Hamacher *et al.*, 2008; Richter *et al.*, 2003). Therapies using gemcitabine as first-line chemotherapeutic agent, as well as target therapies like tyrosine kinase inhibitors, show no more than limited improvement of median survival (Gupta and El-Rayes, 2008; Burris III *et al.*, 1997; Chames *et al.*, 2010). The greatest survival benefit for patients with metastatic pancreatic cancer is currently reached by treatment with the FOLFIRINOX combination (folinic acid, 5-fluorouracil, irinotecan, and oxaliplatin), which increases the median overall survival of patients with good performance status to 11.1 months compared to 6.8 months with gemcitabine treatment. Nevertheless, this has to be taken with caution, as the FOLFIRINOX combination also is affiliated with markedly increased toxicity (Costello *et al.*, 2012).

All these facts illuminate the urgent need for a better understanding of pancreatic cancer pathophysiology for development of new diagnostic methods and therapeutic strategies to improve the outcome of this life-threatening disease.

1.1.1.1 A progression model for pancreatic ductal adenocarcinoma

PDAC develops through several noninvasive precursor lesions, of which the pancreatic intraepithelial neoplasias (PanINs) are the most common. A standard progression model was developed, in which PanINs are graded into stage 1A, 1B, 2, and 3 (Hruban *et al.*, 2001, 2000, Figure 1-1). Whereas regular pancreatic ducts are composed of nonmucinous cuboidal to low-columnar epithelial cells, the earliest lesions termed PanIN1A are built of tall columnar epithelium with basally located nuclei and abundant mucin production. PanIN1B stage is identical to PanIN1A, but further characterized by a papillary, micropapillary, or basally pseudostratified architecture (Hruban *et al.*, 2001). In patients older than 50 years, these lesions are present in up to 40% of nonmalignant pancreata (Schneider *et al.*, 2005). PanIN2 have some nuclear abnormalities, like loss of polarity, crowding, enlargement, or hyperchromatism. These lesions can be flat, but are most likely papillary. PanIN3 are generally papillary or micropapillary with dystrophic goblet cells and show several nuclear abnormalities. They are further characterized by cribriforming, budding into the lumen, and luminal necrosis. PanIN3 lesions are equal to carcinoma *in situ*. They are seen as direct

precursor lesions of invasive PDAC (Hezel *et al.*, 2006; Hruban *et al.*, 2001) and can be found in 30%–50% of pancreata of patients with this diagnosis (Schneider *et al.*, 2005).

Going along with these morphological alterations, the current progression model of PDAC describes a consecutive accumulation of several mutational changes that finally lead to development of PDAC. One of the first genetic alterations during pancreatic cancer development is the activating point mutation of the *KRAS* (v-Ki-ras2 Kirsten rat sarcoma viral oncogene homolog) oncogene, which is found in about 30% of early PanIN lesions and nearly in 100% of advanced PDAC (Almoguera *et al.*, 1988; Rozenblum *et al.*, 1997). The small GTPase KRAS is involved in many cellular functions like proliferation, survival, and differentiation. Bound to guanosine triphosphate (GTP), it activates downstream pathways like mitogen-activated kinase (MAPK) and phosphoinositide-3-kinase (PI3K) signaling (Malumbres and Barbacid, 2003). A frequent one of the possible *KRAS* activating point mutations at codon 12 leads to substitution of glycine with aspartate ($KRAS^{G12D}$), resulting in a decrease of intrinsic GTP hydrolysis rate as well as in insensitivity to GTPase-activating proteins (GAPs). This constitutively activated KRAS acts independently of external stimulation by growth factors (Hezel *et al.*, 2006).

The loss of the tumor suppressor $p16^{INK4A}$ by mutation, deletion, or hypermethylation of the promoter also is a frequent event in moderately advanced PanINs and PDAC, occurring in 80%–95% of patients (Hezel *et al.*, 2006; Rozenblum *et al.*, 1997). The *CDKN2A* locus encodes 2 tumor suppressors, $p16^{INK4A}$ and $p14^{ARF}$ ($p19^{ARF}$ in the mouse). $p16^{INK4A}$ prevents complex formation of cyclin-dependent kinases (CDK) 4 and 6 with cyclin D, thus inhibiting retinoblastoma (RB) phosphorylation and thereby entry into the S phase of the cell cycle. $p14^{ARF}$ inhibits MDM2-dependent proteolysis of TP53 (Trp53 in the mouse), thereby stabilizing it (Bardeesy *et al.*, 2006). For tumor suppression in PDAC, $p16^{INK4A}$ appears to play the more important role, as mutations have been found that affect $p16^{INK4A}$, but spare $p14^{ARF}$ (Bardeesy *et al.*, 2006; Rozenblum *et al.*, 1997).

Further, the tumor suppressor TP53 is mutated in more than 50% of PDAC cases, generally by missense alterations of the DNA-binding domain (Rozenblum *et al.*, 1997). This occurs in advanced stages of PanINs and often goes along with loss of heterozygosity (LOH), leading to loss of wild type TP53 function (Lüttges *et al.*, 2001). Because TP53 is an important regulator of cell cycle, apoptosis, and DNA damage responses, this results in uncontrolled proliferation and genomic instability in pancreatic cancer (Bardeesy and DePinho, 2002).

The transcription factor SMAD4, also known as DPC4, is an additional tumor suppressor, which plays a role in PDAC development. Occurring late during tumorigenesis, loss of SMAD4 by deletion or point mutation can be observed in more than 50% of PDAC and

approximately in 33% of PanIN3 lesions, whereas lower graded PanINs do not show these alterations (Maitra *et al.*, 2003; Wilentz *et al.*, 2000). SMAD4 is a central regulator of the transforming growth factor β (TGFβ) signaling pathway that is supposed to play a role in pancreatic tumorigenesis mediating growth inhibition and controlling effects on tumor-stroma interactions (Bardeesy and DePinho, 2002; Siegel and Massagué, 2003).

Although with a lower frequency than the aforementioned ones, several other gene and pathway alterations can be found, e.g. loss of BRCA2 (Murphy *et al.*, 2002), overexpression of ERBB2 (Safran *et al.*, 2001) and further growth factors, as well as activation of developmental signaling pathways like the Hedgehog (Thayer *et al.*, 2003) and Notch (Mazur *et al.*, 2010) pathway. Also, telomere shortening and dysfunction, chromosomal alterations and epigenetic abnormalities are characteristic for invasive PDAC (Maitra and Hruban, 2008; Hezel *et al.*, 2006).

1.1.2 Acinar cell carcinoma: A rare form of pancreatic neoplasia

Besides PDAC as the most common type of pancreatic cancer, acinar cell carcinoma (ACC) is diagnosed in approximately 1% of cases of pancreatic neoplasia. It is a malignant tumor with early liver metastasis and 5-year survival rates below 5% (Klimstra *et al.*, 1992). Like PDAC, this aggressive disease is often discovered when it has already metastasized, which is due to nonspecific symptoms. Macroscopically, these tumors are generally large, circumscribed, and soft. On microscopical level, ACC is characterized by lack of fibrous stroma as well as high cellular density with different patterns. Nuclei mostly do not differ in shape and size (Klimstra, 2007). Expression of pancreatic enzymes like lipase, chymotrypsin, and trypsin can be observed frequently, whereas amylase is rarely expressed in ACC (Klimstra *et al.*, 1992; Hoorens *et al.*, 1993). In contrast to PDAC, mutations in *KRAS* are extremely rare in ACC (Pellegata *et al.*, 1994). Instead, these tumors exhibit a high grade of LOH, e.g. chromosomes 1p, 4q, and 17p are affected in more than 70% of cases (Rigaud *et al.*, 2000). Furthermore, in 24% of cases, alterations in the adenomatous polyposis coli (APC)/β-catenin pathway can be found, mostly consisting of truncating mutations of *APC* or activating mutations of *β-catenin* (Abraham *et al.*, 2002).

1.1.3 Genetically engineered mouse models for pancreatic cancer

Although there are biological differences between murine and human cells (Rangarajan and Weinberg, 2003; Leach, 2004), genetically engineered mouse models (GEMs) represent an important tool to investigate various human cancer types. Since the 1980s, great effort has been made to recapitulate pancreatic cancer and especially the most common form, PDAC,

in GEMs to gain further insights into the mechanisms that lead to this dismal disease. First attempts in mouse modeling included the generation of transgenic mice expressing the SV40 large T antigen (Ornitz *et al.*, 1987) or activated HRAS (Quaife *et al.*, 1987) under control of the acinar-specific *elastase* (*Ela*) promoter, which both developed acinar cell carcinomas. Using the same promoter for expression of c-Myc (Sandgren *et al.*, 1991) or TGFα, the latter on a *Trp53*-deficient background (Wagner *et al.*, 2001), led to formation of mixed acinar-ductal neoplasias in the pancreas. In a further transgenic approach promoters like c*ytokeratin 19* (*Krt19*) and e*lastase (Ela)* were fused to $Kras^{G12D}$ to express it in the ductal and acinar compartment, respectively (Brembeck *et al.*, 2003; Grippo *et al.*, 2003). Unfortunately, none of these transgenic approaches led to induction of classical PDAC.

However, recognition of 2 transcription factors, pancreatic and duodenal homeobox 1 (Pdx1) and pancreas-specific transcription factor, 1a (Ptf1a, also known as p48) as regulators of pancreatic development, was a milestone in the establishment of GEMs recapitulating PDAC. The homeodomain protein Pdx1 is first detected in the mouse at embryonic day E8.5 with restriction to the dorsal endoderm of the gut. At E9.5 it is expressed in ventral and dorsal pancreatic buds as well as in the duodenal endoderm. In adult mice, its expression is restricted to islet cells and epithelium of the duodenum (Ohlsson *et al.*, 1993; Guz *et al.*, 1995; Offield *et al.*, 1996). The basic helix-loop-helix protein Ptf1a is initially detected at E9.5 in pancreatic progenitor cells. Adult animals exhibit Ptf1a expression in pancreatic acinar cells (Krapp *et al.*, 1998; Kawaguchi *et al.*, 2002). Both Pdx1 and Ptf1a are crucial for pancreatic development and their knock-out turned out to be lethal (Offield *et al.*, 1996; Krapp *et al.*, 1998). Since Ptf1a and Pdx1 expression is relatively restricted to pancreatic precursor cells, this provided a new tool to specifically target $Kras^{G12D}$ to the pancreas (Hingorani *et al.*, 2003) by application of the Cre-loxP system (Orban *et al.*, 1992). Therefore, a mouse line is used, in which the activating G12D mutation is introduced into the second exon of the endogenous *Kras* locus (Jackson *et al.*, 2001). Ubiquitous expression of activated $Kras^{G12D}$ is prevented by inserting a transcriptional stop element, which is flanked by 2 loxP sites (LSL), upstream of the modified second exon. This results in heterozygous expression of the wild type Kras allele. Crossing of these *LSL-*$Kras^{G12D/+}$ mice with the pancreas-specific Cre lines $Ptf1a^{Cre/+}$ (Kawaguchi *et al.*, 2002) or *Pdx1-Cre* (Gannon *et al.*, 2000) leads to excision of the stop element and heterozygous expression of $Kras^{G12D}$ in all pancreatic precursor cells as well as in exocrine and endocrine pancreas of the progeny. These $Ptf1a^{Cre/+}$*;LSL-*$Kras^{G12D/+}$ and *Pdx1-Cre;LSL-*$Kras^{G12D/+}$ mice develop PanINs with complete penetrance that advance in stage with increasing age. Further, from 8 months of age, the animals develop invasive PDAC, which metastasizes to liver and lung (Hingorani *et*

al., 2003), with median survival of 15 months (unpublished data PD Dr. Dieter Saur). This approach for the first time enabled the recapitulation of classical human PanINs and PDAC in a GEM.

Combining Kras activation with pancreatic loss of the frequently mutated tumor suppressors $p16^{INK4A}$/$p19^{ARF}$ causes strong acceleration of tumorigenesis. These mice develop aggressive, locally invasive, and metastatic PDAC resembling human disease with a median survival of 10 weeks (Aguirre *et al.*, 2003). Also, tumorigenesis can be accelerated by interbreeding of *Ptf1a*$^{Cre/+}$*;LSL-Kras*$^{G12D/+}$ and *Pdx1-Cre;LSL-Kras*$^{G12D/+}$ mice with the *LSL-Trp53*$^{R172H/+}$ mouse line. Here, a missense mutation, which is common in human PDAC (Olive *et al.*, 2004), was introduced into the endogenous *Trp53* locus. After deletion of the stop element, mutant $Trp53^{R172H}$ (De Vries *et al.*, 2002) is expressed in the pancreas, leading to development of metastatic ductal PDAC with a median survival of 4 to 5 months (Hingorani *et al.*, 2005, unpublished data PD Dr. Dieter Saur).

Taken together, activated Kras can be regarded as an initiator of pancreatic tumorigenesis, whereas loss of different tumor suppressors, like $p16^{INK4A}$ and $p19^{ARF}$, leads to progression to aggressive human PDAC, which can be recapitulated using GEMs.

1.2 The zinc-finger transcription factor Snail

1.2.1 Structure of Snail

The members of the Snail family of zinc-finger transcription factors play an essential role in a variety of processes in metazoan development and disease (Nieto, 2002). In the early 1980s, the first family member *snail* was described in *Drosophila melanogaster* (Simpson, 1983; Grau *et al.*, 1984; Nüsslein-Volhard *et al.*, 1984), where it was shown to be crucial for mesoderm formation (Alberga *et al.*, 1991). During the next decades, many Snail homologues have been discovered in various species, including mice and humans, where 3 family members have been identified so far: Snai1 (snail homolog 1, hereafter called Snail), Snai2 (Slug), and Snai3 (Smug). They share a highly conserved carboxy-terminal region that contains from 4 to 6 zinc fingers and a more divergent amino-terminal region. The zinc finger motifs of the C_2H_2 type are built of 2 β-strands and 1 α-helix, the latter binding to specific DNA sequences (Barrallo-Gimeno and Nieto, 2009). Several experiments have shown that the consensus binding site for Snail family members is composed of a core of 6 bases, CAGGTG, a motif that is consistent with the so-called E-box (Mauhin *et al.*, 1993; Inukai *et al.*, 1999; Kataoka *et al.*, 2000). When bound to an E-box, Snail proteins are generally thought to function as transcriptional repressors (Peinado *et al.*, 2007). In vertebrates, this

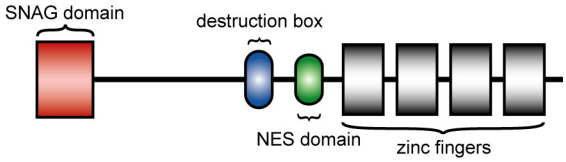

Figure 1-2: The Snail protein structure.
The Snail protein contains a SNAG (Snail/Gfi) domain at the amino-terminal region. In the central region, there can be found a destruction box and a nuclear export signal (NES) domain. Snail has 4 carboxy-terminal zinc-fingers. Adapted by permission from Macmillan Publishers Ltd. (Peinado *et al.*, 2007).

repressor activity further depends on the SNAG (Snail/Gfi) domain, which consists of 7 to 9 conserved amino acids within the amino-terminal region (Grimes *et al.*, 1996). The Snail proteins contain further domains, which vary among the family members.

The murine and the human Snail protein are composed of 264 amino acids, possessing 4 carboxy-terminal zinc fingers and an amino-terminal SNAG domain. Further, 2 different functional domains have been determined in the central region, namely a regular domain which contains a nuclear export signal (NES) and a destruction box domain (Dominguez *et al.*, 2003; Zhou *et al.*, 2004, Figure 1-2). Human and murine Snail proteins are of high similarity, as 87.1% of the amino acids are identical (Twigg and Wilkie, 1999; Jiang *et al.*, 1997).

1.2.2 Function of Snail during epithelial-mesenchymal transition

The best characterized function of Snail is the induction of epithelial-mesenchymal transition (EMT), a process which is necessary for the formation of the body plan during embryonic development but also is of high relevance during tumor progression and metastasis (Barrallo-Gimeno and Nieto, 2009). Epithelial cells have an apicobasal polarity which is defined by the sequential arrangement of extracellular contacts. They interact with the underlying basement membrane via their basal surface and establish close contacts with neighbored cells, forming a layer. During EMT, the cells lose their polarity and cell-cell contacts, leading to the acquisition of a mesenchymal phenotype (Figure 1-3). In contrast to epithelial cells, mesenchymal cells are loosely organized and have an increased motility as well as invasive

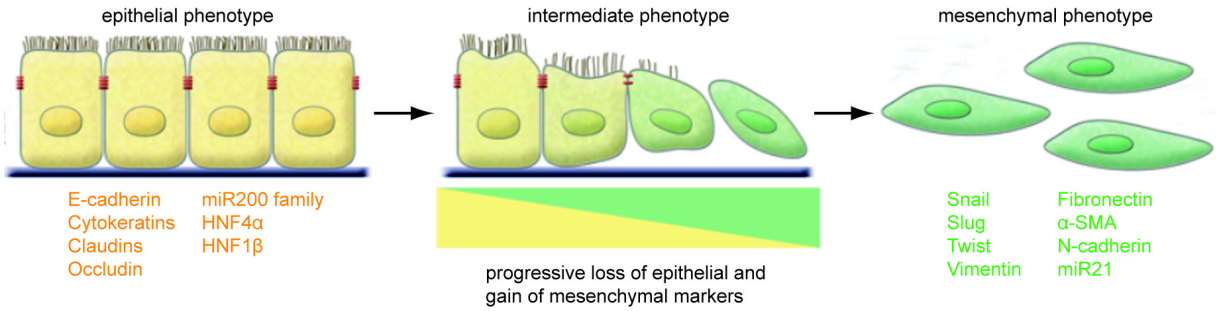

Figure 1-3: Epithelial-mesenchymal transition.
During EMT, polarized epithelial cells convert into loosely organized mesenchymal cells with increased motility and invasive capacity. Common EMT markers are listed. Coexpression of these markers can be observed in cells passing through an intermediate state. miR200, microRNA200; HNF, hepatic nuclear factor; α-SMA, α smooth muscle actin. Adapted by permission from the American Society for Clinical Investigation (Kalluri and Weinberg, 2009).

capacity (Kalluri and Weinberg, 2009; Thiery *et al.*, 2009). A defined level of Snail expression with concomitant EMT is important for cell migrations that occur during several stages of embryonic development. In gastrulating mouse embryos, Snail mRNA expression was observed early during formation of the mesoderm. Later, it is expressed in most mesenchymal cells of mesodermal or neural crest origin (Nieto *et al.*, 1992; Smith *et al.*, 1992). It is obvious that Snail plays a crucial role during murine embryonic development, as *Snail*$^{-/-}$ embryos with ubiquitous Snail knock-out were shown to die due to severe gastrulational defects (Carver *et al.*, 2001).

EMT further has been associated with wound healing, being a physiological response to injury. The third biological setting, in which EMT and Snail play an important role, is cancer progression. Here, EMT allows tumor cells to be released from the primary carcinoma to enter the blood and lymphatic stream and to form distant metastasis. Furthermore, in several experiments it has been shown that EMT in cancer confers resistance to cell death (Valdés *et al.*, 2002; Gal *et al.*, 2008), oncogene-induced senescence (Ansieau *et al.*, 2008), as well as to chemotherapeutic agents (Kajiyama *et al.*, 2007; Yang *et al.*, 2006). EMT can also lead to suppression of the immune system during carcinogenesis (Knutson *et al.*, 2006) and to the acquisition of stem cell properties (Mani *et al.*, 2008). During the process of EMT, several epithelial markers are downregulated, e.g. proteins that account for junctions between cells like E-cadherin, various cytokeratins, claudins, and occludin (Kalluri and Weinberg, 2009), but also microRNAs like the miR200 family (Park *et al.*, 2008; Gregory *et al.*, 2008). This is generally accompanied by the upregulation of mesenchymal markers, e.g. vimentin, fibronectin, Twist, Slug, and Snail. Further, cells in an intermediate state exist that have not completely undergone EMT, expressing both epithelial and mesenchymal markers (Kalluri and Weinberg, 2009).

1.2.3 Activation and regulation of Snail

Numerous signaling molecules and pathways have been demonstrated to induce EMT and thereby activate Snail in different cellular contexts (Barrallo-Gimeno and Nieto, 2005; De Craene *et al.*, 2005 b). Transforming growth factor β (TGFβ), fibroblast growth factor (FGF), bone morphogenetic proteins (BMPs), and epidermal growth factor (EGF) (Valdés *et al.*, 2002; Spagnoli *et al.*, 2000; Peinado *et al.*, 2003; Jamora *et al.*, 2005; Isaac *et al.*, 2000; Ciruna and Rossant, 2001; Montero *et al.*, 2001; Strizzi *et al.*, 2004; Cheng *et al.*, 2010; Lu *et al.*, 2003) induce Snail and concomitant EMT under various experimental conditions. Another pathway that has been connected to Snail expression in several settings is the Notch pathway. This link was shown in multiple species during neural crest development, where

induction of EMT by Snail plays a crucial role. In *Xenopus laevis* and *Drosophila melanogaster*, Snail represses the Notch ligand Delta1, thereby promoting neural crest formation (Cowden and Levine, 2002; Glavic *et al.*, 2004). In contrary, Snail does not seem to play a role in neural crest development in mice, as conditional Snail knock-out mice do not exhibit any severe defects in the neural crest (Murray and Gridley, 2006 a). An association with upregulation of Snail expression was also shown for integrin linked kinase (ILK), as ILK-stimulated human colon carcinoma cells exhibit increased *Snail* promoter activity (Tan *et al.*, 2001).

Besides these numerous Snail-activating signaling pathways, several repressive mechanisms have been described on both pre- and posttranscriptional level. In the context of breast cancer, metastasis-associated protein 3 (MTA3) has been identified to form a transcriptional corepressor complex as response to estrogen receptor (ER) signaling, also known as the Mi-2/NuRD complex. Indeed, in absence of ER signaling or MTA3, aberrant Snail expression was observed (Fujita *et al.*, 2003).

On posttranscriptional level, the subcellular localization of Snail and thus its activity is controlled by 2-stage glycogen synthase kinase 3 beta (GSK3β) phosphorylation. Snail contains a phosphorylation consensus motif for nuclear export and another for protein degradation. As shown in both human embryonic kidney and mammary tumor cells, GSK3β posttranslationally regulates Snail by at first phosphorylating it at the nuclear export motif, thus promoting its export to the cytoplasm. There, Snail secondly is phosphorylated at the protein degradation motif, leading to association with the E3 ubiquitin ligase βTrCP, which results in Snail degradation (Zhou *et al.*, 2004; Yook *et al.*, 2005). This interplay between Snail and GSK3β directly builds a link to the Wnt-β-catenin signaling pathway. Actually, active Wnt signaling inhibits GSK3β-dependent phosphorylation and degradation of Snail, thus leading to its stabilization (Yook *et al.*, 2005). Being consistent with these findings, inhibition of GSK3β in epithelial skin cell lines was shown to induce transcription of Snail (Bachelder *et al.*, 2005). Independently of GSK3β, Snail was also demonstrated to be degraded by the proteasome upon interaction with the E3 ubiquitin ligase FBW14 (Viñas-Castells *et al.*, 2010). Another mechanism of Snail regulation is the binding to and repression of its own promoter, arguing for the existence of an autoregulatory loop (Peiró *et al.*, 2006).

Taken together, Snail is activated and regulated by a variety of factors. In this sensitive system, even slight deregulation of its expression can lead to changed expression of several known downstream targets of Snail and thus to many dysfunctions.

1.2.4 Snail in tumor progression—epithelial-mesenchymal transition and beyond

As stated above, Snail expression seems to be crucial for all EMT-related processes and generally leads to acquisition of a mesenchymal phenotype, accompanied with the loss of epithelial markers, which has been demonstrated in many species (Peinado *et al.*, 2007; Barrallo-Gimeno and Nieto, 2005). Mostly, Snail was shown to act as a transcriptional repressor. The first gene that was published to be directly repressed by Snail was *CDH1*, which encodes the epithelial marker E-cadherin. E-cadherin is a single-span transmembrane glycoprotein which keeps up cellular polarity and intercellular contacts in epithelial tissues (Christofori and Semb, 1999). 2 independent groups could show that Snail expression inversely correlates with E-cadherin expression, which is caused by direct repressive binding of Snail to 3 E-boxes of the *CDH1* promoter. Further, Snail expression was mainly detected in highly malignant cell lines, as well as in dedifferentiated and invasive tumor areas, pointing out the importancy of this transcription factor during tumor progression (Batlle *et al.*, 2000; Cano *et al.*, 2000). For *CDH1* repression, Snail also needs to recruit histone deacetylases (HDAC) 1/2 and mSin3a, building a transcriptional repressor complex (Peinado *et al.*, 2004). Repressive activity of Snail is further promoted by phosphorylation of Ser^{246} by p21-activated kinase 1 (PAK1) (Yang *et al.*, 2005). Beyond *CDH1*, Snail has been demonstrated to directly bind to and repress several other genes that encode epithelial markers, e.g. cytokeratins 17 and 18 (De Craene *et al.*, 2005 a), claudins and occludin (Ikenouchi *et al.*, 2003), hepatic nuclear factor 4α (HNF4α) and HNF1β (Cicchini *et al.*, 2006; Boutet *et al.*, 2006).

Besides EMT, Snail has been implicated in a variety of processes that are of high importance during tumor progression. In mouse mammary epithelial cells and colorectal cancer cells, Snail expression induces stem cell-like properties, which goes along with an increased tumorigenic potential (Mani *et al.*, 2008; Hwang *et al.*, 2011). In cell lines that have undergone EMT, as well as in developing mouse embryos, Snail impairs cell cycle progression by repressing cyclin D2, leading to decreased proliferative potential. Furthermore, it confers resistance to cell death and is a potent pro-survival factor (Martínez-Álvarez *et al.*, 2004; Vega *et al.*, 2004). In human carcinoma cells under genotoxic stress, it was shown that Snail protects from cell death by direct downregulation of proapoptotic genes, e.g. BH3 interacting-domain death agonist (BID) and DNA fragmentation factor (DFF) (Kajita *et al.*, 2004). However, at least the influence of Snail on proliferation seems to be dependent on the experimental context, as transgenic mice expressing Snail ectopically in the skin epidermis exhibit hyperproliferation (Jamora *et al.*, 2005), and murine squamous cell and spindle cell carcinoma cells show decreased proliferation after Snail knockdown (Olmeda *et al.*, 2007).

As both proliferation and survival are 2 critical factors during cancer progression and EMT plays an important role in metastasis, it is no surprise that Snail expression has been shown in many types of cancer, often promoting metastasis and invasion, e.g. in head and neck (Yang *et al.*, 2007), thyroid (Hardy *et al.*, 2007), breast (Moody *et al.*, 2005), hepatocellular (Yang *et al.*, 2009), colorectal (Roy *et al.*, 2005), prostate (Heebøll *et al.*, 2009), and ovarian (Blechschmidt *et al.*, 2008) carcinoma. Also, in 78% of human pancreatic carcinoma samples, Snail expression was observed (Hotz *et al.*, 2007). Furthermore, in an *in vivo* selection model of highly metastatic pancreatic tumor cells, increased Snail levels and repression of E-cadherin expression by a transcriptional repressor complex composed of Snail and HDAC1/2 have been demonstrated (von Burstin *et al.*, 2009).

The last decades have brought enormous advances in our understanding of the molecular mechanisms underlying cancer progression and without doubt, dysregulation of the mesenchymal marker Snail is a critical step in tumorigenesis and the metastatic process. However, a full understanding of its contribution to cancer initiation and progression will be needed to develop potential novel therapeutic strategies of this fatal disease.

1.3 Aims of this work

As depicted above, the transcription factor Snail plays an important role in pancreatic tumorigenesis, but the exact mechanism still needs to be revealed. Existing cell-based models are only partly suitable to investigate Snail function in pancreatic cancer, because here, several factors like tumor microenvironment cannot be considered properly. The aim of this work was to overcome these limitations by *in vivo* examination of the role of Snail in carcinogenesis, metastasis, and EMT in a genetically engineered mouse model of pancreatic cancer. Therefore, a conditional Snail expression model was generated by targeting the murine *Rosa26* locus with a lox-Stop-lox (LSL) silenced *Snail* cassette (*LSL-Rosa26*$^{Snail/+}$). In this model, pancreatic expression of Snail was activated using a pancreas-specific Cre driver line (*Ptf1a*$^{Cre/+}$). To investigate the role of Snail for pancreatic cancer initiation, progression, and metastasis, the *LSL-Rosa26*$^{Snail/+}$ line was crossed into the established Kras^{G12D}-dependent PDAC model (*Ptf1a*$^{Cre/+}$*;LSL-Kras*$^{G12D/+}$, Hingorani *et al.*, 2003). Furthermore, the general influence of Snail expression on pancreatic cell behavior was investigated using *Ptf1a*$^{Cre/+}$*;LSL-Rosa26*$^{Snail/+}$ mice. Survival curves, histological sections, and gene expression profiles of these mice and control cohorts were analyzed to get deeper insight into the contribution of Snail to pancreatic cell differentiation and cancer development. In particular, tightly regulated cellular processes that are dysfunctional in cancer, like proliferation, apoptosis, senescence, and DNA damage repair, were investigated.

2 Materials

2.1 Technical equipment

Table 2-1: Technical equipment.

Device	Source
96-well magnetic ring-stand	Applied Biosystems, Inc., Carlsbad, CA, USA
Amersham Hyperprocessor™ automatic film processor	GE Healthcare Europe GmbH, Munich
Amersham VacuGene™ XL vacuum blotting system	GE Healthcare Europe GmbH, Munich
Analytical balance A 120 S	Sartorius AG, Göttingen
Analytical balance BP 610	Sartorius AG, Göttingen
Autoclave 2540 EL	Tuttnauer Europe B.V., Breda, The Netherlands
AxioCam HRc	Carl Zeiss AG, Oberkochen
AxioCam MRc	Carl Zeiss AG, Oberkochen
Bag sealer Folio FS 3602	Severin Elektrogeräte GmbH, Sundern
Centrifuge Avanti® J25	Beckman Coulter GmbH, Krefeld
Centrifuge Rotina 46R	Andreas Hettich GmbH & Co. KG, Tuttlingen
CO_2 incubator HERAcell®	Heraeus Holding GmbH, Hanau
CO_2 incubator MCO-5AC 17AI	Sanyo Sales & Marketing Europe GmbH, Munich
Cryo 1°C freezing container 5100, "Mr. Frosty"	Thermo Fisher Scientific, Inc., Waltham, MA, USA
Cryostat Microm HM 560	Thermo Fisher Scientific, Inc., Waltham, MA, USA
Dewar carrying flask, type B	KGW-Isotherm, Karlsruhe
Duo therm hybridization oven OV5	Biometra GmbH, Göttingen
Electrophoresis power supply Power Pac 200	Bio-Rad Laboratories GmbH, Munich
Electroporation system Gene Pulser® II	Bio-Rad Laboratories GmbH, Munich
Experion® automated electrophoresis station	Bio-Rad Laboratories GmbH, Munich
Experion® priming station	Bio-Rad Laboratories GmbH, Munich
Experion® vortex station	Bio-Rad Laboratories GmbH, Munich
Flu-o-blu	Biozym Scientific GmbH, Hessisch Oldenburg
Gel Doc™ XR+ system	Bio-Rad Laboratories GmbH, Munich
Glass ware, Schott Duran®	Schott AG, Mainz
Heated paraffin embedding module EG1150 H	Leica Microsystems GmbH, Wetzlar
HERAsafe® biological safety cabinet	Thermo Fisher Scientific, Inc., Waltham, MA, USA
Homogenizer SilentCrusher M with tool 6F	Heidolph Instruments GmbH & Co. KG, Schwabach
Horizontal gel electrophoresis system	Biozym Scientific GmbH, Hessisch Oldenburg
Horizontal shaker	Titertek Instruments, Inc., Huntsville, AL, USA
Incubator shaker Thermoshake	C. Gerhardt GmbH & Co. KG, Königswinter

Device	Source
Laminar flow HERAsafe	Heraeus Holding GmbH, Hanau
Liquid scintillation counter & luminometer Wallac 1450 MicroBeta TriLux	PerkinElmer, Rodgau
Magnetic stirrer, Ikamag® RCT	IKA® Werke GmbH & Co. KG, Staufen
Microcentrifuge 5415 D	Eppendorf AG, Hamburg
Microcentrifuge 5417 R	Eppendorf AG, Hamburg
Microplate reader Anthos 2001	Anthos Mikrosysteme GmbH, Krefeld
Microscope Axio Imager.A1	Carl Zeiss AG, Oberkochen
Microscope Axiovert 25	Carl Zeiss AG, Oberkochen
Microscope DM LB	Leica Microsystems GmbH, Wetzlar
Microtome Microm HM355S	Thermo Fisher Scientific, Inc., Waltham, MA, USA
Microwave	Siemens, Munich
Mini centrifuge MCF-2360	LMS Consult GmbH & Co. KG, Brigachtal
Mini-PROTEAN® Tetra Cell	Bio-Rad Laboratories GmbH, Munich
Multipette® stream	Eppendorf AG, Hamburg
Neubauer hemocytometer, improved	LO-Laboroptik GmbH, Bad Homburg
Odyssey® infrared imaging system	Li-Cor Biosciences, Lincoln, NE, USA
Paraffin tissue floating bath Microm SB80	Thermo Fisher Scientific, Inc., Waltham, MA, USA
pH meter 521	WTW Wissenschaftlich-Technische Werkstätten GmbH, Weilheim
Pipettes Reference®, Research®	Eppendorf AG, Hamburg
Pipetus®	Hirschmann Laborgeräte GmbH & Co. KG, Eberstadt
Power supplies E844, E822, EV243	Peqlab Biotechnologie GmbH, Erlangen
Spectrophotometer NanoDrop 1000	Peqlab Biotechnologie GmbH, Erlangen
StepOnePlus™ real time PCR system	Applied Biosystems, Inc., Carlsbad, CA, USA
Stereomicroscope Stemi SV 11	Carl Zeiss AG, Oberkochen
Surgical instruments	Thermo Fisher Scientific, Inc., Waltham, MA, USA
Thermocycler T1	Biometra GmbH, Göttingen
Thermocycler TGradient	Biometra GmbH, Göttingen
Thermocycler TPersonal	Biometra GmbH, Göttingen
Thermocycler UNO-Thermoblock	Biometra GmbH, Göttingen
Thermomixer compact	Eppendorf AG, Hamburg
Tissue processor ASP300	Leica Microsystems GmbH, Wetzlar
Tumbling table WT 17	Biometra GmbH, Göttingen
Vortex Genius 3	IKA® Werke GmbH & Co. KG, Staufen
Water bath 1003	GFL Gesellschaft für Labortechnik mbH, Burgwedel
Western blot system SE 260 Mighty Small II	Hoefer, Inc., Holliston, MA, USA

2.2 Disposables

Table 2-2: Disposables.

Disposable	Source
Amersham Hybond-N+ membrane	GE Healthcare Europe GmbH, Munich
Amersham micro columns Illustra ProbeQuant™ G-50	GE Healthcare Europe GmbH, Munich
Amersham Rediprime™ II DNA labeling system	GE Healthcare Europe GmbH, Munich
Argentrix® silver nitrate applicator	Ryma-Pharm GmbH, Körle
Cell culture plastics	Becton Dickinson GmbH, Franklin Lakes, NJ, USA; Greiner Bio-One GmbH, Frickenhausen; TPP Techno Plastic Products AG, Trasadingen, Switzerland
Cell scrapers	TPP Techno Plastic Products AG, Trasadingen, Switzerland
Cell strainer, 100 µm, yellow	BD Biosciences, Franklin Lakes, NJ, USA
Chromatography paper, 3 mm	GE Healthcare Europe GmbH, Munich
Combitips BioPur®	Eppendorf AG, Hamburg
Conical tubes, 15 ml	TPP Techno Plastic Products AG, Trasadingen, Switzerland
Conical tubes, 50 ml	Sarstedt AG & Co., Nümbrecht
Cover slips	Gerhard Menzel, Glasbearbeitungswerk GmbH & Co. KG, Braunschweig
CryoPure tubes	Sarstedt AG & Co., Nümbrecht
Cuvettes	Greiner Bio-One GmbH, Frickenhausen
Disposable scalpels	Feather Safety Razor Co., Ltd., Osaka, Japan
Electroporation cuvettes Gene Pulser®/MicroPulser™, 0.2 cm gap	Bio-Rad Laboratories GmbH, Munich
Filtropur S 0.2	Sarstedt AG & Co., Nümbrecht
Filtropur S 0.45	Sarstedt AG & Co., Nümbrecht
Glass slides Superfrost® Plus	Gerhard Menzel, Glasbearbeitungswerk GmbH & Co. KG, Braunschweig
Kodak® BioMax™ MS film	Sigma-Aldrich Chemie GmbH, Munich
MicroAmp® optical 96-well reaction plate	Applied Biosystems, Inc., Carlsbad, CA, USA
Microtome blades S35 and C35	Feather Safety Razor Co., Ltd., Osaka, Japan
Pasteur pipettes	Hirschmann Laborgeräte GmbH & Co. KG, Eberstadt
PCR reaction tubes	Brand GmbH + Co. KG, Wertheim; Eppendorf AG, Hamburg
Petri dishes	Sarstedt AG & Co., Nümbrecht
Phase lock gel light tubes	5 Prime GmbH, Hamburg
Pipette tips	Sarstedt AG & Co., Nümbrecht
Reaction tubes, 0.5 ml, 1.5 ml and 2 ml	Eppendorf AG, Hamburg

Disposable	Source
Safe seal pipette tips, professional	Biozym Scientific GmbH, Hessisch Oldenburg
Safe-lock reaction tubes BioPur®	Eppendorf AG, Hamburg
Serological pipettes	Sarstedt AG & Co., Nümbrecht
Single use needles Sterican® 27 gauge	B. Braun Melsungen AG, Melsungen
Single use syringes Omnifix®	B. Braun Melsungen AG, Melsungen
Spectra/Mesh® polypropylene, 30 x 30 cm square, 500 µm opening	Spectrum Laboratories, Inc., Rancho Dominguez, CA, USA
Tissue embedding cassette system	Medite GmbH, Burgdorf
Transfer membrane Immobilon-P	Millipore GmbH, Schwalbach am Taunus

2.3 Reagents and enzymes

Table 2-3: Reagents and enzymes.

Reagent	Source
1 kb DNA extension ladder	Invitrogen GmbH, Karlsruhe
1,4-Dithiothreitol (DTT)	Carl Roth GmbH + Co. KG, Karlsruhe
2-Log DNA ladder (0.1–10.0 kb)	New England Biolabs GmbH, Frankfurt am Main
2-Mercaptoethanol, 98%	Sigma-Aldrich Chemie GmbH, Munich
2-Propanol (isopropanol)	Carl Roth GmbH + Co.
5-Bromo-2'-deoxyuridine *BioChemica* (BrdU)	AppliChem GmbH, Darmstadt
Agarose	Sigma-Aldrich Chemie GmbH, Munich
Amersham Rapid-hyb™ buffer	GE Healthcare Europe GmbH, Munich
Ammonium persulfate	Sigma-Aldrich Chemie GmbH, Munich
Ampicillin sodium salt	Carl Roth GmbH + Co. KG, Karlsruhe
BBXF agarose gel loading dye mixture	BIO 101, Inc., Carlsbad, CA, USA
Blotting grade blocker non-fat dry milk	Bio-Rad Laboratories GmbH, Munich
Bovine serum albumin, fraction V	Sigma-Aldrich Chemie GmbH, Munich
Bradford reagent	Serva Electrophoresis GmbH, Heidelberg
Bromphenol blue	Sigma-Aldrich Chemie GmbH, Munich
Chloramphenicol	AppliChem GmbH, Darmstadt
Chloroform	Merck KGaA, Darmstadt
Complete, EDTA-free, protease inhibitor cocktail tablets	Roche Deutschland Holding GmbH, Grenzach-Wyhlen
Deoxycytidine 5'-triphosphate, [alpha-32P]- (EasyTides)	PerkinElmer, Rodgau
Dimethylsulfoxide (DMSO)	Carl Roth GmbH + Co. KG, Karlsruhe
dNTP mix, 10mM each	Fermentas GmbH, St. Leon-Rot
Dodecylsulfate Na-salt in pellets (SDS)	Serva Electrophoresis GmbH, Heidelberg

Reagent	Source
Dulbecco's phosphate buffered saline, powder	Biochrom AG, Berlin
Ethanol (100%)	Merck KGaA, Darmstadt
Ethidium bromide	Sigma-Aldrich Chemie GmbH, Munich
Ethylenediaminetetraacetic acid (EDTA)	Invitrogen GmbH, Karlsruhe
Etoposide Calbiochem®	Merck KGaA, Darmstadt
Forene® isoflurane	Abbott GmbH & Co. KG, Ludwigshafen
Gateway® LR Clonase™ enzyme mix	Invitrogen GmbH, Karlsruhe
Gel loading dye, blue	New England Biolabs GmbH, Frankfurt am Main
GelStar® nucleic acid gel stain	Biowhittaker Molecular Applications, Rockland, ME, USA
GeneRuler™ 100bp DNA ladder	Fermentas GmbH, St. Leon-Rot
Glycerol	Sigma-Aldrich Chemie GmbH, Munich
Glycin Pufferan®	Carl Roth GmbH + Co. KG, Karlsruhe
HEPES Pufferan®	Carl Roth GmbH + Co. KG, Karlsruhe
Histosec® pastilles (without DMSO)	Merck KGaA, Darmstadt
HotStarTaq DNA polymerase	Qiagen GmbH, Hilden
Hydrochloric acid (HCl)	Merck KGaA, Darmstadt
Isotonic sodium chloride solution	Braun Melsungen AG, Melsungen
Kanamycin sulphate	Carl Roth GmbH + Co. KG, Karlsruhe
LB agar (Luria/Miller)	Carl Roth GmbH + Co. KG, Karlsruhe
LB broth (Luria/Miller)	Carl Roth GmbH + Co. KG, Karlsruhe
Magnesium chloride	Carl Roth GmbH + Co. KG, Karlsruhe
Methanol	Merck KGaA, Darmstadt
Mouse diet LASCRdiet™ CreActive TAM400	LASvendi GmbH, Soest
Mouse diet M-Z low phytoestrogen + 10g/kg Pancrex-Vet	Ssniff Spezialdiäten GmBH, Soest
N,N-dimethylformamide	Sigma-Aldrich Chemie GmbH, Munich
Nonidet P40	Roche Deutschland Holding GmbH, Grenzach-Wyhlen
Orange G	Carl Roth GmbH + Co. KG, Karlsruhe
Peanut oil	Sigma-Aldrich Chemie GmbH, Munich
PfuUltra™ high fidelity DNA polymerase	Agilent Technologies, Inc., Santa Clara, CA, USA
Phosphatase inhibitor mix I	Serva Electrophoresis GmbH, Heidelberg
Polyethylene glycol 4000	Merck KGaA, Darmstadt
Precision Plus Protein™ all blue standard	Bio-Rad Laboratories GmbH, Munich
Proteinase K, recombinant, PCR grade	Roche Deutschland Holding GmbH, Grenzach-Wyhlen
QuantiFast® SYBR® green PCR master mix	Qiagen GmbH, Hilden

Reagent	Source
rAPid alkaline phosphatase	Roche Deutschland Holding GmbH, Grenzach-Wyhlen
REDTaq® ReadyMix™ PCR reaction mix	Sigma-Aldrich Chemie GmbH, Munich
Restriction endonucleases	New England Biolabs GmbH, Frankfurt am Main
RNase-free DNase set	Qiagen GmbH, Hilden
RNaseA	Fermentas GmbH, St. Leon-Rot
Roti® phenol / chloroform / isoamyl-alcohol	Carl Roth GmbH + Co. KG, Karlsruhe
Rotiphorese® gel 30	Carl Roth GmbH + Co. KG, Karlsruhe
S.O.C. medium	Invitrogen GmbH, Karlsruhe
Sodium acetate buffer solution	Sigma-Aldrich Chemie GmbH, Munich
Sodium chloride (NaCl)	Merck KGaA, Darmstadt
Sodium hydroxide solution (NaOH)	Merck KGaA, Darmstadt
SSC buffer concentrate	Sigma-Aldrich Chemie GmbH, Munich
T4 DNA ligase	Invitrogen GmbH, Karlsruhe
Tamoxifen	Sigma-Aldrich Chemie GmbH, Munich
TaqMan® reverse transcription reagents	Applied Biosystems, Inc., Carlsbad, CA, USA
TE buffer, pH 8.0	AppliChem GmbH, Darmstadt
TEMED	Carl Roth GmbH + Co. KG, Karlsruhe
Tissue-Tek® O.C.T.™ compound	Sakura Finetek Europe B.V, Alphen aan den Rijn, Netherlands
Tris hydrochloride	J.T.Baker® Chemicals, Phillipsburg, NJ, USA
Tris Pufferan®	Carl Roth GmbH + Co. KG, Karlsruhe
Triton® X-100	Merck KGaA, Darmstadt
TUNEL dilution buffer	Roche Deutschland Holding GmbH, Grenzach-Wyhlen
Tween® 20	Carl Roth GmbH + Co. KG, Karlsruhe

2.4 Antibodies

Table 2-4: Antibodies.

Antibody	Source
AlexaFluor® 680 goat anti-mouse IgG, A21058	Invitrogen GmbH, Karlsruhe
AlexaFluor® 750 goat anti-mouse IgG, A21037	Invitrogen GmbH, Karlsruhe
Anti-mouse IgG (H+L) (DyLight® 680 Conjugate), #5470	Cell Signaling Technology, Inc., Danvers, MA, USA
Anti-mouse IgG (H+L) (DyLight® 800 Conjugate), #5257	Cell Signaling Technology, Inc., Danvers, MA, USA
Anti-rabbit IgG (H+L) (DyLight® 680 Conjugate), #5366	Cell Signaling Technology, Inc., Danvers, MA, USA

Antibody	Source
Anti-rabbit IgG (H+L) (DyLight® 800 Conjugate), #5151	Cell Signaling Technology, Inc., Danvers, MA, USA
BrdU, MCA2060	AbD Serotec, Düsseldorf
Cleaved Caspase 3 (Asp175) (5A1E), #9664	Cell Signaling Technology, Inc., Danvers, MA, USA
Cytokeratin 19, TROMA 3	Developmental Studies Hybridoma Bank, Iowa City, IA, USA
E-cadherin, 610181	BD Biosciences, Franklin Lakes, NJ, USA
p21 (C-19), sc-397	Santa Cruz Biotechnology, Inc., Santa Cruz, CA, USA
p44/42 MAPK (Erk1/2) (L34F12), #4696	Cell Signaling Technology, Inc., Danvers, MA, USA
p53 (CM5), Novocastra™	Leica Microsystems GmbH, Wetzlar
pan-Akt (C67E7), #4691	Cell Signaling Technology, Inc., Danvers, MA, USA
Phospho-Akt (Ser473), #9271	Cell Signaling Technology, Inc., Danvers, MA, USA
Phospho-Akt (Thr308), #9275	Cell Signaling Technology, Inc., Danvers, MA, USA
Phospho-Histone H2A.X (Ser139) (JBW301)	Millipore GmbH, Schwalbach am Taunus
Phospho-p44/42 MAPK (Erk1/2) (Thr202/Tyr204) (D13.14.4E) XP™, #4370	Cell Signaling Technology, Inc., Danvers, MA, USA
Phospho-Rb (Ser807/811) (D20B12) #8516	Cell Signaling Technology, Inc., Danvers, MA, USA
Snail (L70G2), #3895	Cell Signaling Technology, Inc., Danvers, MA, USA
Snail, ab17732	Abcam plc, Cambridge, UK
α-Amylase, A8273	Sigma-Aldrich Chemie GmbH, Munich
α-Tubulin, T6199	Sigma-Aldrich Chemie GmbH, Munich
β-Actin, A5316	Sigma-Aldrich Chemie GmbH, Munich

2.5 Molecular biology

All buffers were prepared with bidistilled H_2O.

Table 2-5: Buffers and solutions for molecular biology.

Buffer	Component
IP buffer, pH 7.9	50 mM HEPES
	150 mM NaCl
	1 mM EDTA
	0.5% Nonidet P40
	10% Glycerol
	Phosphatase inhibitor (add prior to use)
	Protease inhibitor (add prior to use)
Stacking gel buffer	0.5 M Tris, adjusted to pH 6.8 with HCl
Separating gel buffer	1.5 M Tris, adjusted to pH 8.8 with HCl

Buffer	Component
Running buffer	25 mM Tris
	192 mM Glycine
	0.1% SDS
Transfer buffer, pH 8.3	25 mM Tris
	192 mM Glycine
	20% Methanol
5x Protein loading buffer (Laemmli), pH 6.8	10% SDS
	50% Glycerol
	228 mM Tris hydrochloride
	0.75 mM Bromphenol blue
	5% 2-Mercaptoethanol
6x Loading buffer orange G	60% Glycerol
	60 mM EDTA
	0.24% Orange G
10x Gitschier's buffer	670 mM Tris, pH 8.8
	166 mM $(NH_4)_2SO_4$
	67 mM $MgCl_2$
PCR lysis buffer (Soriano)	0.5% Triton® X-100
	1% 2-Mercaptoethanol
	1x Gitschier's buffer
	400 µg/ml Proteinase K (add prior to use)
ES cell lysis buffer	100 mM Tris, pH 8.5
	5 mM EDTA
	0.8 mM HCl
	0.2% SDS
	200 mM NaCl
	0.1 mg/ml Proteinase K (add prior to use)
Tris buffered saline (TBS), pH 7.6	0.5 M Tris
	1.5 M Sodium chloride
50x Tris acetate EDTA (TAE) buffer, pH 8.5	2 M Tris
	50 mM EDTA
	5.71% Acetic acid
Tryptic soy broth (TSB) buffer	10% Polyethylene glycol 4000
(ad 100 ml with LB broth, pH 6.1)	5% DMSO
	10 mM $MgCl_2$
	10 mM $MgSO_4$

Buffer	Component
5x KCM buffer	500 mM KCl
	150 mM $CaCl_2$
	250 mM $MgCl_2$

Table 2-6: Kits for molecular biology.

Kit	Source
Ambion® WT expression kit	Applied Biosystems, Inc., Carlsbad, CA, USA
Amersham Rediprime™ II DNA labeling system	GE Healthcare Europe GmbH, Munich
EndoFree® plasmid maxi kit	Qiagen GmbH, Hilden
Experion™ RNA StdSens analysis kit	Bio-Rad Laboratories GmbH, Munich
GeneChip® 3' IVT express kit	Affymetrix, Inc., Santa Clara, CA, USA
GeneChip® poly-A RNA control kit	Affymetrix, Inc., Santa Clara, CA, USA
GeneChip® WT terminal labeling kit	Affymetrix, Inc., Santa Clara, CA, USA
QIAamp DNA mini kit	Qiagen GmbH, Hilden
QIAfilter plasmid midi kit	Qiagen GmbH, Hilden
QIAprep® spin miniprep kit	Qiagen GmbH, Hilden
QIAquick® gel extraction kit	Qiagen GmbH, Hilden
QIAshredder	Qiagen GmbH, Hilden
QuantiFast SYBR green PCR kit	Qiagen GmbH, Hilden
Quick Blunting™ kit	New England Biolabs GmbH, Frankfurt am Main
Ras activation assay kit	Millipore GmbH, Schwalbach am Taunus
RNeasy mini kit	Qiagen GmbH, Hilden
Topo® TA cloning® kit	Invitrogen GmbH, Karlsruhe
Zero Blunt® TOPO® PCR cloning kit	Invitrogen GmbH, Karlsruhe

Table 2-7: Bacterial strains.

Bacterial strain	Source
DB3.1™ chemically competent *E. coli*	Invitrogen GmbH, Karlsruhe
One Shot® Stbl3™ chemically competent *E. coli*	Invitrogen GmbH, Karlsruhe
One Shot® TOP10 chemically competent *E. coli*	Invitrogen GmbH, Karlsruhe

Table 2-8: Plasmids and cDNAs.

Plasmid	Source
pBroad3	InvivoGen, San Diego, CA, USA
pENTR™-LSL-MCS-pA	Generated in Saur laboratory, Munich, modification of pENTR™/D-TOPO®, Invitrogen GmbH, Karlsruhe

Plasmid	Source
pENTR™-MCS-EF1a-dsRed	Generated in Saur laboratory, Munich, modification of pENTR™/D-TOPO®, Invitrogen GmbH, Karlsruhe
pENTR™/D-TOPO®	Invitrogen GmbH, Karlsruhe
pMC1neo	Agilent Technologies, Inc., Santa Clara, CA, USA
pRosa26-3-2	Generated in Saur laboratory, Munich
pRosa26-Att-CCDB-Att	Generated in Saur laboratory, Munich
RCASBP(A)	Kindly provided by Ph.D. Stephen H. Hughes, Frederick, MD, USA
RCASBP(A)-Att-CCDB-Att	Generated in Saur laboratory, Munich, modification of RCASBP(A)
Snai1 cDNA; Library: IRAV MGC Mouse verified full length amp cDNA; Clone: IRAVp968A0443D6	RZPD Deutsches Ressourcenzentrum für Genomforschung GmbH, Berlin

Table 2-9: Microarray chips.

Chip	Source
GeneChip® mouse gene 1.0 ST array	Affymetrix, Inc., Santa Clara, CA, USA
GeneChip® mouse genome 430 2.0 array	Affymetrix, Inc., Santa Clara, CA, USA

2.5.1 Primers

Primers were synthesized by Eurofins MWG GmbH (Ebersberg), and diluted in H_2O to a concentration of 10 µM.

Table 2-10: Primers for genotyping.

Name of PCR	Name of primer	Sequence (5' – 3')
Ptf1a^{Cre}	Ptf1a-Cre-GT-LP-URP	CCTCGAAGGCGTCGTTGATGGACTGCA
	Ptf1a-Cre-GT-wt-UP	CCACGGATCACTCACAAAGCGT
	Ptf1a-Cre-GT-mut-UP-neu	GCCACCAGCCAGCTATCAA
LSL-Kras^{G12D}	Kras-WT-UP1	CACCAGCTTCGGCTTCCTATT
	Kras-URP-LP1	AGCTAATGGCTCTCAAAGGAATGTA
	KrasG12D-mut-UP	CCATGGCTTGAGTAAGTCTGC
LSL-Trp53^{R172H}	Trp53R172H-WT-UP2	AGCCTTAGACATAACACACGAACT
	Trp53R172H-URP-LP	CTTGGAGACATAGCCACACTG
	Trp53R172H-mut-UP4	GCCACCATGGCTTGAGTAA
LSL-Rosa26^{Snail}	R26-Tva-GT-UP	AAAGTCGCTCTGAGTTGTTAT
	pGL3-pA-pause-4645-UP	TGAATAGTTAATTGGAGCGGCCGCAATA
	Snail-geno-rev	GCGCTCCTTCCTGGT

Name of PCR	Name of primer	Sequence (5' – 3')
LSL-Rosa26$^{Tva\text{-}lacZ}$	R26-Tva-GT-UP	AAAGTCGCTCTGAGTTGTTAT
	R26-Tva-GT-SA-mut-LP	GCGAAGAGTTTGTCCTCAACC
	R26-Tva-GT-WT LP	GGAGCGGGAGAAATGGATATG
	Tva-LP-353	CATCTCACCAGCTCACAGCAA
Ela1-Cre^{ERT2}	Cre-ERTM-UP	AACCTGGATAGTGAAACAGGGGC
	Cre-ERTM-LP	CATGGAGCGAACGACGAGA
Cdkn2a^{lox}	Ink4a-UP	CCAAGTGTGCAAACCCAGGCTCC
	Ink4a-LP	TTGTTGGCCCAGGATGCCGACAT
Ink*	VBC-Ink4a-PM-UP	GCAGTGTTGCAGTTTGAACCC
	VBC-Ink4a-PM-LP	TGTGGCAACTGATTCAGTTGG
Cdkn2a integrity	Cdkn2a-UP	AGTTCGGGGCGTTGGG
	Cdkn2a-Int1-LP	GCACAGGCTCTGGAATGCA

Table 2-11: Primers for cloning.

Name of PCR	Name of primer	Sequence (5' – 3')
Cloning Snail	Snail1-ATG-AatII-for	AAGACGTCGCCAACATGCCGCGCT
	Snail1-Stop-NdeI-rev	GGAATTCCATATGTCAGCGAGGGCCTCCG

Table 2-12: Murine primers for quantitative real time PCR.

Gene	Name of primer	Sequence (5' – 3')
Amy2	Amy2-TM-for	TGGCGTCAAATCAGGAACATG
	Amy2-TM-rev	AAAGTGGCTGACAAAGCCCAG
CD44	CD44-TM-for2	CACATATTGCTTCAATGCCTCAG
	CD44-TM-rev2	CCATCACGGTTGACAATAGTTATG
Cdh1	Cdh1-TM-for	GAGCGTGCCCCAGTATCG
	Cdh1-TM-rev	CGTAATCGAACACCAACAGAGAGT
Cel	Cel-TM-for	AAGTTGCCCGTGAAAAAGCAG
	Cel-TM-rev	ATGGTAGCAAATAGGTGGCCG
Cela1	Cela1-TM-for	CGTGGTTGCAGGCTATGACAT
	Cela1-TM-rev	TTGTTAGCCAGGATGGTTCCC
Cpa1	Cpa1-TM-for	TACACCCACAAAACGAATCGC
	Cpa1-TM-rev	GCCACGGTAAGTTTCTGAGCA
Ins1	Insulin1-TM-for	GAAGTGGAGGACCCACAAGTG
	Insulin1-TM-rev	CTGAAGGTCCCCGGGGCT
Ptf1a	Ptf1a-TM-for	ACAAGCCGCTAATGTGCGAGA
	Ptf1a-TM-rev	TTGGAGAGGCGCTTTTCGT

Gene	Name of primer	Sequence (5' – 3')
$p16^{INK4A}$	p16-TM-for	CCCAACGCCCCGAACT
	p16-TM-rev	GTGAACGTTGCCCATCATCA
$p19^{ARF}$	p19-TM-for	TCGCAGGTTCTTGGTCACTGT
	p19-TM-rev	GAACTTCACCAAGAAAACCCTCTCT
Rbpj	Rbpj-TM-for	GTGTTCCTCAGCAAGCGGATA
	Rbpj-TM-rev	TGCCACCTTCGTTCCTGA
Rbpjl	Rbpjl-TM-for	ATGCCAAGGTGGCTGAGAAAT
	Rbpjl-TM-rev	CTTGGTCTTGCATTGGCTTCA
Snail	Snail-TM-for3	GCCGGAAGCCCAACTATAGC
	Snail-TM-rev3	GGTCGTAGGGCTGCTGGAA

Table 2-13: Primers for embryonic stem cell clone screening.

Name of PCR	Name of primer	Sequence (5' – 3')
ES screen Snail	RosES UP2	GCTCCTCAGAGAGCCTCGGCTAGGTAG
	RosES LP2	ACCTCGAGGGTACCCGGTGAAGG

2.6 Cell culture

Table 2-14: Cell lines.

Cell line	Source
DF-1 chicken fibroblasts	American Type Culture Collection, Manassas, VA, USA
W4/129S6 embryonic stem ells	Taconic Farms, Inc., Hudson, NY, USA

Table 2-15: Reagents and kits for cell culture.

Reagent / kit	Source
Collagenase type 2	Worthington Biochemical Corporation, Lakewood, NJ, USA
Dulbecco's modified eagle medium (D-MEM) with L-glutamine	Invitrogen GmbH, Karlsruhe
Dulbecco's modified eagle medium (D-MEM) without L-glutamine (for ES cell medium)	Invitrogen GmbH, Karlsruhe
Dulbecco's phosphate buffered saline (PBS)	Invitrogen GmbH, Karlsruhe
ES-FCS (for ES cell medium)	Biochrom AG, Berlin
ESGRO® (LIF)	Millipore GmbH, Schwalbach am Taunus
Fetal bovine serum, South America (for DF-1 medium)	PAN-Biotech GmbH, Aidenbach

Reagent / kit	Source
Fetal calf serum (FCS)	Biochrom AG, Berlin
Fungizone® antimycotic	Invitrogen GmbH, Karlsruhe
G418, Geneticin®	Invitrogen GmbH, Karlsruhe
Gelatin	Sigma-Aldrich Chemie GmbH, Munich
Hygromycin	Merck KGaA, Darmstadt
L-Glutamine 200 mM	Invitrogen GmbH, Karlsruhe
MEM non essential amino acids	Invitrogen GmbH, Karlsruhe
Penicillin (10000 units/ml)-streptomycin (10000 µg/ml) solution	Invitrogen GmbH, Karlsruhe
Puromycin dihydrochloride	Sigma-Aldrich Chemie GmbH, Munich
Sodium pyruvate MEM	Invitrogen GmbH, Karlsruhe
SuperFect transfection reagent	Qiagen GmbH, Hilden
Trypsin, 0.05% with 0.53 mM EDTA 4Na	Invitrogen GmbH, Karlsruhe
Venor® *GeM* mycoplasma detection kit	Minerva Biolabs GmbH, Berlin

Table 2-16: Media for cell culture.

Medium	Components
DF-1 cell medium	D-MEM
	10% FCS (PAN-Biotech GmbH)
	1% Penicillin-streptomycin
	1% MEM non essential amino acids
MEF medium	D-MEM
	10% FCS (Biochrom AG)
	1% Penicillin-streptomycin
	1% L-Glutamine
Embryonic stem cell medium	D-MEM without glutamine
	15% ES-FCS
	1% Penicillin-streptomycin
	1% L-Glutamine
	1% Sodium pyruvate MEM
	1% MEM non essential amino acids
	0.1% 0.1 M 2-Mercaptoethanol
	1000 U/mL LIF
Tumor cell medium	D-MEM
	10% FCS (Biochrom AG)
	1% Penicillin-streptomycin

Medium	Components
Freezing medium	70% D-MEM
	20% FCS
	10% DMSO

2.7 Histology

Table 2-17: Reagents and kits for histological analysis.

Reagent / kit	Source
Acetic acid (glacial)	Merck KGaA, Darmstadt
Alcian blue 8GX	Sigma-Aldrich Chemie GmbH, Munich
Aluminium sulfate	Honeywell Specialty Chemicals Seelze GmbH, Seelze
Antigen unmasking solution, citric acid based	Vector Laboratories, Inc., Burlingame, CA, USA
Avidin/biotin blocking kit	Vector Laboratories, Inc., Burlingame, CA, USA
Certistain® Nuclear fast red	Merck KGaA, Darmstadt
DAB peroxidase substrate kit, 3,3'-diaminobenzidine	Vector Laboratories, Inc., Burlingame, CA, USA
Donkey serum D9663	Sigma-Aldrich Chemie GmbH, Munich
Eosine	Waldeck GmbH & Co KG, Münster
Goat serum G9023	Sigma-Aldrich Chemie GmbH, Munich
Hematoxylin	Merck KGaA, Darmstadt
Hydrogen peroxide 30%	Merck KGaA, Darmstadt
In situ cell death detection kit, POD	Roche Deutschland Holding GmbH, Grenzach-Wyhlen
Pertex mounting medium	Medite GmbH, Burgdorf
Rabbit serum R9133	Sigma-Aldrich Chemie GmbH, Munich
Roti® Histofix 4%	Carl Roth GmbH + Co. KG, Karlsruhe
Roti® Histol	Carl Roth GmbH + Co. KG, Karlsruhe
Senescence β-galactosidase staining kit	Cell Signaling Technology, Inc., Danvers, MA, USA
Sucrose (saccharose)	Merck KGaA, Darmstadt
TUNEL dilution buffer	Roche Deutschland Holding GmbH, Grenzach-Wyhlen
Vectashield® mounting medium with DAPI	Vector Laboratories, Inc., Burlingame, CA, USA
Vectastain® elite ABC kit	Vector Laboratories, Inc., Burlingame, CA, USA

Table 2-18: Buffers for histological analysis.

Buffer	Source
Alcian blue, pH 2.5	1% Alcian blue 3% Acetic acid
Nuclear fast red	0.1% Nuclear fast red 2.5% Aluminium sulphate

Table 2-19: Secondary antibodies for histological analysis.

Antibody	Source
Biotinylated anti-goat IgG (H+L)	Vector Laboratories, Inc., Burlingame, CA, USA
Biotinylated anti-mouse IgG (H+L)	Vector Laboratories, Inc., Burlingame, CA, USA
Biotinylated anti-rabbit IgG (H+L)	Vector Laboratories, Inc., Burlingame, CA, USA
Biotinylated anti-rat IgG (H+L)	Vector Laboratories, Inc., Burlingame, CA, USA

3 Methods

If not stated otherwise, all procedures were carried out according to manufacturer's protocol.

3.1 Molecular techniques

3.1.1 DNA analysis

3.1.1.1 Generation and transformation of competent bacteria

For the generation of KCM competent bacteria, the bacteria were first streaked on agar-plates for colony purification. A 5 ml overnight culture from an isolated colony was grown at 37°C in LB medium. 4 ml of this saturated culture were used to inoculate 250 ml of LB medium. These bacteria were grown for approximately 1–2 h until OD was 0.3–0.6 (early log phase) and placed on ice immediately. After centrifugation for 10 min at 1000 g and 4°C, the cells were resuspended in 25 ml cold TSB buffer, incubated on ice for 10 min, aliquoted and snap-frozen in liquid nitrogen. KCM competent bacteria were stored at -80°C until use.
Just before transformation, the bacteria were thawed on ice. 20 µl 5x KCM buffer and 200–500 ng of the DNA of interest were mixed and filled up with H_2O to 100 µl. This solution was added to 100 µl of the competent bacteria and kept at 4°C for 20 min. After a second incubation step at RT for 10 min, 1 ml S.O.C. medium was added and the bacteria were shaken horizontally for 1 h at 37°C (Top10) or for 2 h at 25°C (Stbl3). The bacteria were streaked in various amounts on agar plates supplied with the appropriate antibiotic (100 µg/ml) and incubated at 37°C or 25°C, respectively.

3.1.1.2 Isolation and cloning of plasmid DNA

Isolation of plasmid DNA. To isolate plasmid DNA, single colonies of bacteria transformed with the plasmid of interest (→ 3.1.1.1) were taken to inoculate 5 ml of selective LB medium. After shaking it at 37°C for 16 h (Top10) or 25°C for up to 36 h (Stbl3), the saturated culture (OD ca. 1) was used to carry out DNA preparation with the QIAprep® spin miniprep kit. When a higher amount of DNA was required, 50 ml of LB medium were inoculated to perform a preparation with the QIAfilter™ plasmid midi kit, or 250 ml LB medium for the use of the EndoFree® plasmid maxi kit, respectively. DNA concentration was measured with the spectrophotometer NanoDrop 1000. Glycerol stocks were produced by mixing freshly shaken bacteria and glycerol 1:1 and stored at -80°C.

Ethanol precipitation. For concentration and cleanup of isolated DNA, a 1/10 volume of sodium acetate (3 M, pH 5.2) was pipetted to the sample. Thereafter, a 2.5-fold volume of 100% ethanol, calculated after addition of sodium acetate, was added. After incubation for 2 h at -80°C, centrifugation at 13000 rpm for 30 min at 4°C was performed and the supernatant was discarded. The pellet was washed with 70% ethanol and dried for 10 min at room temperature. DNA was resolved in water and stored at -20°C.

Restriction digests were performed either for cloning or plasmid analysis. For cloning, generally 30 µg of plasmid DNA were digested in a mixture of 120 µl. After gel electrophoresis with an 0.8% agarose gel (→ 3.1.1.5) using GelStar® nucleic acid gel stain as a loading dye, DNA isolation was done with the QIAquick® gel extraction kit. If required, nucleotide overhangs were removed with the Quick Blunting™ kit. DNA ends of linearized vectors were dephosphorylated by rAPid alkaline phosphatase.

Ligation and screening. T4 DNA ligase was used to ligate generally 30 fM of the vector to 90 fM of the insert. The ligation product was transformed into bacteria (→ 3.1.1.1) and up to 48 single colonies were picked with an autoclaved toothpick and streaked out on a fresh agar plate. By touching the inside of a PCR reaction tube with the same toothpick, a sufficient amount of DNA was transferred. For heat denaturation of the bacteria, 50 µl of H_2O were added and the mixture was cooked at 95°C for 5 min. Analysis of every single clone was done by screening PCR (→ 3.1.1.4) on 5 µl of the denaturated bacteria using specific primers. Plasmid DNA from up to 6 colonies showing the correct band size was isolated (see above) and fragment size was validated by restriction digest and subsequent gel electrophoresis (→ 3.1.1.5) of ca. 1 µg DNA.

3.1.1.3 Isolation of genomic DNA

Generally, isolation of genomic DNA for subsequent PCR analysis (→ 3.1.1.4) was done by adding 50–100 µl of PCR lysis buffer (Soriano) to a piece of tissue (→ 3.3.4 , 3.3.5) or a cell pellet (→ 3.2.1). DNA lysis was performed in a thermocycler at 55°C for 1 h and 30 min. Proteinase K was inactivated for 15 min at 95°C. Thereafter, the tube was vortexed vigorously for 10 sec, the DNA-containing supernatant was separated from the debris by centrifugation at 13000 g and 4°C for 10 min and transferred into a new tube, which was stored at -20°C until use.

Embryonic stem cell DNA for PCR-based screening of 96-well plates (→ 3.1.1.4) was lysed in 20 µl PCR lysis buffer for 1 h at 55°C in a wet chamber. DNA was transferred into PCR reaction tubes and proteinase K was heat inactivated at 95°C for 10 min. DNA was stored at -20°C.

Genomic DNA from embryonic stem cells for subsequent Southern blot (→ 3.1.1.6) was harvested from 6-wells and lysed in 2 ml of ES cell lysis buffer overnight at 55°C in a wet chamber. 4 ml of 100% ethanol were added and this mixture was incubated overnight at RT. The third day, ethanol was removed and the DNA was washed 3 x with 70% ethanol. After drying at RT, DNA was dissolved in 100–200 µl H_2O and stored at 4°C.

3.1.1.4 Polymerase chain reaction

Polymerase chain reaction (PCR). Standard PCR for DNA analysis, genotyping and screening (Mullis *et al.*, 1986) was performed using the REDTaq® ReadyMix™ PCR reaction mix. 1.2 µl of genomic DNA (→ 3.1.1.3) or ca. 20 ng of plasmid DNA were applied. If necessary, DMSO was added to improve PCR output. Primer amounts were optimized depending on the PCR product. The standard PCR reaction setup and conditions can be seen in Table 3-1. PCR products were stored at 4°C or -20°C until further analysis by gel electrophoresis (→ 3.1.1.5).

Table 3-1: Reaction mix and conditions for standard PCR.

Reaction mix		Conditions		
12.5 µl	REDTaq® ReadyMix™	95°C	5 min	
0.5–1.2 µl	Forward primer (10 µM)	95°C	45 sec	
0.5–1.2 µl	Reverse primer (10 µM)	53°C–62°C	1 min	40x
1.2 µl	DNA	72°C	1 min, 30 sec	
ad 25 µl	H_2O	72°C	5 min	

Genotyping. To determine the genotype of mouse tissue or cells, PCRs with primers, which were designed individually for each genotype of interest (Table 2-10), were run on genomic DNA. Annealing temperatures and band sizes varied and are indicated in Table 3-2.

Table 3-2: Annealing temperatures and band sizes of genotyping PCR.
stop = mutated with translational stop element; rec = without translational stop element after recombination.

Name of PCR	Annealing	Wild type	Mutated
Ptf1a^{Cre}	60°C	600 bp	400 bp
LSL-Kras^{G12D}	55°C	270 bp	170 bp (stop); 300 bp (rec)
LSL-Trp53^{R172H}	60°C	270 bp	570 bp (stop); 600 bp (rec)
LSL-Rosa26$^{Tva\text{-}lacZ}$	62°C	600 bp	310 bp (*LSL-Rosa26*$^{Tva\text{-}lacZ}$); 410 bp (*LSL-Rosa26*^{Snail})
LSL-Rosa26$^{Tva\text{-}lacZ}$ *Stop*	53°C	no product	900 bp (rec)
LSL-Rosa26^{Snail}	60°C	no product	300 bp (stop); 590 bp (rec)

Name of PCR	Annealing	Wild type	Mutated
Ela1-Cre^{ERT2}	58°C	no product	410 bp
Cdkn2a^{lox}	58°C	140 bp	180 bp
*Ink**	60°C	600 bp	500 bp
Cdkn2a integrity	60°C	415 bp	no product (deletion)

PCR with proof-reading polymerase Pfu. To avoid errors that occur during PCR with standard Taq polymerase, the proof-reading polymerase Pfu was used for error-sensitive applications. The conditions can be found in Table 3-3.

Table 3-3: Reaction mix and conditions for PCR with proof-reading polymerase.

Reaction mix		Conditions		
5 µl	10x Pfu PCR buffer	95°C	3 min	
1 µl	dNTP mix, 10 mM each	95°C	30 sec	
2 µl	Forward primer (10 µM)	58°C	30 sec	18x
2 µl	Reverse primer (10 µM)	72°C	1 min 30 sec	
1.5 µl	PfuUltra™ high fidelity DNA polymerase	72°C	5 min	
1 µl	Plasmid (100 ng/µl)			
ad 50 µl	H_2O			

Screening PCR for embryonic stem cell clones. To check for correct homologous recombination of the targeting constructs, isolated genomic DNA from embryonic stem cell clones (→ 3.1.1.3) was used for screening PCR with HotStarTaq DNA as seen in Table 3-4. Clones with correct recombination showed a PCR product of 1230 bp.

Table 3-4: Reaction mix and conditions for ES cell screening PCR.

Reaction mix		Conditions		
11 µl	5x Q-solution	95°C	16 min	
5 µl	10x PCR buffer	95°C	40 sec	
2 µl	dNTP mix, 10 mM each	63°C	45 sec	45x
2 µl	Primer: RosES UP2 (10 µM)	65°C	4 min + 3 sec each cycle	
2 µl	Primer: RosES LP2 (10 µM)	65°C	10 min	
0.35 µl	HotStar Taq polymerase			
2 µl	DNA			
ad 50 µl	H_2O			

Sequencing. DNA sequencing was accomplished by GATC Biotech AG (Konstanz).

3.1.1.5 Gel electrophoresis

For analytical gel electrophoresis, 1x TAE buffer was used both in agarose gels and as running buffer. Depending on the band size, 1%–2% agarose gels were prepared. 24 µl of 1 mg/ml ethidium bromide were added. The amounts of loaded DNA depended on the experiment. For analysis, regularly 12 µl of DNA solution were loaded and, if necessary, Orange G was added as a loading dye. The gel was run generally at 110 V for 1 h and 30 min or until the bands had been separated sufficiently for subsequent analysis by UV transillumination.

3.1.1.6 Southern blot

The standard Southern blot protocol (Southern, 1975) was used to confirm correct integration of the sequence of interest into the genome of embryonic stem cells after homologous recombination. 50 µl of isolated genomic DNA (→ 3.1.1.3) from ES cell clones showing the correct band size in the screening PCR (→ 3.1.1.4) as well as DNA from wild type ES cells were digested for 24 h with EcoRV and additional RNaseA (12 µg/ml). As 5' probe, pBroad3, digested with NotI (330 bp), was used.

Gel electrophoresis. The restriction digests, as well as 1 kb DNA extension ladder, were loaded on a 1% agarose gel with BBXF agarose gel loading dye. pBroad, digested with SacI and StuI, was used as positive control. Gel electrophoresis was run for 14 h at 40 V. As length reference, a part of the gel containing digested wild type DNA and 1 kb extension ladder was stained in ethidium bromide, aligned to a ruler and photographed under UV illumination.

Blotting. Using a vacuum blotting system, the DNA was transferred onto a Hybond-N+ membrane. To improve transfer efficiency, the gel was depurinated for 60–75 min by incubation in 0.25 M HCl following denaturation in 0.4 M NaOH. After blotting for 4 h at 55 mbar, the membrane was incubated shortly in 2x SSC buffer and then baked at 80°C for 2 h to fix the DNA.

Prehybridization of the membrane was done in a roller bottle for 2 h at 65°C. 0.1 ml Amersham Rapid-hyb™ buffer were used per 1 cm^2 membrane.

Probe labeling. By use of Amersham Rediprime™ II DNA labeling system, 25 ng of the probe was labeled with deoxycytidine 5'-triphosphate, [alpha-32P] during prehybridization. Purification of the labeled probe was carried out with Amersham micro columns Illustra ProbeQuant™ G-50. Incorporation was measured with a liquid scintillation counter.

Hybridization. The freshly labeled probe was denaturated for 5 min at 95°C and cooled for 5 min on ice before mixing them with pre-warmed Amersham Rapid-hyb™ buffer. Probe

hybridization was done at 65°C overnight with gentle agitation. Stringency washing of the membranes was carried out at 65°C (Table 3-5). Ultimately, the membrane was exposed to Kodak® BioMax™ MS film.

Table 3-5: Stringency washing of membranes after hybridization with radioactively labeled probes.

Probe	Buffer	Duration	Repeats
	2x SSC / 0.1% SDS	20 min	1
5' probe	1x SSC / 0.1% SDS	60 min	2
	0.1x SSC / 0.1% SDS	60 min	1

3.1.1.7 Cloning strategies

3.1.1.7.1 pRosa26-LSL-Snail

A conditional Snail expression mouse model was generated by inserting a loxP-Stop-loxP (LSL) silenced Snail expression cassette into the ubiquitously active *Rosa26* locus. The generated targeting vector contained as basic elements a loxP-flanked stop cassette, the *Snail* full length cDNA and 2 homology regions of the *Rosa26* locus.

Initially, the transcriptional region of the *Snail* cDNA (Table 2-8) was amplified by PCR using PfuUltra™ high fidelity DNA polymerase (→ 3.1.1.4) The primers Snail1-ATG-AatII-for and Snail1-Stop-NdeI-rev that included both AatII and NdeI restriction sites, as well as the *Snail* stop codon, were employed. The PCR product was cloned into the pCR®-Blunt II-TOPO® vector by using the Zero Blunt® TOPO® PCR cloning kit. After restriction digest with AatII and NdeI, the *Snail* cDNA was ligated (→ 3.1.1.2) to a modified pENTR™/D-TOPO® vector (pENTR™-LSL-MCS-pA) carrying a loxP-flanked stop cassette 5' to the Snail insertion side. By using the Gateway® LR Clonase™ enzyme mix, the LSL-Snail cassette of the resulting plasmid was cloned into the pRosa26-Att-CCDB-Att vector to get the final targeting construct pRosa26-LSL-Snail. Preparation was performed using the EndoFree® plasmid maxi kit, before the plasmid was ethanol precipitated (→ 3.1.1.2) and linerarized with the single cutter PacI to be introduced into embryonic stem cells (→ 3.2.2.3).

3.1.1.7.2 RCASBP(A)-Att-Snail-Att

The transcriptional region of the *Snail* cDNA (Table 2-8) was amplified and cloned into the pCR®-Blunt II-TOPO® vector. After restriction digest with AatII and NdeI, the *Snail* cDNA was ligated (→ 3.1.1.2) to a modified pENTR™/D-TOPO® vector (pENTR™-MCS-EF1a-dsRed),

carrying the red fluorescing protein dsRed under control of the *EF1α* promoter 3' to the *Snail* insertion side. Further cloning into RCASBP(A)-Att-CCDB-Att was performed using the Gateway® LR Clonase™ mix to acquire the final targeting construct RCASBP(A)-Att-Snail-Att for transduction of cells (→ 3.2.1.2).

3.1.2 RNA analysis

3.1.2.1 RNA isolation and cDNA synthesis

RNA isolation from tissue and cells. A piece of tissue (→ 3.3.5) with 2 mm diameter was put into 1 ml of RLT buffer containing 10 µl 2-mercaptoethanol, quickly homogenized using SilentCrusher M, immediately snap-frozen in liquid nitrogen and kept at -80°C until use. For extraction of RNA from cells (→ 3.2.1), they were cultured in plates with 10 cm diameter until ca. 80% confluency was reached. Medium was aspirated and 600 µl of RLT buffer containing 6 µl 2-mercaptoethanol were added to the plate, the lysate was collected with a scraper and kept at -80°C until use. For RNA isolation, QIAshredder columns and the RNeasy mini kit were employed. DNA was digested using the RNase-free DNase set. RNA concentration was measured with the spectrophotometer NanoDrop 1000. Samples were stored at -80°C.
cDNA synthesis was carried out with the TaqMan® reverse transcription reagents. 1 µg of mRNA was used for generation of 50 µl cDNA, which was stored at -20°C.

3.1.2.2 Quantitative real time PCR

Primer design. Primers for quantitative real time PCR (qPCR) were generated using Primer3 software (Rozen and Skaletsky, 2000) with DNA sequences acquired at www.ensembl.org. Melting temperature optimum was 60°C and length of the amplicons was 50–150 bp. The binding sites of forward and reverse primer were always separated by an intron to avoid unwanted amplification of genomic DNA.
Quantitative real time PCR was performed with the StepOnePlus™ real time PCR system. As fluorescent DNA binding dye, QuantiFast® SYBR® green PCR master mix was used in a 25 µl mixture. 300 nM both forward and reverse primer were added. mRNA expression was analyzed on 5 µl of 1:5 in TE buffer diluted cDNA in either duplicate or triplicate. All mRNA expression values were normalized to the housekeeping gene Cyclophilin (CypA). A melt curve was always performed after the run to check for unwanted primer dimerization. Data analysis was done with StepOne™ software (Applied Biosystems, Inc., Carlsbad, CA, USA) and Excel (Microsoft Corporation, Redmont, WA, USA). Either a standard curve was included into the run, or subsequent analysis was carried out according to $2^{-\Delta\Delta Ct}$ method (see below).

Primer efficiency test. To test whether the primers were efficient enough to use the $2^{-\Delta\Delta Ct}$ method, a dilution series of a mixture of cDNA was generated. Pure cDNA (20 ng/µl) of up to 10 cell lines and tissue samples was mixed and diluted 6 x 1:5 in TE buffer. A qPCR was performed on the resulting 6 samples and the primers of interest. The slope of the standard curve given by StepOne™ software was used to calculate the efficiency:

$$10^{\frac{-1}{\text{slope}}} = \text{primer efficiency}$$

Ideally, the efficiency of a primer pair should be 2.0 (Mukhopadhyay *et al.*, 2008).

$2^{-\Delta\Delta Ct}$ analysis method. If primer efficiency was between 1.8 and 2.2, the $2^{-\Delta\Delta Ct}$ method (Pfaffl, 2001) was applied for relative mRNA expression analysis, otherwise, a standard curve was used. Calculation was performed as follows:

$$C_t[\text{gene of interest}] - C_t[\text{control}] = \Delta C_t$$

$$\Delta C_t[\text{treated sample}] - \Delta C_t[\text{reference sample}] = \Delta\Delta C_t$$

$2^{-\Delta\Delta Ct}$ was used for further data analysis and demonstration.

Cloning of standard curves. If the efficiently was not sufficient or if exact quantification of the absolute amounts of mRNA within a special sample was required, a standard curve with samples containing known copy numbers was included into the run. Therefore, a standard PCR (→ 3.1.1.4) using both qPCR primers for the gene of interest was run on 5 µl cDNA and the generated PCR product was checked for specificity and size by gel electrophoresis (→ 3.1.1.5). Correct PCR products were cloned into pCR®II-Topo® vector by use of the Topo® TA cloning® kit. The integration of the PCR product into the vector was tested by screening PCR. Plasmid DNA of confirmed clones was isolated using the QIAprep® spin miniprep kit (→ 3.1.1.2 , 3.1.1.4).

The number of molecules per µl was calculated as follows:

$$\text{plasmid concentration } \frac{\text{g}}{\mu\text{l}} \cdot \frac{6.022 \cdot 10^{23} \frac{\text{molecules}}{\text{mol}}}{\text{bp plasmid} \cdot 660 \frac{\text{g}}{\text{mol}}} = \frac{\text{molecules}}{\mu\text{l}}$$

Serial dilutions in TE buffer were prepared from the isolated plasmid DNA according to Table 3-6. 5 µl of 5 standards for each gene of interest were included into every run, the used dilutions were determined by particular mRNA expression level.

Table 3-6: Standard curve dilution for quantitative real time PCR.

Name	Molecules per µl	Molecules per 5 µl
S I	$1 \cdot 10^9$	$5 \cdot 10^9$
S II	$1 \cdot 10^8$	$5 \cdot 10^8$
S III	$1 \cdot 10^7$	$5 \cdot 10^7$

Name	Molecules per µl	Molecules per 5 µl
S IV	$1 \cdot 10^6$	$5 \cdot 10^6$
S V	$1.5 \cdot 10^5$	$7.5 \cdot 10^5$
S VI	$3 \cdot 10^4$	$1.5 \cdot 10^5$
S VII	6000	$3 \cdot 10^4$
S VIII	1200	6000
S IX	240	1200
S X	48	240
S XI	9.6	48

3.1.2.3 Microarrays

To determine and compare gene signatures and underlying signaling pathways, whole genome expression analysis of murine pancreatic tumor cells and tissue was performed. mRNA was extracted as described in 3.1.2.1 . Quality was checked by use of Experion™ RNA StdSens analysis kit.

Cells. For cell mRNA analysis, 250 ng of each sample without any degradation or salt contamination were taken for further processing with the GeneChip® 3' IVT express kit. Fragmentation and hybridization of the resulting aRNA to GeneChip® mouse genome 430 2.0 array chips was performed by the team of PD Dr. Reinhard Hoffmann (Institute for Medical Microbiology, Immunology and Hygiene, Technical University of Munich).

Tissue samples. To analyze mRNA expression of pancreatic tissue samples, 500 ng of isolated mRNA were processed with the Ambion® WT expression kit. Purified single-stranded cDNA was fragmented and labeled by using the GeneChip® WT terminal labeling kit. Hybridization to GeneChip® mouse gene 1.0 ST array chips was carried out by the team of Prof. Thorsten Buch (Institute for Medical Microbiology, Immunology and Hygiene, Technical University of Munich).

3.1.3 Protein analysis

3.1.3.1 Protein isolation and quantification

Whole cell lysates. Cells were cultured (→ 3.2.1) in plates of 10 cm diameter until they reached confluency of 80%. Medium was aspirated and the plates were washed with PBS. Instantly, 200 µl of chilled IP buffer containing phosphatase and protease inhibitors were given onto the plate. Cells were harvested on ice with a cell scraper and immediately snap-frozen in liquid nitrogen. The lysate was stored at -80°C. Before use, it was centrifuged for 20

min at 13200 rpm and 4°C and the supernatant was transferred into a new reaction tube.

Protein concentration determination. Protein concentration was measured by Bradford assay (Bradford, 1976). Therefore, Bradford reagent was diluted 1:5 and 300 µl were placed into a 96 well of a microplate. 1 µl of the sample of interest was added. Measurement was carried out in triplicate. After 10 min of incubation, absorbance was measured at 600 nm with the microplate reader Anthos 2001 and protein concentration was calculated using a defined BSA dilution series as reference. Subsequently, protein concentration of all samples was adjusted to one level by adding IP buffer and protein loading buffer (Laemmli, 1970). After denaturation for 5 min at 95°C, the samples were stored at -20°C.

3.1.3.2 Western blot

Sodium dodecyl sulfate polyacrylamide gel electrophoresis (SDS-PAGE). Standard SDS-PAGE (Laemmli, 1970) using a gel containing a 10% to 20% linear gradient was performed to separate the proteins by size. At first, every reagent for the 3 gels except TEMED was mixed according to Table 3-7. Then TEMED was added to both separating gels for polymerization. Quickly, 2.9 ml of the heavy separating gel and then an equal amount of the light separating gel were aspirated with the same serological pipette, following an air bubble to let the gradient develop. After pouring into a gel caster, the gel was covered with a layer of 2-propanol and allowed to polymerize. Next, TEMED was added to the stacking gel mixture and it was poured as well. After polymerization, up to 100 µg of the protein extract (→ 3.1.3.1) were loaded onto the gel. Protein separation was carried out at 80–300 V for 1–4 h in running buffer with additional cooling, depending on the molecular weight of the proteins of interest.

Table 3-7: SDS gradient gel electrophoresis of proteins.

Stacking gel		**Heavy separating gel**		**Light separating gel**	
2250 µl	H_2O	400 µl	Glycerol	1641 µ	H_2O
975 µl	Stacking gel buffer	1000 µl	Separating gel buffer	1000 µl	Separating gel buffer
563 µl	Rotiphorese® gel 30	2540 µl	Rotiphorese® gel 30	1326 µl	Rotiphorese® gel 30
37.5 µl	10% SDS	40 µl	10% SDS	40 µl	10% SDS
18.75 µl	APS	20 µl	APS	20 µl	APS
7.5 µl	TEMED	2 µl	TEMED	2 µl	TEMED

Blotting and immunodetection. The proteins were blotted onto a PVDF membrane, which was activated in methanol before (Immobilon-P). Standard wet blot was performed for 1–2 h at 100 V or overnight at 30 V in transfer buffer (Towbin *et al.*, 1979). After blotting, the

membrane was incubated for 30 min in blocking solution (TBS, containing 0.1% Tween® 20 and 5% non-fat dry milk or BSA) to block unspecific antibody binding. Next, incubation with the primary antibody was carried out by gently shaking overnight at 4°C. Antibodies for immunodetection were generally diluted 1:1000 in blocking solution. Subsequently, the membrane was washed 3 x for 10 min in TBS containing 0.1% Tween® and incubated with gentle agitation in the dark for 1 h with 1:10000 diluted secondary antibody. After another 3 washing steps, the membrane was scanned at 700 nm or 800 nm wavelength using Odyssey® infrared imaging system. Loading control was performed generally with β-actin or α-tubulin.

3.2 Cell culture

All cell culture experiments were carried out within biological safety cabinets under sterile conditions. Cells were cultivated in corresponding media according to Table 2-16 at 37°C and 5% CO_2.

3.2.1 Tumor cells

3.2.1.1 Isolation and handling of pancreatic tumor cells

Isolation. All conditions were kept as sterile as possible. During mouse dissection (→ 3.3.5), a piece of the tumor with 1–2 mm diameter was cut out and put into sterile PBS. Under a biological safety cabinet, it was separated into small pieces with a scalpel and solved in 5 ml tumor cell medium supplied with 3.9 mg collagenase type 2. After incubation at 37°C for 24–48 h it was centrifuged for 5 min at 1200 rpm, supernatant was aspirated and the pellet was resolved in 5 ml tumor cell medium for further culturing.

Culturing and passaging. Cells were supplied with fresh pre-warmed tumor cell medium and passaged regularly. To subculture them, cells were washed with PBS, trypsinized at 37°C until they dissociated and put into a new vessel with fresh medium. Cell number and vessel type depended on experimental conditions.

Cell counting was conducted using a Neubauer hemocytometer.

Cryopreservation. Trypsinized cells were taken up in fresh medium and centrifuged at 1200 rpm for 5 min. The pellet was dissolved in ice-cold freezing medium, transferred to CryoPure tubes, frozen at -80°C for 24 h and subsequently processed to liquid nitrogen, where the cells were stored until further use.

3.2.1.2 Transduction of cells via the RCAS-Tva system

The RCAS (replication-competent avian sarcoma-leukosis virus long terminal repeat with a splice acceptor)-Tva (tumor virus A) system (Hughes *et al.*, 1987) was applied to overexpress genes of interest in murine tumor cell lines containing the Tva receptor by retroviral transduction. At first, the chicken fibroblast cell line DF-1 was transfected with 2.5 µg of the purified RCAS plasmid DNA containing the cDNA of the gene of interest and a reporter gene, e.g. eGFP. Superfect was used as transfection reagent. DF-1 cells were generally cultured at 39°C in DF-1 cell medium. The successfully transfected cells released virus particles that led to subsequent infection of further cells. Fresh virus-containing supernatant was filtered through 0.45 µm pores and added to the medium of murine tumor cells carrying the Tva receptor (*Rosa26*$^{Tva\text{-}LacZ}$, → 3.3.1) for transduction with the gene of interest. In these cells, no infectious virus is replicated. Transduction with fresh supernatant was repeated daily until 80% of the cells showed eGFP fluorescence. All cells were cryopreserved (→ 3.2.1.1) until further use.

3.2.2 Embryonic stem cell culture

3.2.2.1 Generation of the *LSL-Rosa26*$^{Snail/+}$ mouse line

During this study, a mouse line was generated: *LSL-Rosa26*$^{Snail/+}$. Therefore, a targeting construct was cloned as described in 3.1.1.7.1 . This construct was inserted into embryonic stem cells by electroporation (→ 3.2.2.3) to undergo homologous recombination with the embryonic stem cell DNA. Positive clones were cryopreserved and sent to PolyGene AG (Switzerland) for blastocyst injection and subsequent generation of germline chimeras. Chimeras were bred with C57BL/6J females to get heterozygous *LSL-Rosa26*$^{Snail/+}$ progeny on a mixed 129S6;C57BL/6J genetic background.

3.2.2.2 Culture conditions, passaging and cryopreservation

Culture conditions and passaging. W4/129S6 embryonic stem (ES) cells were grown in daily renewed ES cell medium on a monolayer of mitotically inactivated mouse embryonic fibroblasts (MEFs). Inactivation of the MEFs was accomplished by irradiation with 34 gray. Generally, MEFs were cultured in MEF medium on plates coated with 0.1% gelatin. They were seeded the day before thawing of ES cells. ES cells were passaged regularly (→ 3.2.1.1) before they reached confluency to keep them in undifferentiated state.

Cryopreservation. Trypsinized ES cells were centrifuged at 1200 rpm for 5 min at RT, supernatant was discarded and the pellet was resuspended in ES cell medium containing

10% DMSO. The suspension was transferred into CryoPure tubes, put into a precooled freezing container filled with 2-propanol and slowly cooled down to -80°C for 24 h. The tubes were processed to liquid nitrogen where they were stored until further use.

3.2.2.3 Transfection and subsequent handling of embryonic stem cells

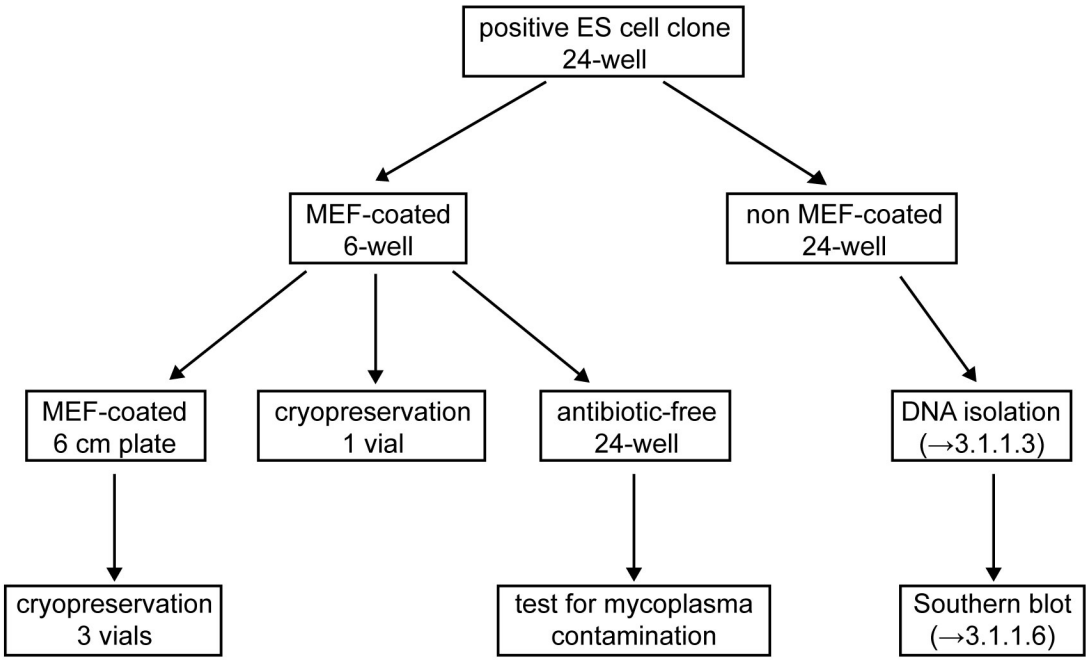

Figure 3-1: Culture procedure for positive ES cell clones.

$1 \cdot 10^7$ trypsinized ES cells were resuspended in 750 µl ice-cold PBS, transferred to a pre-cooled electroporation cuvette and mixed with 25 µg of the linearized targeting construct (→ 3.1.1.7.1). Electroporation was carried out at 250 V and 500 µF using the electroporation system Gene Pulser® II. Thereafter, the electroporated cells were added to 50 ml of pre-warmed ES cell medium and pipetted onto plates covered with MEFs. As wild type control for later analysis, a residue of non-electroporated ES cells was seeded onto a gelatin-coated 6-well plate.

20 h after electroporation, ES cell medium was replaced by selective ES cell medium supplied with 250 µg/ml Geneticin® to select for cell clones that contain a neomycin cassette providing resistance to Geneticin®. Medium was changed daily for 7 days. Single clones were picked into MEF-covered 24-well plates for further culturing as well as into 96-well plates for genomic DNA extraction (→ 3.1.1.3) and subsequent PCR screening (→ 3.1.1.4). Positive clones were passaged according to Figure 3-1 and cryopreserved as described in 3.2.2.2 .

3.3 Mouse experiments

All animal studies were conducted meeting the requirements of the European guidelines for the care and use of laboratory animals and were approved by the local authorities.

3.3.1 Mouse strains and breeding

The Cre-loxP system (Orban *et al.*, 1992) was applied for both tissue-specific overexpression of genes and expression of mutated alleles. Therefore, a mouse strain expressing a Cre recombinase under the control of a tissue-specific promoter was interbred with a mouse line that carries the transgene or the mutated allele silenced by a translational stop element flanked by loxP sites (LSL) (Hingorani *et al.*, 2003). Recombination of the loxP sites by the Cre recombinase resulted in a deletion of the stop cassette and tissue-specific expression of the gene of interest in the offspring.

***Ptf1a*$^{Cre/+}$ (Nakhai *et al.*, 2007).** This knock-in mouse strain was kindly provided by Dr. Hassan Nakhai (Klinikum rechts der Isar, Technical University of Munich). *Ptf1a*$^{Cre/+}$ mice express Cre recombinase under control of the *Ptf1a* promoter that is specifically expressed in pancreatic precursor cells as well as in adult exocrine and endocrine pancreas. Expression was also observed in retinal neurons, cerebellum and neural tube.

***Ela1-Cre*^{ERT2} *(Stanger et al., 2005)*.** This transgenic mouse strain was kindly provided by Prof. Doug Melton (Harvard Medical School, Boston, MA, USA). The transgene insert is constructed of a Cre recombinase which is fused to a mutant form of the human estrogen receptor ligand binding domain. Upon tamoxifen induction, *Ela1-Cre*^{ERT2} mice express Cre recombinase under control of the *rat elastase 1* (*Ela1*) promoter, which is specifically expressed in acinar cells of the pancreas.

***LSL-Kras*$^{G12D/+}$ (Hingorani *et al.*, 2003; Jackson *et al.*, 2001)**. This knock-in mouse strain was kindly provided by Prof. Tyler Jacks (Massachusetts Institute of Technology, Cambridge, MA, USA). *LSL-Kras*$^{G12D/+}$ mice carry a mutation in codon 12 that is frequently found in human pancreatic ductal adenocarcinoma. After deletion of the loxP-flanked stop cassette, this mutation impairs the GTPase activity of Kras which leads to constitutive activity of Ras signaling pathways.

***LSL-Trp53*$^{R172H/+}$ (Hingorani *et al.*, 2005; Olive *et al.*, 2004)**. This knock-in mouse strain was kindly provided by Prof. Tyler Jacks (Massachusetts Institute of Technology, Cambridge, MA, USA). *LSL-Trp53*$^{R172H/+}$ mice carry a missense mutation in codon 172 of endogenous *Trp53*, which is often observed in patients with Li-Fraumeni syndrome as well as in spontaneous human tumors. After deletion of the loxP-flanked stop cassette, this mutation leads to expression of dominant-negative oncogenic Trp53 (Liu *et al.*, 2000; de Vries *et al.*, 2002).

***LSL-Rosa26$^{Tva\text{-}lacZ/+}$* (Seidler *et al.*, 2008).** The mouse strain was generated in PD Dr. Dieter Saur's group (Klinikum rechts der Isar, Technical University of Munich). Here, the *Rosa26* locus is targeted to get Cre-loxP-based conditional expression of tumor virus A (Tva) receptor as well as nuclear lacZ (β-galactosidase). Due to the Tva receptor, which is normally expressed endogenously in avian cells, these mice and isolated tumor cells from these animals can be transduced with the gene of interest by the RCAS-Tva system (→ 3.2.1.2 ; Hughes *et al.*, 1987).

***Ink4a$^{*/+}$* (Krimpenfort *et al.*, 2001).** This knock-out mouse strain was kindly provided by Prof. Anton Berns (The Netherlands Cancer Institute, Amsterdam, The Netherlands). A TGG to TAG nonsense mutation was introduced into codon 101 of exon 2 of the *Cdkn2a* gene, leading to ubiquitous destabilization of the mutated p16^{INK4A} protein. The mutation does not have any effect on p19^{ARF} expression.

***Cdkn2a$^{lox/+}$* (Aguirre *et al.*, 2003).** This knock-out mouse strain was kindly provided by Prof. Nabeel Berdeesy (Harvard Medical School, Boston, MA, USA). The murine *Cdkn2a* locus codes for the tumor suppressors p16^{INK4A} and p19^{ARF} by alternative usage of the first exon and alternative reading frames (Krimpenfort *et al.*, 2001). In this mouse line, exon 2 and 3 are flanked with loxP sites, permitting conditional deletion of both p16^{INK4A} and p19^{ARF} at the same time.

3.3.2 Control animals

If not stated otherwise, wild type, *LSL-Rosa26$^{Snail/+}$*, *LSL-Rosa26$^{Tva\text{-}lacZ/+}$* or *Ptf1a$^{Cre/+}$* mice were used as control animals.

Table 3-8: Nomenclature of mouse strains.

Complete genotype	Abbreviation
Ptf1a$^{Cre/+}$;LSL-Rosa26$^{Snail/+}$	*Snail$^{KI/+}$*
Ptf1a$^{Cre/+}$;LSL-Rosa26$^{Snail/Snail}$	*Snail$^{KI/KI}$*
Ptf1a$^{Cre/+}$;LSL-Rosa26$^{Snail/+}$;LSL-Trp53$^{R172H/+}$	*Snail$^{KI/+}$;p53$^{mut/+}$*
Ptf1a$^{Cre/+}$;LSL-Rosa26$^{Snail/Snail}$;LSL-Trp53$^{R172H/+}$	*Snail$^{KI/KI}$;p53$^{mut/+}$*
Ptf1a$^{Cre/+}$;LSL-Kras$^{G12D/+}$	*Kras*
Ptf1a$^{Cre/+}$;LSL-Kras$^{G12D/+}$;LSL-Rosa26$^{Snail/+}$	*Kras;Snail$^{KI/+}$*
Ptf1a$^{Cre/+}$;LSL-Kras$^{G12D/+}$;LSL-Rosa26$^{Snail/Snail}$	*Kras;Snail$^{KI/KI}$*
Ptf1a$^{Cre/+}$;LSL-Kras$^{G12D/+}$;LSL-Rosa26$^{Snail/+}$;Ink4a$^{*/+}$	*Kras;Snail$^{KI/+}$;Ink$^{*/+}$*
Ptf1a$^{Cre/+}$;LSL-Kras$^{G12D/+}$;LSL-Rosa26$^{Snail/+}$;Cdkn2a$^{lox/+}$	*Kras;Snail$^{KI/+}$;Cdkn2a$^{lox/+}$*
Ela1-Cre^{ERT2};LSL-Kras$^{G12D/+}$	*Kras^{Ac}*
Ela1-Cre^{ERT2};LSL-Kras$^{G12D/+}$;LSL-Rosa26$^{Snail/Snail}$	*Kras^{Ac};Snail$^{Ac/Ac}$*

3.3.3 Mouse nomenclature

For better readability of the text, mouse genotypes in the results and discussion parts were abbreviated as listed in Table 3-8.

3.3.4 Genotyping

At the age of 2–3 weeks, a ca. 1 mm long piece of tail was cut off the previously anesthetized mouse with a sterile scalpel. The wound was disinfected with a silver nitrate applicator. For later identification, every mouse got explicit earmarks representing a number code. DNA for genotyping was extracted from the tails as described in 3.1.1.3 .

3.3.5 Mouse dissection

All instruments and general conditions were kept as sterile as possible. 2 h before sacrification, 5 mg/kg 5-bromo-2'-deoxyuridine (BrdU), dissolved in sterile PBS, was injected intraperitoneally for subsequent proliferation assays. Prior to dissection, the mouse was euthanasized with isoflurane, fixed and disinfected with 70% ethanol. The abdomen was cut open and samples of approximately 1–2 mm diameter were removed from the pancreas for following RNA and protein isolation (→ 3.1.2.1 , 3.1.3.1) as well as samples for subsequent DNA isolation (→ 3.1.1.3) and cryosectioning (→ 3.4.1). If the mouse developed any pancreatic tumor, measurements were taken. Pancreas, spleen, stomach, intestine, liver, lung, heart and kidneys were fixed overnight in 4% Roti® Histofix to be processed to histological analysis (→ 3.4).

3.4 Histological analysis

3.4.1 Tissue fixation, sectioning and documentation

Paraffin sections. Tissue from mouse dissection (→ 3.3.5) was fixed in 4% Roti® Histofix for 16 h, dehydrated by use of tissue processor ASP300, embedded in paraffin and stored at RT until further use. For subsequent staining, series of 3 µm thick sections were cut using the microtome Microm HM355S.

Cryosections. A tissue sample from mouse dissection (→ 3.3.5) was fixed in 4% Roti® Histofix for 2 h, dehydrated in a sucrose series (15% sucrose for 4 h and 30% sucrose overnight), embedded in Tissue-Tek® O.C.T.™ compound and stored long term at -80°C. 6 µm thick sections for staining were cut with the cryostat Microm HM 560 and stored at -20°C until further use.

Documentation. Slides were photographed using the microscope Axio Imager.A1 with AxioCam HRc and software AxioVision 4.8 (Carl Zeiss AG, Oberkochen). Generally, representative images were shown in the results part. Scale bars generally indicate 50 µm.

3.4.2 Hematoxylin and eosin (H&E) staining of tissue sections

Paraffin-embedded sections were dewaxed and rehydrated for 5 min in Roti® Histol and a decreasing ethanol series (2 x 99%, 2 x 96% and 2 x 80%). Then slides were stained in hematoxylin for 5 sec and in eosin for 20 sec. Next, the sections were dehydrated in an increasing ethanol series (2 x 80%, 2 x 96% and 2 x 99%) and incubated in Roti® Histol for 5 min before mounting with Pertex mounting medium.

3.4.3 Alcian blue staining

Paraffin-embedded sections were dewaxed and rehydrated (→ 3.4.2). Then slides were stained in alcian blue solution for 5 min and washed in water. Counterstaining was performed in nuclear fast red solution for 5 min and slides were rehydrated and mounted as described in 3.4.2 .

3.4.4 Immunohistochemistry

Paraffin-embedded sections were dewaxed and rehydrated as described in 3.4.2 . Antigen retrieval was generally performed in a microwave at 360 W for 10 min using citric acid based antigen unmasking solution. Slides were left at RT for at least 30 min and washed with H_2O. Next, endogenous peroxidase activity was inhibited by incubation of the slides in 3% H_2O_2 for 10 min. They were washed with H_2O and blocked for 1 h at RT with 5% serum in PBS before primary antibody incubation overnight at 4°C. The primary antibody was diluted in blocking solution at dilution ranges from 1:50 to 1:500. The avidin/biotin blocking kit was generally applied.

After a washing step with PBS, slides were incubated in biotinylated secondary antibody, which was diluted in blocking solution 1:500, for 1 h at RT. Slides were washed again with PBS. Detection was performed using Vectastain® elite ABC kit and DAB peroxidase substrate kit. Finally, slides were counterstained with hematoxylin, dehydrated and mounted as described in 3.4.2 .

3.4.5 Immunocytochemistry

Cells were grown as described in 3.2.1.1 . They were washed 3 x in cold PBS and fixated 10 min in cold methanol. Washing was repeated and cells were permeabilized in 0.3% Triton® X-

100 in PBS for 10 min. Blocking was done for 30 min at 37°C with 5% serum before incubation with the primary antibody for 2 h at 37°C. After washing 3 x with PBS, cells were incubated with the secondary antibody at 1:400 dilution for 30 min at 37°C. Washing was repeated and cells were covered with a cover glass using Vectashield® mounting medium with DAPI.

3.5 Statistical analysis

General statistics. Graphical depiction, data correlation and statistical analysis were conducted with GraphPad Prism 5 (La Jolla, CA, USA). If not stated otherwise, data were obtained from at least 3 independent experiments and are presented as arithmetic mean ± standard deviation (SD) or standard error of the mean (SEM). Cell culture-based assays were performed in triplicate. To calculate statistical differences between certain data sets, two-tailed Student's t test was employed and resulting p-values are indicated in the respective figures. The significance level was set to 0.05. If more than 1 statistical test was performed simultaneously on a single data set, a Bonferroni-adjusted significance level was calculated to account for the increased possibility of false-positive results. For survival analysis, Kaplan-Meier estimator was applied. Log rank test was used for statistical analysis of survival curves.

Microarray analysis. Analysis of raw data was performed using R and Bioconductor (Gentleman *et al.*, 2004) by the teams of PD Dr. Reinhard Hoffmann and Prof. Thorsten Buch (Institute for Medical Microbiology, Immunology and Hygiene, Technical University of Munich). Arrays were assessed for quality and normalized using the robust multi-array average (RMA) approach. Principal component analysis and heat map generation were done by Philipp Eser (Gene Center, Ludwig Maximilian University of Munich).

Gene set enrichment analysis. To test for enriched gene sets in a mRNA expression profile, gene set enrichment analysis (GSEA) was conducted (Subramanian *et al.*, 2005). GSEA software was provided by the Broad Institute (http://www.broadinstitute.org, Massachusetts Institute of Technology, Cambridge, MA, USA). Gene sets were obtained from the Molecular Signatures Database v3.1. Following GSEA parameters were used: permutation type: gene set, permutation number: 1000, metric for ranking genes: Signal2Noise, enrichment statistic: weighted, gene set size restrictions: minimum 15 / maximum 500. The enrichment score (ES) marks the degree of which a gene set of interest is enriched at the bottom or top of a ranked list of genes. The ES is calculated by walking down the list of genes. When a gene is present in the gene set, a running-sum statistic is increased, when the gene is not present, it is decreased. The final ES is the maximum

deviation of zero found by walking the list of genes. A positive ES marks the enrichment of the gene set of interest, whereas a negative ES means that the gene set is underrepresented. The normalized ES (NES) is used to compare results across different gene sets. It is calculated by dividing the ES by the mean of all permutations of the dataset. Statistical significance of the ES was determined by using the nominal (NOM) p-value. Because significance of the results can be influenced by multiple testing, the false discovery rate (FDR) was further used to calculate the estimated probability that a false-positive result was obtained (Benjamini and Hochberg, 1995). The cutoff for a significant FDR q-value as well as NOM p-value was set at 0.05.

4 Results

4.1 Generation of the *LSL-Rosa26*$^{Snail/+}$ mouse line

In this study, a conditional mouse line was created that is able to express Snail in any cell type after Cre recombinase-mediated removal of a loxP-flanked transcriptional and translational stop element (loxP-stop-loxP, LSL, Seidler *et al.*, 2008) that silences the Snail transgene. To create this mouse strain, the ubiquitously expressed *Rosa26* locus was targeted by homologous recombination in embryonic stem (ES) cells (Soriano, 1999). The

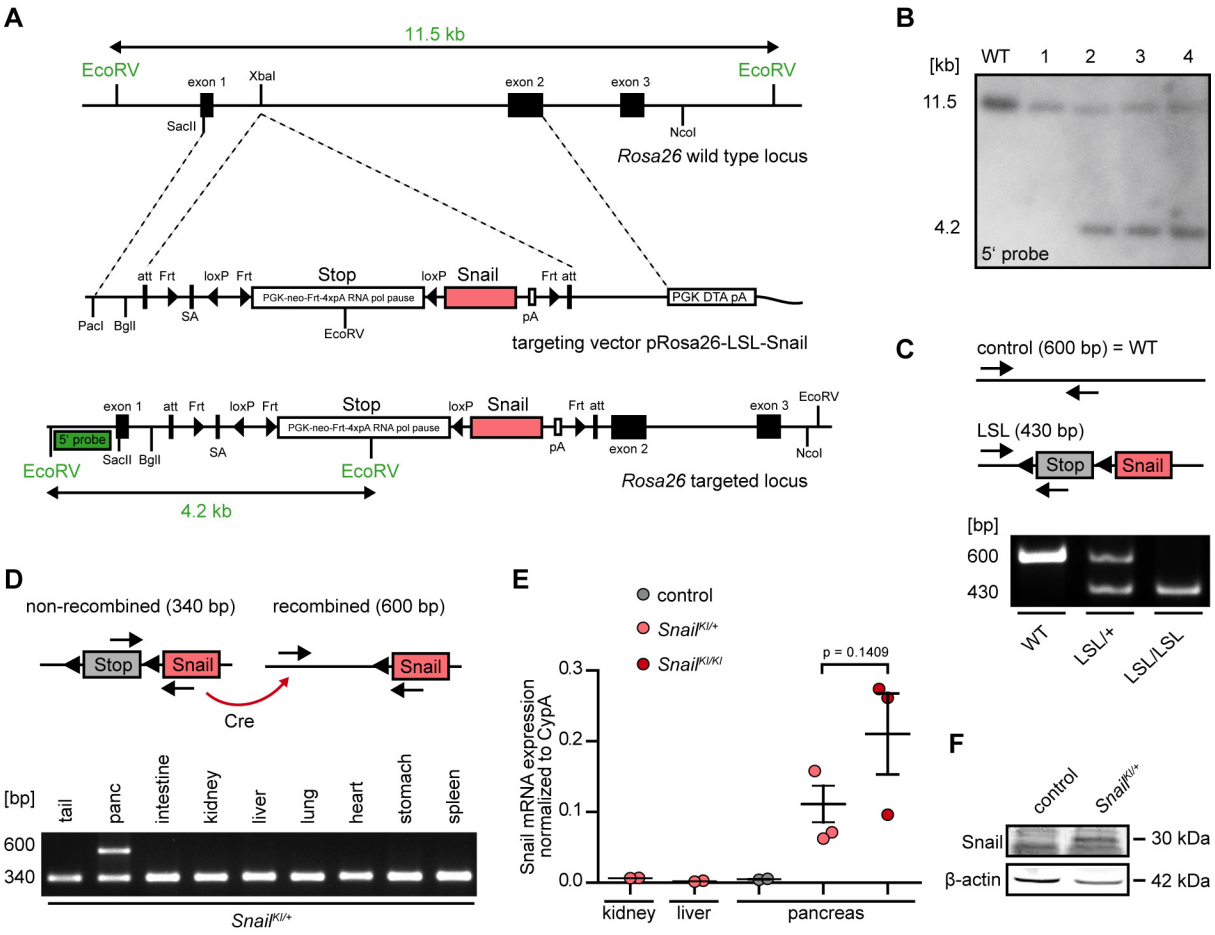

Figure 4-1: Targeting of a loxP-stop-loxP-silenced Snail cassette to the murine *Rosa26* locus.
A) From top to bottom: *Rosa26* wild type locus, the targeting vector pRosa26-LSL-Snail and the targeted *Rosa26* locus. The targeting vector consists of 2 homological regions of the *Rosa26* locus, a splice acceptor (SA), a loxP-flanked transcriptional and translational stop element and a Snail expression cassette. Restriction sites, location of the 5' probe, and sizes of DNA fragments are indicated. **B)** Southern blot analysis of DNA from wild type (WT) and targeted ES cells (1–4) after EcoRV digestion. The 11.5 kb band is expected for the WT allele, the 4.2 kb band represents the mutant allele. **C)** PCR analysis of DNA from wild type (WT), heterozygous (LSL/+), and homozygous (LSL/LSL) *Rosa26*^{Snail} mice with retained stop element. **D)** Recombination scheme and PCR analysis DNA from different tissues of *Snail*$^{KI/+}$ mice after Cre-mediated recombination. **E)** qPCR analysis of total Snail mRNA expression in pancreas, liver, and kidney of 1-month-old mice. mRNA expression levels were normalized to CypA. Data are mean ± SEM, indicated p-value by t-test. **F)** Western blot analysis of total Snail protein expression in pancreatic tissue of 1-month-old mice of indicated genotypes.

targeting vector pRosa26-LSL-Snail (Figure 4-1A) was electroporated into W4/129S6 ES cells. 120 geneticin-resistant colonies were picked and checked by screening PCR (data not shown). The resulting 8 positive clones were further checked by Southern blot. Finally, 3 clones remained that had undergone correct homologous recombination (Figure 4-1B). Clone 3 was sent to PolyGene AG (Switzerland) for blastocyst injection and subsequent generation of germline chimeras. These were bred with C57BL/6J females to get heterozygous *LSL-Rosa26*$^{Snail/+}$ progeny on a mixed 129S6;C57BL/6J genetic background. Both heterozygous *LSL-Rosa26*$^{Snail/+}$ and homozygous *LSL-Rosa26*$^{Snail/Snail}$ mice did not show any abnormalities, were viable, fertile and had normal lifespan (data not shown). By PCR analysis of tail DNA, the genotype of the progeny could be clearly determined (Figure 4-1C).

4.2 Snail is expressed in the pancreas of *Snail*$^{KI/+}$ mice

In order to investigate the effect of ectopic Snail expression in the pancreas *in vivo*, *LSL-Rosa26*$^{Snail/+}$ mice were bred with the pancreas-specific Cre driver line *Ptf1a*$^{Cre/+}$ (*Ptf1a*$^{Cre/+}$*; LSL-Rosa26*$^{Snail/+}$, hereafter referred to as *Snail*$^{KI/+}$ mice). In *Ptf1a*$^{Cre/+}$ mice, the Cre recombinase under the control of the *Ptf1a* promoter is expressed in precursors of acini, ductal cells, and islets from 9.5 d.p.c. on (Kawaguchi *et al.*, 2002) as well as in retinal neurons, dorsal neural tube, and cerebellum (Nakhai *et al.*, 2007). Cre recombinase-mediated excision of the LSL element in the adult pancreas was verified by PCR analysis of *Snail*$^{KI/+}$ mice, but not in tail, intestine, kidney, liver, lung, heart, stomach, and spleen (Figure 4-1D). qPCR analysis showed increased Snail mRNA expression levels in the pancreas, but not in liver and kidney of 1-month-old *Snail*$^{KI/+}$ mice. Expressing Snail from both alleles of the *Rosa26* locus in *Snail*$^{KI/KI}$ mice resulted in further increase of pancreatic Snail mRNA expression, although a high variance between individuals was observed. As expected, control mice without Cre recombinase did not exhibit any increase of Snail mRNA expression (Figure 4-1E). This could be confirmed on protein level (Figure 4-1F).

4.3 Expression of high gene doses of Snail in the pancreas leads to dramatic growth retardation

Whereas *Snail*$^{KI/+}$ mice exhibited a normal phenotype with no obvious alterations of appearance, increased Snail gene dose in *Snail*$^{KI/KI}$ mice led to dramatic growth retardation and severely reduced body weight. *Snail*$^{KI/KI}$ mice were born with no obvious weight reduction compared to their littermates (data not shown), but shortly after birth a strong growth retardation was observed that went along with a significantly reduced body weight. This phenotype was more severe in male mice than in females (Figure 4-2A and B).

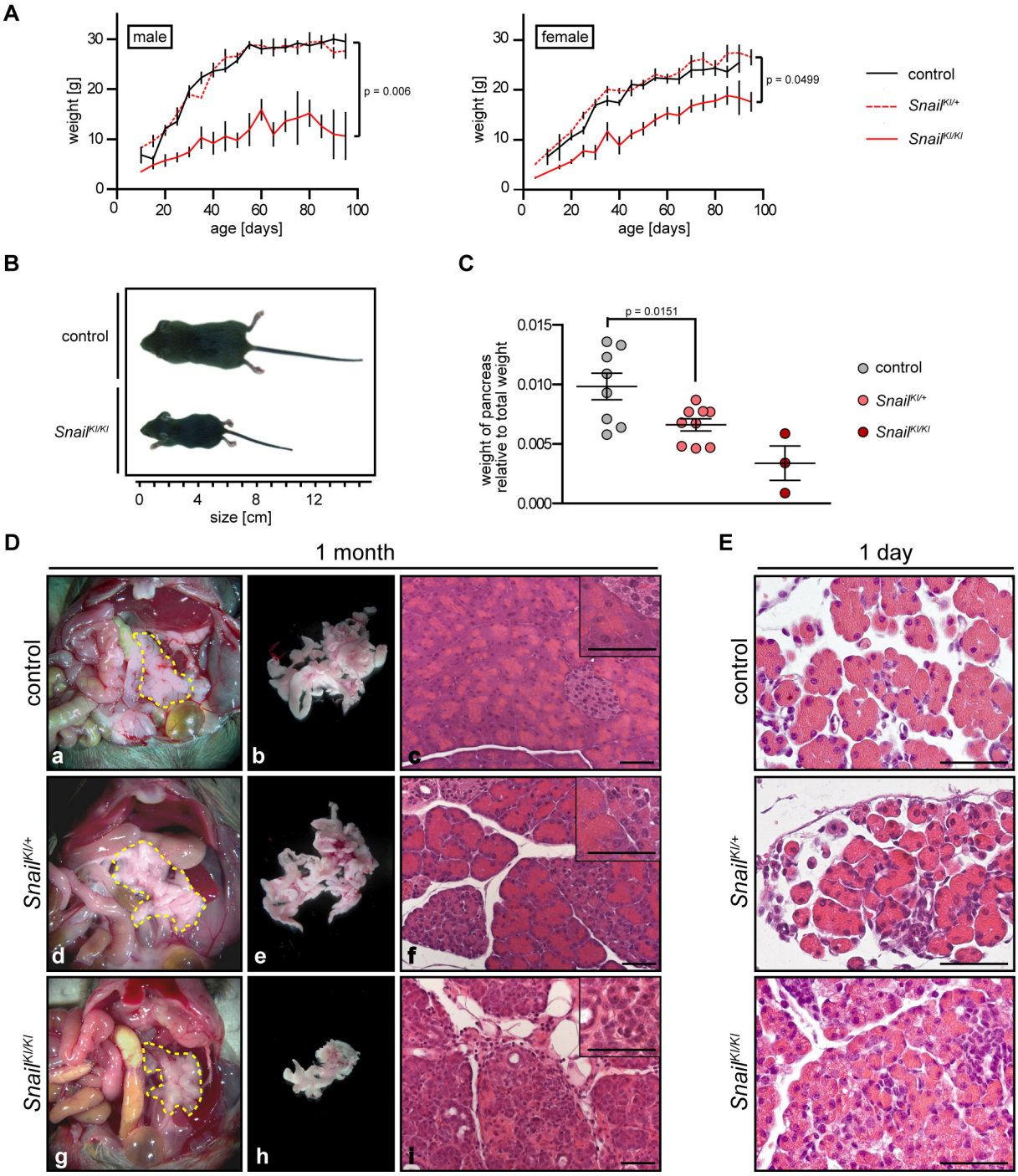

Figure 4-2: Growth retardation and reduced body weight in *Snail*$^{KI/KI}$ mice.
A) Weight analysis of male and female *Snail*$^{KI/KI}$ mice (n = 6) in comparison with *Snail*$^{KI/+}$ (n = 6) and control mice (n = 6) until the age of 3 months. Data are mean ± SEM, indicated p-values by t test. **B)** Photographic documentation of appearance of 1-month-old *Snail*$^{KI/KI}$ mice. **C)** Pancreas weight in relation to total body weight of 1-month-old mice of indicated genotypes. Data are mean ± SEM, indicated p-value by t test. **D)** Gross picture of sacrificed mice with indicated pancreas (a,d,g), detailed view of the excised pancreas (b,e,h) and H&E staining of paraffin sections of the pancreas (c,f,i) in 1-month-old mice with indicated genotypes. **E)** H&E staining of paraffin sections of the pancreas of 1-day-old mice with indicated genotypes. Scale bars represent 50 µm.

Comparing the pancreata of 1-month-old *Snail*$^{KI/+}$ mice and control mice on macroscopical level did not reveal any obvious differences. Nevertheless, pancreata of *Snail*$^{KI/+}$ mice had a

significantly lower weight than control organs (Figure 4-2C). Concerning the macroscopical appearance of pancreata of *Snail*$^{KI/KI}$ mice it was observed that in general they looked smaller and often granulomatous and fatty. Also, the pancreas weight in relation to total weight was significantly lower than in control mice (Figure 4-2C and D). Whereas most acinar cells of *Snail*$^{KI/+}$ mice were regular regarding histological appearance, focal parts of the pancreas contained dedifferentiated acinar cells that never appeared in control animals (Figure 4-2D). *Snail*$^{KI/KI}$ mice exhibited an even more severe phenotype with a totally disorganized pancreas and abnormal acinar cells. In general, the acinar cells of 1-month-old *Snail*$^{KI/KI}$ mice had nuclei of regular appearance, but were of reduced size and contained less amount of cytoplasm (Figure 4-2D). To a lesser extend, these histological alterations could be already observed in 1-day-old mice (Figure 4-2E).

4.4 Overexpression of Snail in the pancreas induces dedifferentiation of acinar cells

To confirm dedifferentiation of acinar cells in *Snail*$^{KI/+}$ and *Snail*$^{KI/KI}$ mice on molecular level, expression levels of several acinar and pancreatic differentiation markers were examined in detail. Immunohistochemical analysis of pancreata of Snail-expressing mice showed an obviously reduced expression level of the adult acinar marker alpha-amylase 1 (Amy1) in acinar cells. Cells expressing the ductal marker cytokeratin 19 (Krt19) were present in all genotypes (Figure 4-3A).

Microarray analysis of pancreatic tissue of 1-month-old *Snail*$^{KI/+}$ mice and control cohorts further revealed the downregulation of various markers for acinar differentiation (Figure 4-3B), which was confirmed by qPCR (Figure 4-3C). Although the number of analyzed animals was too small for statistical analysis, a tendency could be observed in most of the tested pancreatic differentiation markers. Concerning the adult pancreatic transcription factor 1 (PTF1) complex, Ptf1a and recombination signal binding protein for immunoglobulin kappa J region-like (Rbpjl) mRNA levels were reduced to less than 50% of initial expression levels in *Snail*$^{KI/+}$ mice. Increasing Snail gene dose led to even further reduction to approximately 20%. However, recombination signal binding protein for immunoglobulin kappa J region (Rbpj), which is part of the embryonic PTF1 complex, was not markedly altered. Coding transcript levels of digestive enzymes like alpha amylase 1 (Amy1), carboxypeptidase A1 (Cpa1), carboxyl ester lipase (Cel), and chymotrypsin-like elastase family, member 1 (Cela1) were all downregulated to less than 50% in *Snail*$^{KI/+}$ mice, although the levels varied strongly. In comparison, *Snail*$^{KI/KI}$ mice hardly expressed any of these enzymes, mRNA levels all being less than 5% of the initial levels. The ductal marker cytokeratin 19 (Krt19) was slightly

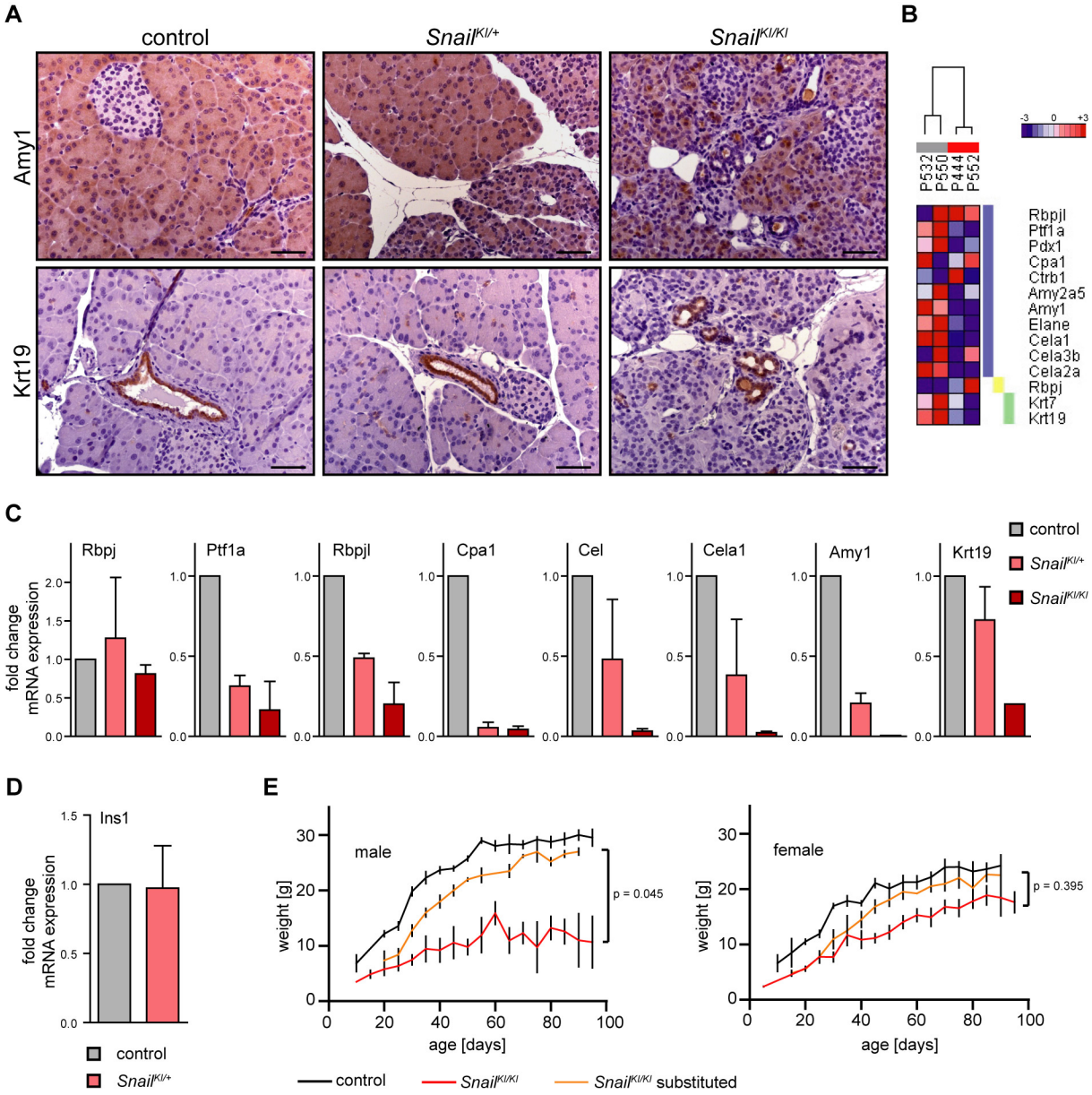

Figure 4-3: Snail expression in the pancreas leads to acinar dedifferentiation.
A) Amy1 and Krt19 immunohistochemical staining of pancreatic tissue from 1-month-old mice of indicated genotypes. Scale bars represent 50 µm. **B)** mRNA was isolated from pancreatic tissue of 1-month-old *Snail*$^{KI/+}$ and control mice (n = 2), labeled, and hybridized onto GeneChip mouse gene 1.0 ST array. Heat map of indicated pancreatic differentiation markers. Horizontal bars: gray, control mice; red, *Snail*$^{KI/+}$ mice. Vertical bars: blue, adult marker; yellow, embryonic marker; green, ductal marker. **C)** Quantitative mRNA expression of the pancreatic differentiation markers Rbpj, Ptf1a, Rbpjl, Cpa1, Cel, Cela1, Amy1, and Krt19. Total mRNA was prepared from pancreatic tissue of 1-month-old *Snail*$^{KI/+}$ mice (n = 3), *Snail*$^{KI/KI}$ mice (n = 2), and control cohorts (n = 3). **D)** Quantitative Ins1 mRNA expression in pancreatic tissue of 1-month-old *Snail*$^{KI/+}$ and control mice (n = 3). mRNA expression levels were normalized to CypA. Data are mean ± SD. **E)** *Snail*$^{KI/KI}$ mice (n = 6) were substituted with pancreatic enzymes. Their weight was monitored until the age of 3 months and compared with untreated *Snail*$^{KI/KI}$ mice (n = 6) as well as control cohorts (n = 6). Data are mean ± SEM, indicated p-values by t test.

reduced in *Snail*$^{KI/+}$ mice to approximately 70%. Stronger reduction to 20% was observed in *Snail*$^{KI/KI}$ animals (Figure 4-3C).

In order to reveal any possible dysfunctions of the endocrine department caused by Snail

expression, insulin 1 (Ins1) mRNA levels of 1-month-old Snail-expressing mice were compared with those of control mice, showing no difference between the mouse cohorts (Figure 4-3D).

To evaluate whether growth retardation in *Snail*$^{KI/KI}$ mice was due to exocrine pancreatic insufficiency, mice were substituted with a diet containing all essential pancreatic enzymes beginning at the age of 1 month. Monitoring body weight of male mice until the age of 3 months revealed a significant difference compared to untreated mice. Females also exhibited a slight gain of weight and thereby nearly reached the weight of control cohorts, although the change was not significant (Figure 4-3E).

In summary, these data show that aberrantly increased Snail expression in the pancreas leads to overt morphological alterations and loss of pancreatic differentiation markers in acinar cells. This results in reduced body weight due to exocrine pancreatic insufficiency.

4.5 Snail expression induces a stem cell-like signature

Snail is involved in embryogenesis, a process which has been associated with the participation of stem cells (Mani *et al.*, 2008; Barrallo-Gimeno and Nieto, 2005). CD44 is a cell-surface protein that is generally observed in stem cells and has been widely used as a stem cell marker (Mani *et al.*, 2008). Indeed, mRNA levels of CD44 were increased 1.8-fold in 1-month-old *Snail*$^{KI/+}$ mice and 2.7-fold in *Snail*$^{KI/KI}$ mice when compared with control cohorts (Figure 4-4A). To verify this, Gene set enrichment analysis (GSEA) was performed using mRNA gene expression profiles of pancreatic tissue of 1-month-old mice. GSEA showed a significantly enriched expression of embryonic stem cell core genes (Wong *et al.*, 2008) in 1-month-old pancreata of *Snail*$^{KI/+}$ mice (Figure 4-4B). Due to the low number of

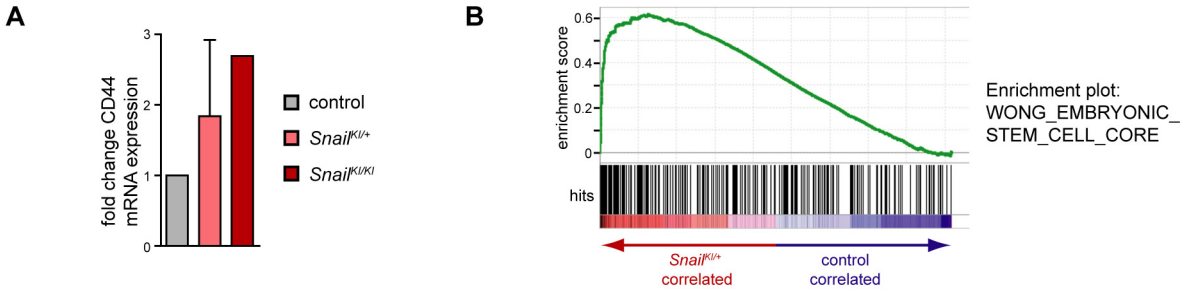

Figure 4-4: Snail induces a stem cell-like signature.
A) Quantitative mRNA expression of the stem cell marker CD44. Total mRNA was prepared from pancreatic tissue of 1-month-old *Snail*$^{KI/+}$ (n = 3), *Snail*$^{KI/KI}$ mice (n = 1), and control cohorts (n = 3). mRNA expression levels were quantified by qPCR and normalized to CypA. Data are mean ± SD. **B)** GSEA using mRNA profiles (GeneChip mouse gene 1.0 ST array) showed significant enrichment of embryonic stem cell core genes in *Snail*$^{KI/+}$ (red, n = 2) vs. control pancreata (blue, n = 2) from 1-month-old mice. Genes were ranked using Signal-to-Noise ratio statistics according to their correlation with indicated genotypes. Vertical black lines mark the position of each gene in the data set. The green curve represents the ES (enrichment score), which is the running sum of the weighted ES calculated by GSEA software. Normalized enrichment score (NES): 2.54; False discovery rate q-value (FDR q) < 0.001; nominal p-value (NOM p) < 0.001.

mice, the changes in CD44 mRNA level were not significant, although a clear tendency could be shown. In summary, Snail expression in the pancreas leads at least in part to induction of a stem cell-like signature.

4.6 Pancreatic Snail expression leads to development of metastatic acinar cell carcinoma

In a cohort of longitudinally monitored animals with pancreas-specific Snail expression, metastatic acinar cell carcinoma (ACC) development was observed at advanced age in 55% of *Snail*$^{KI/+}$ mice (n = 11) and in 94% of *Snail*$^{KI/KI}$ animals (n = 17). This resulted in a shortened median survival of 14.5 months in *Snail*$^{KI/+}$ mice compared to 24 months in control mice. Increasing Snail gene dose in *Snail*$^{KI/KI}$ animals led to significant reduction of the median survival to 10 months. Expression of Snail in combination with the established mutant gain-of-function Trp53 model (Olive *et al.*, 2004, *LSL-Trp53*$^{R172H/+}$, hereafter called *p53*$^{mut/+}$) in *Snail*$^{KI/+}$*;p53*$^{mut/+}$ mice significantly accelerated tumor progression with a median survival of 7 months, which was even shorter with 5 months in *Snail*$^{KI/KI}$*;p53*$^{mut/+}$ mice (Figure 4-5A).

22 tumor-bearing mice (*Snail*$^{KI/+}$, n = 6; *Snail*$^{KI/KI}$, n = 16) were further investigated. They generally developed 1 or multiple large, hemorrhagic masses in the pancreatic region, which were soft and capsular (Figure 4-5B). These characteristics also have been observed in human ACC (Klimstra, 2007). Blood-filled cystic tumor parts were exhibited by 45% of mice. 32% of tumors showed invasion into adjacent organs like the duodenum or the peritoneum (data not shown). In 27%, the mesenterial lymph nodes were enlarged due to metastasis (Figure 4-5D, upper panel). In 9% of animals, macroscopic lung metastases were observed and 36% of mice developed macroscopic liver metastasis (Figure 4-5D, middle panel and data not shown).

The histopathological features of the tumors resembled ACC of the pancreas with dysplastic acini of variable cell sizes, growth patterns, and grades of differentiation, respectively. The tumors were characterized by a high neoplastic cellularity and a lack of fibrous stroma, although frequently cell clusters were separated by stroma-rich areas. The nuclei were relatively uniform with only moderate variation in size and shape, generally containing 1 large single nucleolus, which is also characteristic for ACC (Klimstra, 2007, Figure 4-5C). In some areas, fat vacuoles could be noticed. Acinar origin of the tumor cells was confirmed by immunohistochemical staining for amylase, which showed heterogeneous expression levels that were generally of lower intensity than in control tissue and sometimes absent (data not shown). Both macroscopic and microscopic liver and lung metastasis were seen in *Snail*$^{KI/+}$ (25% liver, 25% lung) and in *Snail*$^{KI/KI}$ (27% liver, 18% lung) mice, respectively (Figure 4-5D,

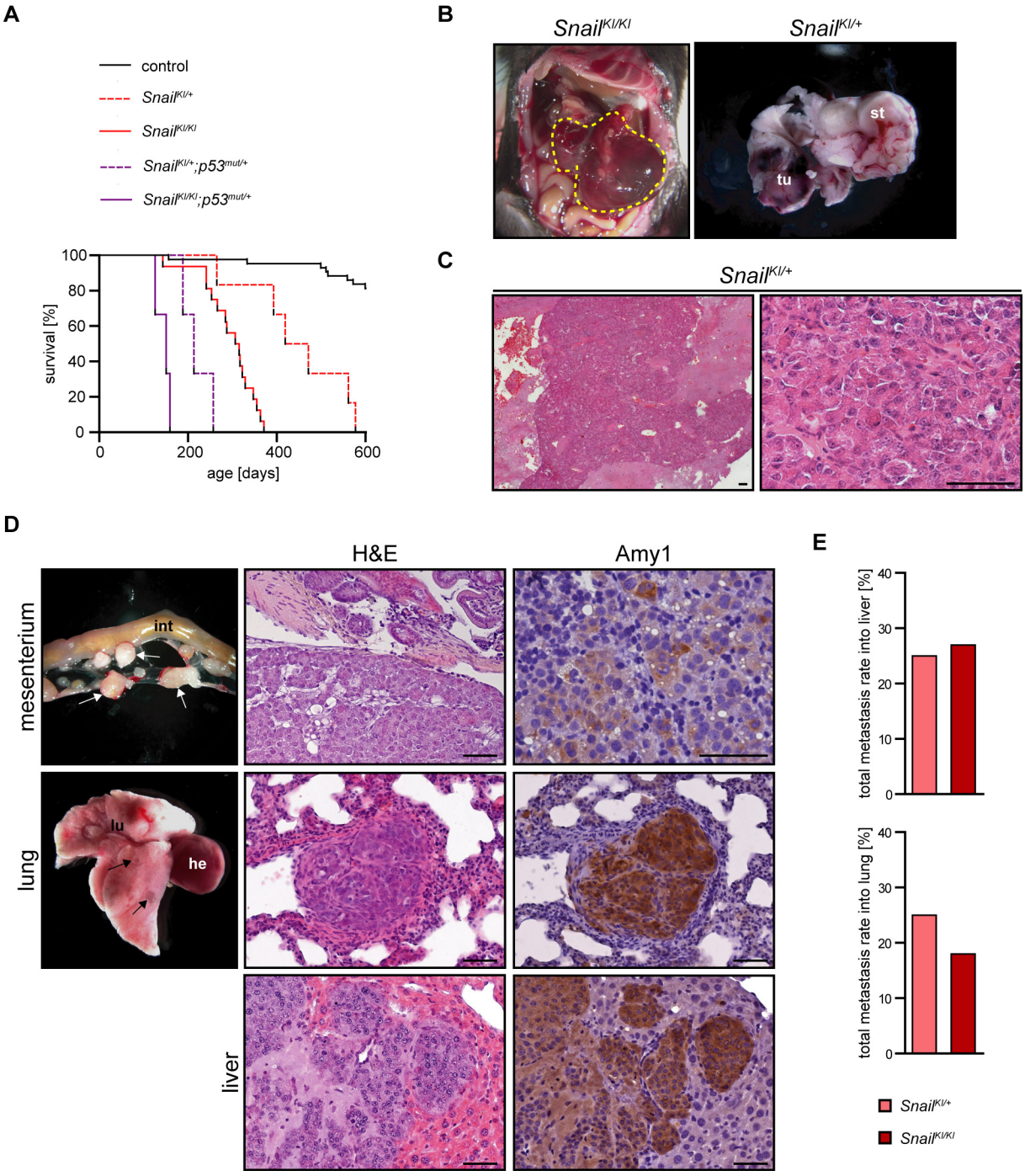

Figure 4-5: Snail-expressing mice develop metastatic acinar cell carcinoma.
A) Kaplan-Meier survival curves show a significantly decreased median survival of *Snail*$^{KI/+}$ mice (n = 6; 445 d), compared with wild type animals (n = 43; 731 d; p < 0.0001; log rank test). Increasing gene dose in *Snail*$^{KI/KI}$ mice further decreased the median survival when compared with *Snail*$^{KI/+}$ mice (n = 17; 310.5 d; p = 0.0011; log rank test). Inactivation of Trp53 accelerated tumor development and led to a further reduced median survival in *Snail*$^{KI/+}$;*p53*$^{mut/+}$ mice when compared with *Snail*$^{KI/+}$ animals (n = 3; 213 d; p = 0.0018; log rank test) and *Snail*$^{KI/KI}$;*p53*$^{mut/+}$ animals when compared with *Snail*$^{KI/KI}$ mice (n = 3; 151 d; p < 0.0001; log rank test). **B)** Macroscopic view of ACC arising in a *Snail*$^{KI/KI}$ mouse and of the excised tumor in a *Snail*$^{KI/+}$ mouse (tu, tumor; st, stomach). **C)** H&E-stained paraffin sections of ACC in *Snail*$^{KI/+}$ mice. **D)** Macroscopic pictures of metastases (left panel, indicated by arrows) in the mesenterium (int, intestine), and lung (lu, lung; he, heart) of *Snail*$^{KI/KI}$ mice. H&E (middle panel) and Amy1 (right panel) staining of metastases in the mesenterium, lung and liver of *Snail*$^{KI/KI}$ mice. Scale bars represent 50 µm. **E)** Metastasis rate to liver and lung of *Snail*$^{KI/+}$ (n = 4) and *Snail*$^{KI/KI}$ mice (n = 11) with ACC.

left and middle, Figure 4-5E). These metastatic cells strongly resembled the primary tumors. Affiliation to the acinar compartment was further supported by positive immunohistochemical amylase staining (Figure 4-5D, right).

Collectively, these data show that Snail alone has the capability to cause *in vivo* development of metastatic ACC when it is overexpressed in the pancreas.

4.7 Snail accelerates progression of Kras^{G12D}-induced pancreatic ductal adenocarcinoma

To analyze the role of Snail in PDAC initiation, development, and metastasis, the well-established Kras^{G12D}-dependent mouse model, which recapitulates the entire spectrum of pancreatic carcinogenesis (Hingorani *et al.*, 2003), was used in this study (*Ptf1a$^{Cre/+}$;LSL-Kras$^{G12D/+}$*, referred to as *Kras* mice). The *LSL-Rosa26$^{Snail/+}$* line was crossed into this model to characterize the resulting *Ptf1a$^{Cre/+}$;LSL-Kras$^{G12D/+}$;LSL-Rosa26$^{Snail/+}$* animals (referred to as *Kras;Snail$^{KI/+}$* mice).

Snail mRNA and protein levels in *Kras;Snail$^{KI/+}$* animals were markedly increased compared to *Kras* and control mice at the age of 1 month (Figure 4-6A and B). At this point, *Kras* animals have a low number of neoplastic lesions and morphologically resemble control mice. Animals were longitudinally monitored and sacrificed either when they showed signs of disease or at defined age for postmortal analysis. The mice developed invasive and metastatic PDAC with complete penetrance. Median survival of *Kras;Snail$^{KI/+}$* animals was dramatically shortened to 6 months compared to 15 months in *Kras* mice. Increasing Snail gene dose by biallelic expression in *Kras;Snail$^{KI/KI}$* mice led to further acceleration of PDAC formation and a drastically reduced median survival of 2 months (Figure 4-6C).

By histology, compound mutant *Kras;Snail$^{KI/+}$* mice exhibited pancreatic ductal lesions (PanINs) of all grades, which resembled the PanINs in *Kras* mice (Figure 4-6D and F). Characteristic elongation of the normal duct cells as well as mucin accumulation, which was proofed by Alcian blue staining, were observed, going along with loss of polarity, atypical nuclei and budding into the lumen in high-grade PanINs (Figure 4-6F).

1-month-old *Kras;Snail$^{KI/+}$* mice displayed a significantly increased acinar-to-ductal metaplasia (ADM) rate (1.73 lesions/field) in comparison to *Kras* compound mutant mice (0.85 lesions/field). Further, Snail expression led to PanIN progression, as *Kras;Snail$^{KI/+}$* mice exhibited slightly more PanIN1A (0.49 lesions/field) and significantly more PanIN1B (0.31 lesions/field) than *Kras* animals (PanIN1A, 0.41 lesions/field; PanIN1B, 0.04 lesions/field). In contrast to *Kras* cohorts, *Kras;Snail$^{KI/+}$* mice also showed high-grade PanINs (PanIN2, 0.37 lesions/field; PanIN3, 0.62 lesions/field; Figure 4-6E and F).

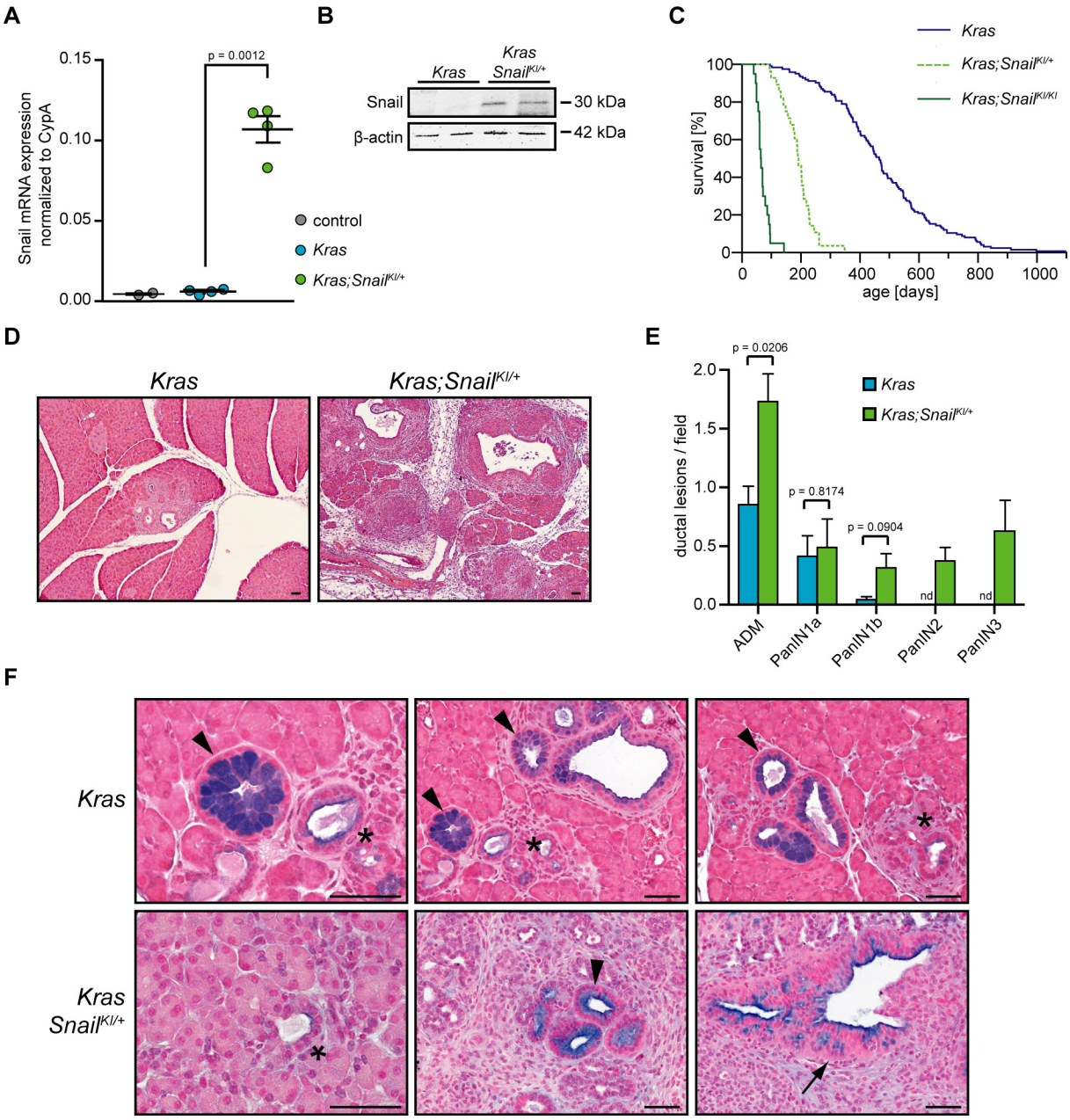

Figure 4-6: Snail in cooperation with Kras^{G12D} accelerates PanIN progression and PDAC development.
A) qPCR analysis of total Snail mRNA expression in the pancreas of 1-month-old *Kras;Snail*$^{KI/+}$ mice compared to *Kras* and control cohorts. Data are mean ± SEM, indicated p-value by t test. **B)** Western blot analysis of total Snail protein expression in pancreatic tissue of 1-month-old mice. **C)** Kaplan-Meier survival curves show a significantly decreased median survival of *Kras;Snail*$^{KI/+}$ mice (n = 28; 191 d), compared to *Kras* animals (n = 124; 466 d; p < 0.0001; log rank test). Increasing gene dose in *Kras;Snail*$^{KI/KI}$ mice further decreased the median survival (n = 20; 65 d; p < 0.0001; log rank test). **D)** Overview of the H&E stained pancreas of a 1-month-old *Kras;Snail*$^{KI/+}$ mouse compared to *Kras*. **E)** Number of PanINs was counted per 200x field in 1-month-old *Kras* (n = 4) and *Kras;Snail*$^{KI/+}$ mice (n = 5). nd, not detectable. Data are mean ± SEM, indicated p-values by t test. **F)** Alcian blue-stained pancreatic tissue of 1-month-old *Kras;Snail*$^{KI/+}$ mice compared to same aged *Kras* animals. Asterisks indicate ADMs, arrowheads point to PanIN1A and the arrow indicates PanIN3. Note the absence of high-grade PanINs in *Kras* animals. Scale bars represent 50 µm.

These data strongly support the importance of Snail in development of PDAC, which could be demonstrated by the Kras^{G12D}-dependent mouse model of pancreatic cancer.

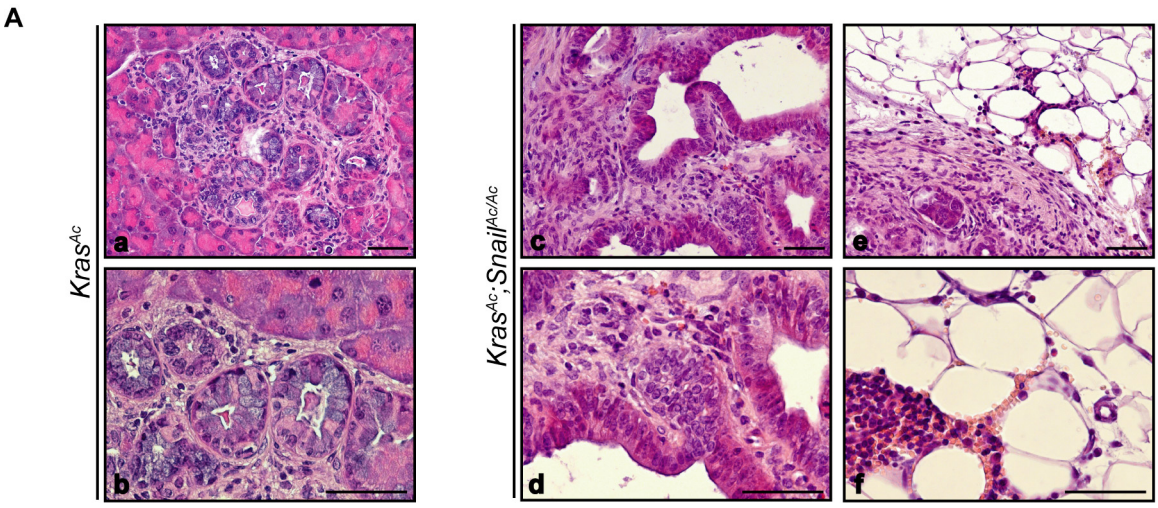

Figure 4-7: Acinar expression of Kras^{G12D} and Snail by the *Ela1-Cre^{ERT2}* line.
A) H&E-stained microscopic view of the pancreas of 6-month-old *Kras^{Ac}* and *Kras^{Ac};Snail$^{Ac/Ac}$* mice. (a,b) Low-grade PanIN lesions in *Kras^{Ac}* mice. (c,d) Invasive pancreatic ductal adenocarcinoma in *Kras^{Ac};Snail$^{Ac/Ac}$* mice. (e,f) Fatty degeneration of the pancreas in *Kras^{Ac};Snail$^{Ac/Ac}$* mice. Scale bars represent 50 µm.

4.8 Acceleration of pancreatic cancer evolution by Snail when expressed in the acinar compartment

In this work, the *Ptf1a$^{Cre/+}$* line was generally used to specifically target Snail expression to all pancreatic cells. To exclude an influence of Snail expression in islet or ductal cells on PDAC development, Snail was specifically expressed in acinar cells. A transgenic mouse line, which expresses tamoxifen-inducable Cre recombinase under the control of the *elastase* promoter (*Ela1-Cre^{ERT2}*), provides a tool to particularly target genes of interest, like in this case Kras^{G12D} and Snail to the acinar compartment of the pancreas (Stanger *et al.*, 2005), hereafter referred to as *Kras^{Ac}* and *Snail$^{Ac/Ac}$* mice). Starting at the age of 1 month, *Kras^{Ac}* mice and *Kras^{Ac};Snail$^{Ac/Ac}$* animals were fed for 2 weeks with a tamoxifen-containing diet, monitored, and sacrificed when they were 6 months old. Whereas *Kras^{Ac}* mice exhibited mostly regular pancreatic tissue with few low-grade PanINs, the *Kras^{Ac},Snail$^{Ac/Ac}$* animals showed invasive ductal pancreatic tumor areas as well as fatty degeneration besides normal pancreas (Figure 4-7A). Therefore, Snail is also capable to accelerate PDAC development in context of concomitant Kras^{G12D}, when the expression is restricted to the acinar compartment of the pancreas.

4.9 Snail and epithelial-mesenchymal transition in pancreatic cancer

Because Snail generally is seen as a marker and inducer of epithelial-mesenchymal transition (EMT) (Barrallo-Gimeno and Nieto, 2005) and represses the epithelial marker and cell-adhesion molecule E-cadherin (Cdh1) (Cano *et al.*, 2000; Batlle *et al.*, 2000), the

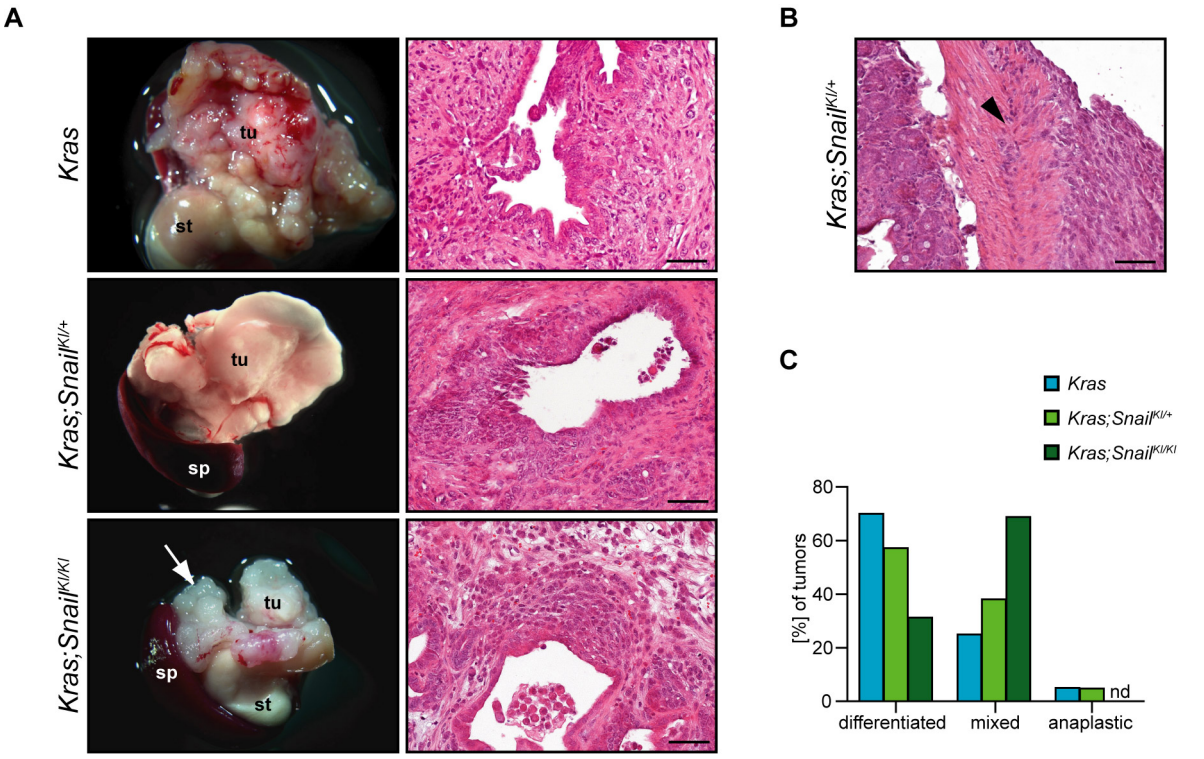

Figure 4-8: Snail-expressing mice develop moderately differentiated PDAC.
A) Macroscopic and H&E-stained microscopic view of pancreatic tumors of *Kras;Snail*$^{KI/+}$ and *Kras;Snail*$^{KI/KI}$ mice in comparison to *Kras* mice (tu, tumor; st, stomach; sp, spleen; arrow, papillary structure). **B)** H&E-stained view of pancreatic tumor tissue showing invasion into adjacent duodenal muscle layer (arrowhead). Scale bars represent 50 µm. **C)** Tumor grading. Percentage of well-differentiated, mixed, and anaplastic pancreatic tumors of *Kras;Snail*$^{KI/+}$ (n = 21) and *Kras;Snail*$^{KI/KI}$ mice (n = 16) in comparison to *Kras* mice (n = 40).

influence of Snail on Cdh1 and EMT in pancreatic cancer was examined *in vivo*.

PDACs of Snail-expressing mice were closely investigated for signs of EMT in appearance and differentiation grade. Macroscopically, tumors of investigated *Kras;Snail*$^{KI/+}$ animals were comparable to those in *Kras* mice. They were mainly of white-beige color and all of solid consistence. 25% of malignancies had a cystic aspect and 50% infiltrated adjacent organs like the intestine. Tumors of *Kras;Snail*$^{KI/KI}$ mice with biallelic Snail expression were solid. Additionally, they were of a papillary structure in 70% of cases. 15% of tumors contained cysts and 15% infiltrated into adjacent tissue (Figure 4-8A and B). By histology, ductal structures with changing degrees of cellular abnormalities and differentiation levels, which is common for PDAC (Hezel *et al.*, 2006), were seen in both genotypes. The nuclei exhibited a great variance in size and shape. Further, in most parts of the tumor, cells were surrounded by a high amount of fibrous stroma. In *Kras* mice, 70% of tumors were well-differentiated, 25% were mixed, and 5% were anaplastic. With 57%, the number of well-differentiated tumors was only slightly decreased in *Kras;Snail*$^{KI/+}$ animals. 38% of tumors were mixed and 5% were anaplastic. Only 31% of tumors in *Kras;Snail*$^{KI/KI}$ mice were well-differentiated, whereas 69% were mixed, and none of them was anaplastic (Figure 4-8C). Pancreatic tumor

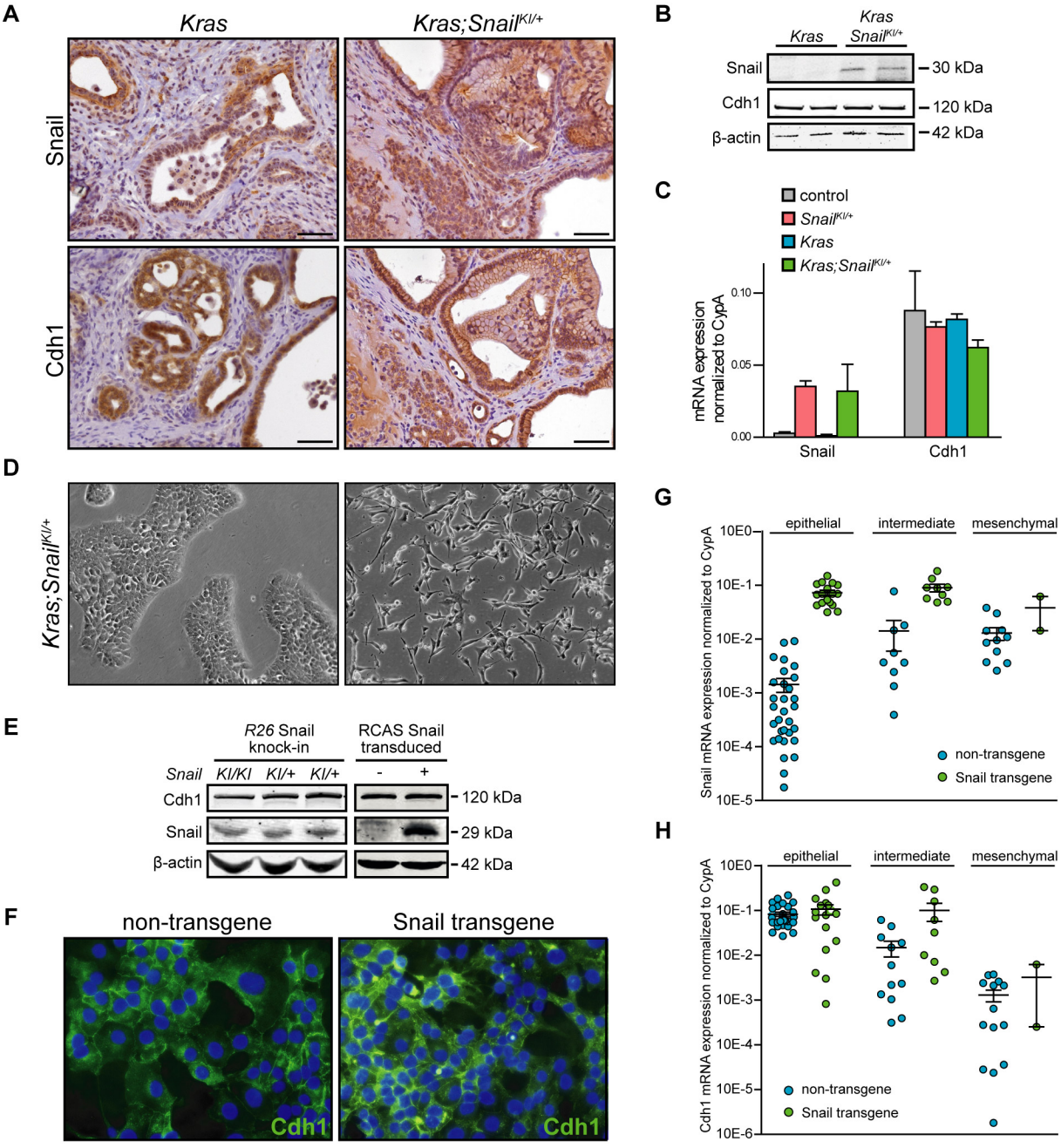

Figure 4-9: Snail and EMT in PDAC.
A) Snail and Cdh1 staining of PDAC tissue of indicated genotypes. Scale bars represent 50 µm. **B)** Western blot analysis of total Cdh1 protein expression in pancreatic tissue of 1-month-old *Kras* and *Kras;Snail*$^{KI/+}$ mice (as already shown in Figure 4-6B). **C)** qPCR analysis of total Snail and Cdh1 mRNA expression in the pancreas of 1-month-old mice of indicated genotypes. mRNA expression levels were normalized to CypA. Data are mean ± SEM. **D)** Primary PDAC cells from *Kras;Snail*$^{KI/+}$ mice with epithelial (left) and mesenchymal (right) morphology. **E)** Western blot analysis of total Snail and Cdh1 protein expression of primary PDAC cells (left panel) and Snail-transduced PDAC cells via the RCAS-Tva system (right panel). **F)** Immunocytochemistry showing membraneous localization of Cdh1 (green) in cells isolated from PDACs of the Kras^{G12D}-dependent mouse model with or without transgenic Snail expression. DAPI counterstain (blue). **G)** qPCR analysis of total Snail and **H)** Cdh1 mRNA expression of cells isolated from PDACs of the Kras^{G12D}-dependent mouse model with or without transgenic Snail expression classified by morphology. mRNA expression levels were normalized to CypA. Data are mean ± SEM.

tissue of *Kras;Snail*$^{KI/+}$, *Kras;Snail*$^{KI/KI}$ mice, as well as of *Kras* mice, exhibited nuclear and cytosolic Snail expression (Figure 4-9A). Also, on protein and mRNA level of pancreatic

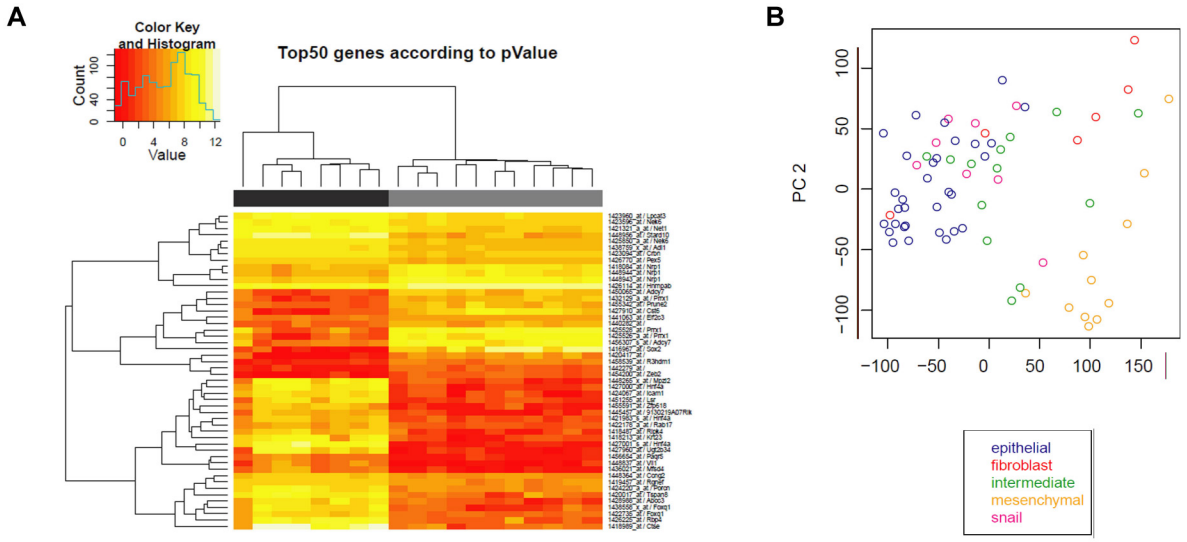

Figure 4-10: PDAC cells with transgenic Snail expression exhibit an epithelial expression profile.
Global mRNA expression profiles from epithelial, intermediate, and mesenchymal PDAC cells from the Kras^{G12D} dependent model as well as fibroblasts were compared with the expression profile from epithelial PDAC cells from *Kras;Snail*$^{KI/+}$ mice (GeneChip mouse genome 430 2.0 array). **A)** Heat map of the top 50 differentially expressed genes according to p-value. Bars: dark gray, *Kras;Snail*$^{KI/+}$ cells, light gray, mesenchymal PDAC cells. **B)** Principal component analysis (PCA) of the mRNA expression profile of epithelial, intermediate, and mesenchymal PDAC cells from the Kras^{G12D} dependent model, fibroblasts and epithelial PDAC cells from *Kras;Snail*$^{KI/+}$ mice. PCA is a mathematical algorithm which reduces the dimensions of large data sets with many variables (probes) per sample (cell line), while most of the variation of the data set is retained. This reduction is achieved by identification of directions with maximal data variation, named principal components. By use of few components instead of expression levels of thousands of probes in the plot, each cell line can be represented visually. Differences and similarities between each cell line then can be accessed at a glance in such a PCA plot (Ringnér, 2008).

tumor tissue, Snail did not have any repressive effect on Cdh1 (Figure 4-9B and C).

Primary pancreatic tumor cells were isolated from Snail-expressing mice and positively checked for Cre recombinase-mediated excision of the LSL element by PCR (data not shown). They were compared with already deeply characterized epithelial, intermediate, and mesenchymal cells, which were isolated from PDACs of the Kras^{G12D}-dependent mouse model (von Burstin *et al.*, 2009 and unpublished data). Regardless of the genotype, the morphology strongly varied among the different cell lines, as both epithelial and mesenchymal, as well as intermediate primary cell lines, were present, although epithelial cell lines predominated (Figure 4-9D). Whereas Snail protein and mRNA levels were increased in cells from Snail-expressing mice (Figure 4-9E and G), Cdh1 was expressed on comparable levels in Snail-transgenic and non-Snail transgenic mice, with decreasing tendency in cells with mesenchymal morphology (Figure 4-9E and H). Further, membraneous localization of Cdh1 was present in epithelial cells of all genotypes (Figure 4-9F and data not shown). Also, in Snail-transduced PDAC cells, neither Cdh1 levels were altered nor any EMT could be observed (Figure 4-9E and data not shown).

The mRNA gene expression profiles of PDAC cells from *Kras;Snail*$^{KI/+}$ mice with epithelial

morphology were compared with aforementioned PDAC cells (von Burstin *et al.*, 2009 and unpublished data) as well as fibroblasts. As seen by both heat map and principle component analysis (PCA), *Kras;Snail*$^{KI/+}$ tumor cells strongly differed from mesenchymal tumor cells not only on morphological, but also on molecular level. They clustered with epithelial cells from the Kras^{G12D}-dependent mouse model and exhibited a clear epithelial phenotype (Figure 4-10A and B).

Consequently, exclusive expression of Snail does not lead to Cdh1 repression and does not induce EMT in PDAC *in vivo* and *in vitro*.

4.10 Snail-expressing mice do not show increased metastatic rates

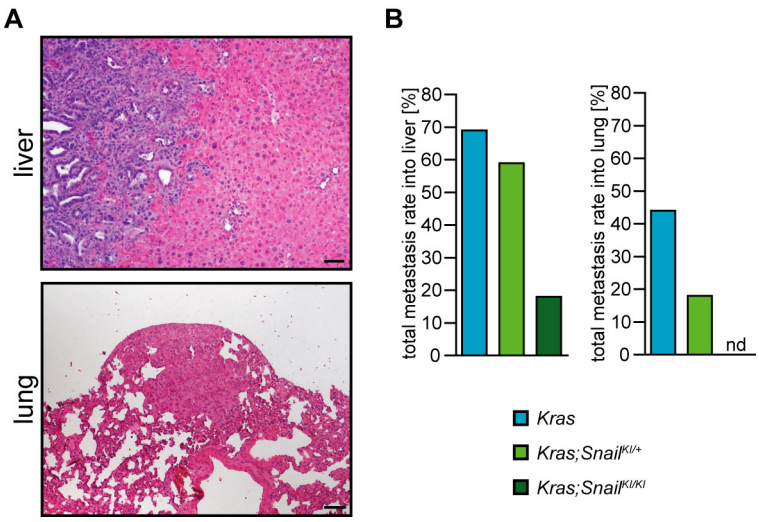

Figure 4-11: Snail-expressing mice do not show increased metastatic rates.
A) H&E staining of metastases in the liver and lung of *Kras;Snail*$^{KI/+}$ mice. Scale bars represent 50 µm. **B)** Metastasis rate to liver and lung of *Kras;Snail*$^{KI/+}$ (n = 17) and *Kras;Snail*$^{KI/KI}$ mice (n = 17) in comparison to *Kras* mice (n = 16) with PDAC.

As EMT is a crucial process for metastasis development, metastatic rates were compared in the mouse lines described above. At time of sacrification, macroscopic liver and lung metastases were observed in 56% and 38% of *Kras* mice, respectively. Due to shortened median survival (→ 4.7), Snail-expressing mice were sacrificed at a much lower age than *Kras* mice. This may explain that a much lower number of macroscopic metastases was detected in *Kras;Snail*$^{KI/+}$ (6% liver, 6% lung) and *Kras;Snail*$^{KI/KI}$ mice (6% liver, 0% lung), respectively. However, including micrometastases, *Kras* (69% liver, 44% lung) and *Kras;Snail*$^{KI/+}$ animals (59% liver, 18% lung) exhibited comparable metastatic rates, whereas metastasis in *Kras;Snail*$^{KI/KI}$ animals was still low (18% liver, 0% lung, Figure 4-11A and B).

In summary, these *in vivo* data show no overt influence of Snail expression on PDAC metastasis in the context of concomitant Kras^{G12D}, which is in agreement with the finding that Snail does not induce any obvious EMT in the PDAC model used in this study.

4.11 Aberrant Snail expression in the pancreas bypasses senescence and increases cell proliferation, DNA damage, and apoptosis

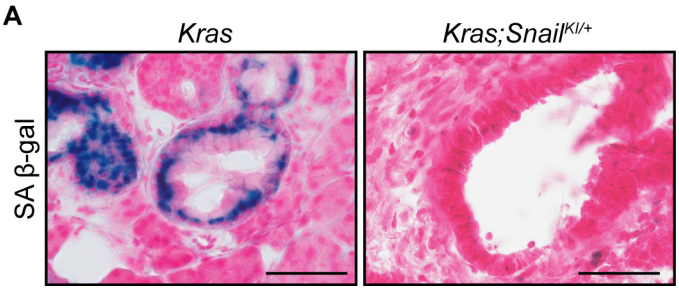

Figure 4-12: Snail bypasses senescence.
A) Senescence-associated β-galactosidase (SA β-gal) staining in the pancreas of 3-month-old *Kras* and *Kras;Snail*$^{KI/+}$ mice. Scale bars represent 50 µm.

Oncogene-induced senescence (OIS), which can be found in premalignant lesions of the pancreas and other organs, is a cellular stress response which effectively blocks proliferation and therefore is a mechanism to protect from cancer development (Collado and Serrano, 2010). Confirming previous studies (Morton *et al.*, 2010), low-grade PanINs in 3-month-old *Kras* mice displayed positive senescence-associated β-galactosidase (SA β-gal) staining. In contrast, senescence was not detectably present in preneoplastic lesions of same-aged *Kras;Snail*$^{KI/+}$ mice (Figure 4-12A), indicating a role of Snail in overcoming of OIS.

Bypass of senescence is associated with maintenance of proliferation, which is one of the hallmarks of cancer (Hanahan and Weinberg, 2011). Depending on the context and the model (*in vivo* vs. *in vitro*), Snail was shown to have both pro- and antiproliferative effects (Jamora *et al.*, 2005; Olmeda *et al.*, 2007; Vega *et al.*, 2004). To investigate the impact of Snail expression on pancreatic cell proliferation, BrdU incorporation was used as an indicator. In comparison to control mice, proliferation in 1-month-old *Snail*$^{KI/+}$ animals was 2.4-fold increased. In *Snail*$^{KI/KI}$ mice, proliferation was even higher with 4.4-fold increase (Figure 4-13A and B). This was verified on molecular level by GSEA, which revealed a significantly enriched expression of Kegg pathways cell cycle genes in 1-month-old *Snail*$^{KI/+}$ mice when compared to control cohorts (Figure 4-13C).

The influence of Snail on proliferation in pancreatic cancer was further investigated in preneoplastic lesions using the Kras^{G12D}-dependent mouse model of PDAC. A slight but not significant increase of BrdU-positive cells was observed in ADMs of *Kras;Snail*$^{KI/+}$ mice (36.4%) when compared to *Kras* mice (18.4%). There was a trend towards increased proliferation in PanIN1A lesions of *Kras;Snail*$^{KI/+}$ animals (5.94%) when compared to *Kras* mice (4.14%). Higher-graded PanINs exhibited a significantly increased proliferation rate in *Kras;Snail*$^{KI/+}$ mice (PanIN1B, 12.0%; PanIN2, 19.7%; PanIN3, 16.6%) in comparison to *Kras* animals (PanIN1B, 2.2%; PanIN2, 1.3%; PanIN3, 1.7%, Figure 4-13D and E). Accordingly, GSEA showed a significantly enriched expression of Kegg pathways cell cycle genes in pancreata of 1-month-old *Kras;Snail*$^{KI/+}$ mice when compared to *Kras* mice (Figure 4-13F).

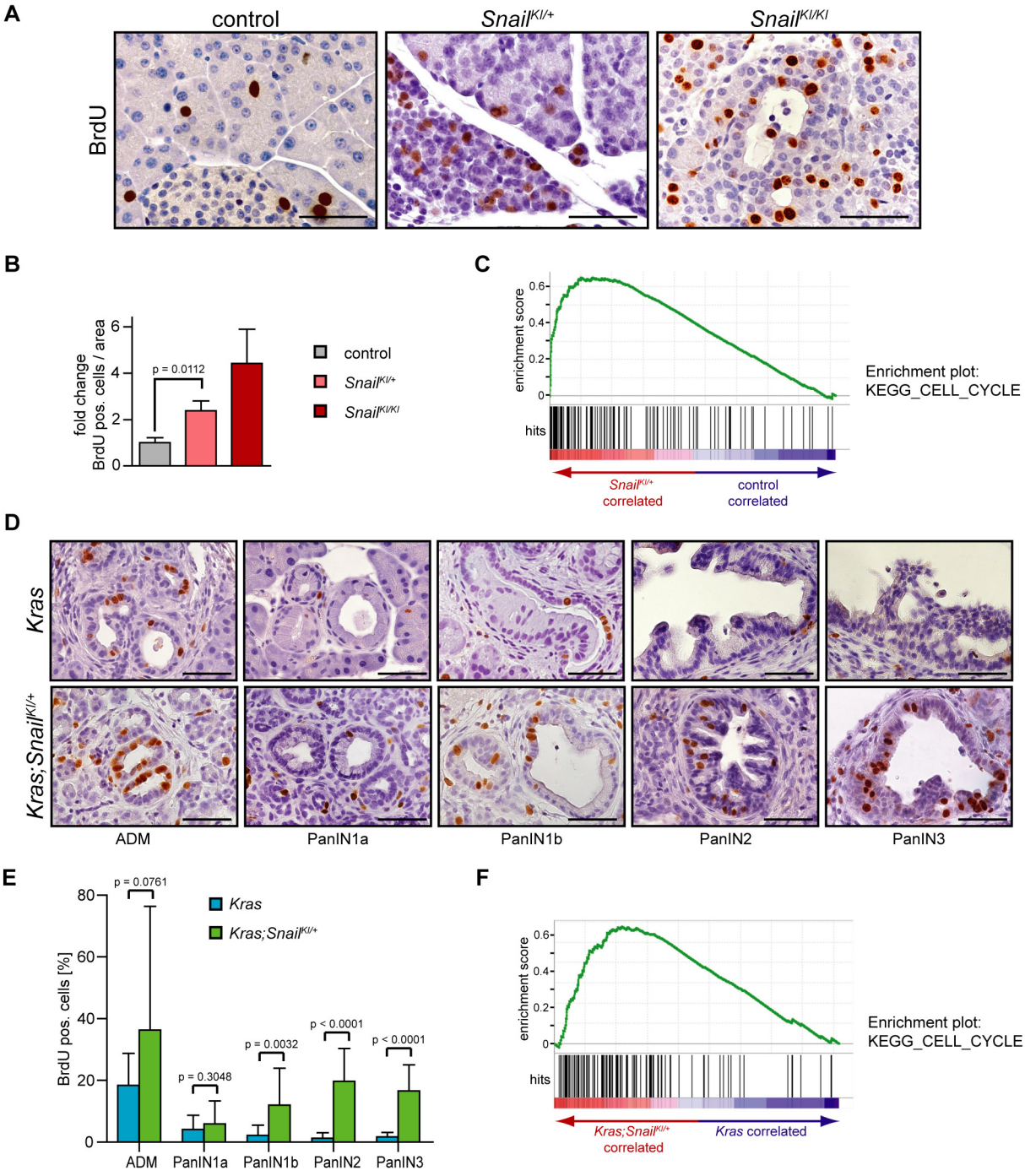

Figure 4-13: Snail expression increases proliferation.
A) Immunohistochemical BrdU staining of pancreatic tissue from 1-month-old mice of indicated genotypes. **B)** Proliferation index of pancreatic tissue from 1-month-old *Snail*$^{KI/+}$ (n = 4), *Snail*$^{KI/KI}$ (n = 3) and control mice (n = 3) was defined by dividing the number of BrdU-incorporated cells by area. Data are mean ± SEM, indicated p-value by t test. **C)** GSEA showing significant enrichment of Kegg pathways cell cycle genes in *Snail*$^{KI/+}$ (red, n = 2) vs. control pancreata (blue, n = 2) isolated from 1-month-old mice. NES = 2.43; FDR q < 0.001; NOM p < 0.001. **D)** Immunohistochemical BrdU staining of pancreata from 1-month-old *Kras;Snail*$^{KI/+}$ and 1-month-old (ADM, PanIN1A), 3-month-old (PanIN1B), and 2-year-old (PanIN2 and 3) *Kras* mice. Scale bars represent 50 µm. **E)** Proliferation index of neoplastic lesions of *Kras;Snail*$^{KI/+}$ mice (n = 5, 1-month-old to 3-month-old) in comparison with *Kras* animals (n = 11, 1-month-old to 2-year-old). Data are mean ± SD, indicated p-values by t test. **F)** GSEA showing significant enrichment of Kegg pathways cell cycle genes in *Kras;Snail*$^{KI/+}$ (red, n = 2) vs. *Kras* pancreata (blue, n = 2) isolated from 1-month-old mice. NES = 2.43; FDR q < 0.001; NOM p < 0.001.

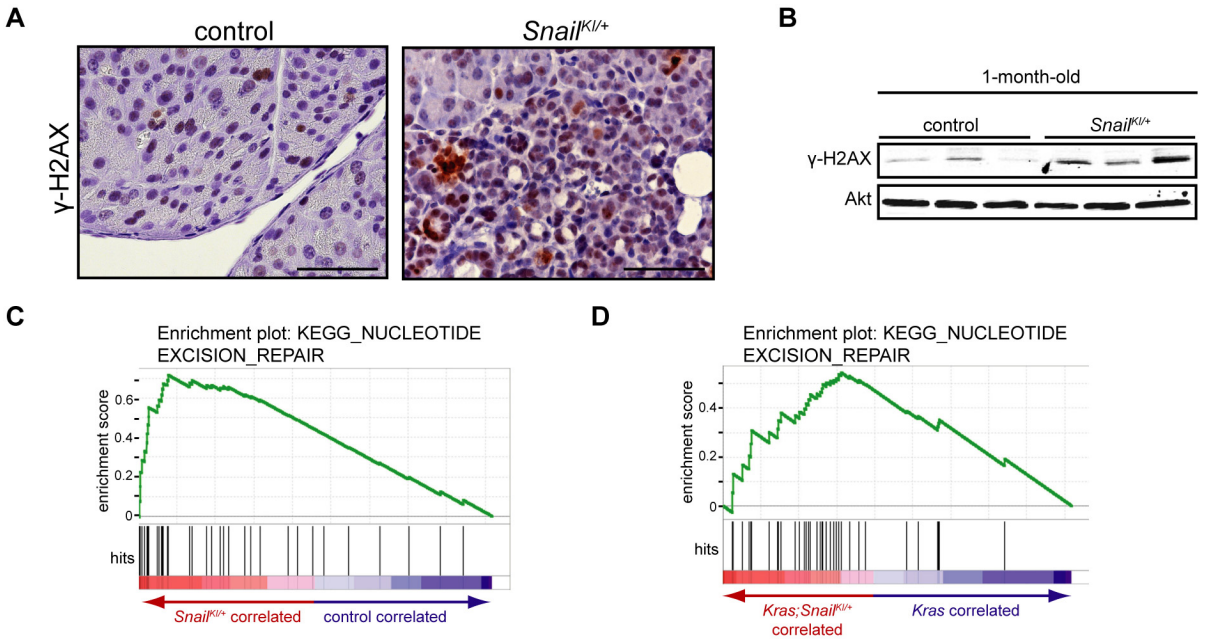

Figure 4-14: Influence of Snail on DNA damage.
A) Immunohistochemical γ-H2AX staining of pancreatic tissue from 1-month-old *Snail*$^{KI/+}$ mice and control cohorts. Scale bars represent 50 µm. **B)** Western blot analysis of γ-H2AX of pancreatic tissue of 1-month-old *Snail*$^{KI/+}$ mice and control cohorts. Total Akt was used as loading control. **C)** and **D)** GSEA showing significant enrichment of Kegg pathways nucleotide excision repair genes in pancreata of 1-month-old Snail-expressing mice. **C)** *Snail*$^{KI/+}$ (red, n = 2) vs. control pancreata (blue, n = 2). NES = 2.22; FDR q < 0.001; NOM p < 0.001. **D)** *Kras;Snail*$^{KI/+}$ (red, n = 2) vs. *Kras* pancreata (blue, n = 2). NES = 1.89; FDR q = 0.0013; NOM p = 0.06.

Sustained proliferation often results in DNA damage due to replication stress, which goes along with activation of the cellular DNA damage response machinery (Malumbres and Barbacid, 2009). γ-H2AX was taken as readout for DNA damage repair in pancreatic tissue samples. In contrast to control mice, 1-month-old *Snail*$^{KI/+}$ animals showed a strongly positive staining for γ-H2AX in the nuclei of acinar cells, which was even more intense in less differentiated cells (Figure 4-14A). This was confirmed by western blot analysis (Figure 4-14B). Further, Kegg pathways nucleotide excision repair genes were strongly enriched in *Snail*$^{KI/+}$ mice, as shown by GSEA (Figure 4-14C). Accordingly, GSEA revealed a significantly enriched expression of Kegg pathways nucleotide excision repair genes in pancreata of 1-month-old *Kras;Snail*$^{KI/+}$ mice when compared to *Kras* animals (Figure 4-14D).

In the presence of unrepaired DNA double-strand breaks, the DNA damage response machinery can trigger apoptotic cell death (Cotter, 2009). Cleaved caspase 3 staining and terminal deoxynucleotidyl transferase dUTP nick end labeling (TUNEL) reaction were taken as readout for apoptosis in pancreatic tissue samples (Figure 4-15A and B). In spite of high variances between individuals, the calculated apoptotic index in *Snail*$^{KI/+}$ animals (cleaved caspase 3, mean = 0.44; TUNEL, mean = 0.81) was significantly higher than in control cohorts (cleaved caspase 3, mean = 0.05; TUNEL, mean = 0.03, Figure 4-15C). Also, GSEA showed a significantly enriched expression of Kegg pathways apoptosis genes in 1-month-

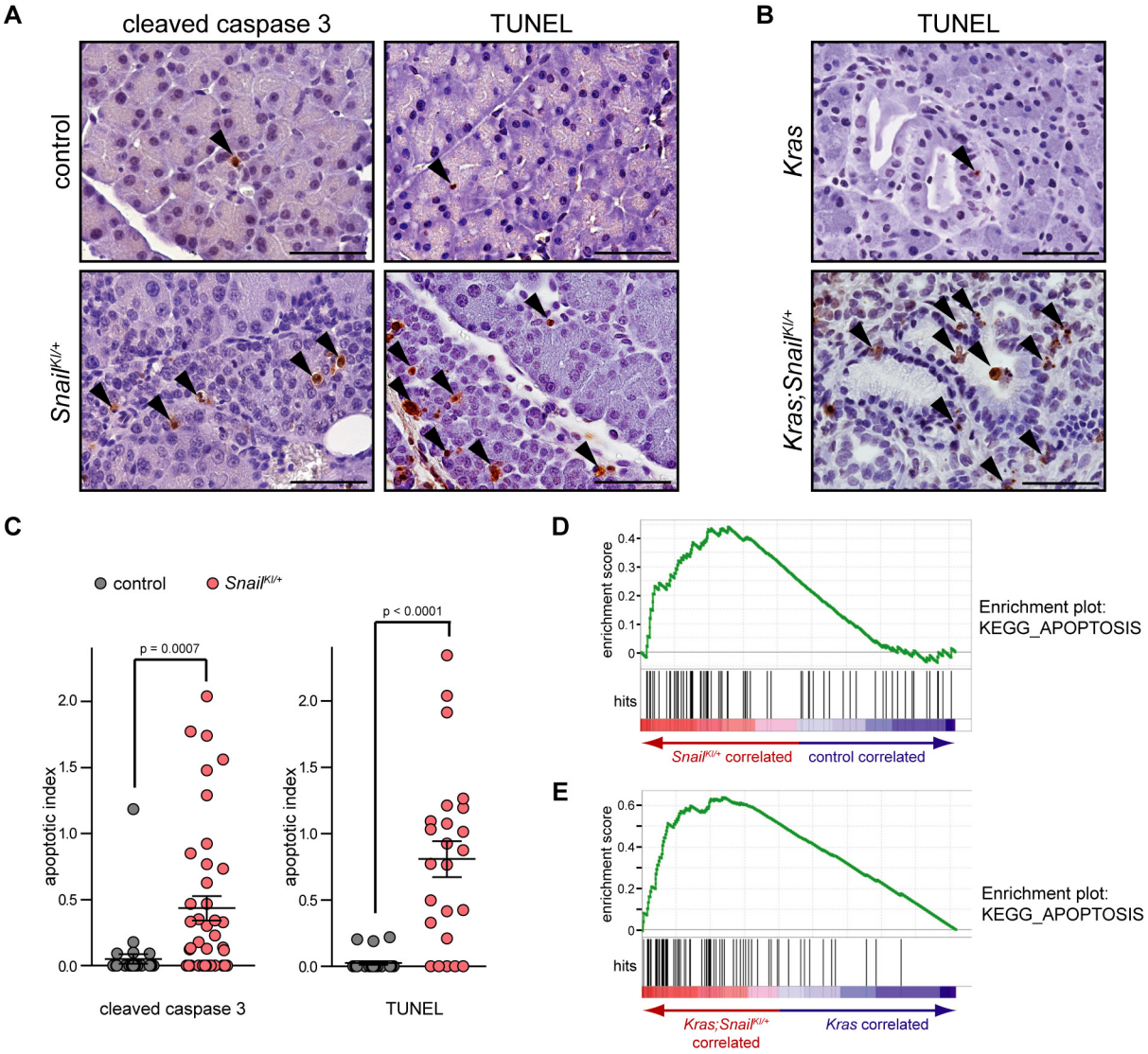

Figure 4-15: Increased apoptosis in Snail-expressing mice.
A) and **B)** Immunohistochemical cleaved caspase 3 staining and TUNEL labeling of pancreatic tissue from 1-month-old mice of indicated genotypes as readout for apoptosis. Scale bars represent 50 µm. **C)** Cleaved caspase 3 (left panel) and TUNEL-based (right panel) apoptotic index (positive cells x 100 / total cells) of pancreatic tissue from 1-month-old *Snail*$^{KI/+}$ (cleaved caspase, n = 5; TUNEL, n = 3) and control mice (n = 3). Data are mean ± SEM, indicated p-values by t test. **D)** and **E)** GSEA showing significant enrichment of Kegg pathways apoptosis genes in pancreata of 1-month-old Snail-expressing mice. **D)** *Snail*$^{KI/+}$ (red, n = 2) vs. control pancreata (blue, n = 2). NES = 1.54; FDR q = 0.08; NOM p = 0.01. **E)** *Kras;Snail*$^{KI/+}$ (red, n = 2) vs. *Kras* pancreata (blue, n = 2). NES = 2.50; FDR q < 0.001; NOM p < 0.001.

old pancreata of *Snail*$^{KI/+}$ mice (Figure 4-15D). Even clearer was the enrichment of Kegg pathways apoptosis genes in *Kras;Snail*$^{KI/+}$ mice when compared to *Kras* animals, supporting the findings of the TUNEL labeling (Figure 4-15E).

Thus, Snail overexpression in the pancreas leads to a bypass of OIS with a distinct increase of proliferation, which is accompanied by a high rate of DNA damage response and apoptosis.

4.12 The mitogen-activated protein kinase and phosphoinositide 3-kinase pathway in Snail-expressing mice

To determine how Snail alters the senescence program and induces proliferation, molecular pathways that have been associated with these processes were examined if they come into question as possible downstream targets of Snail.

The mitogen-activated protein kinase (MAPK) pathway is relevant for OIS but also drives cellular proliferation (Collado and Serrano, 2010; Pylayeva-Gupta *et al.*, 2011). Here, activation of Kras activates the protein kinase Raf, which then phosphorylates and activates Mek, finally leading to phosphorylation of the protein kinase Erk, which results in active MAPK signaling (Malumbres and Barbacid, 2003). Further, the phosphoinositide 3-kinase (PI3K) pathway, which is frequently altered during onset of cancer, plays an important role in senescence and proliferation (Collado and Serrano, 2010; Yuan and Cantley, 2008).

Akt phosphorylation at sites S473 and T308, which is a surrogate for PI3K pathway activation, was not increased in neither 1-month-old nor 3-month-old *Snail*$^{KI/+}$ mice when compared with control animals. Erk phosphorylation was also comparable in *Snail*$^{KI/+}$ mice and same-aged control animals (Figure 4-16A).

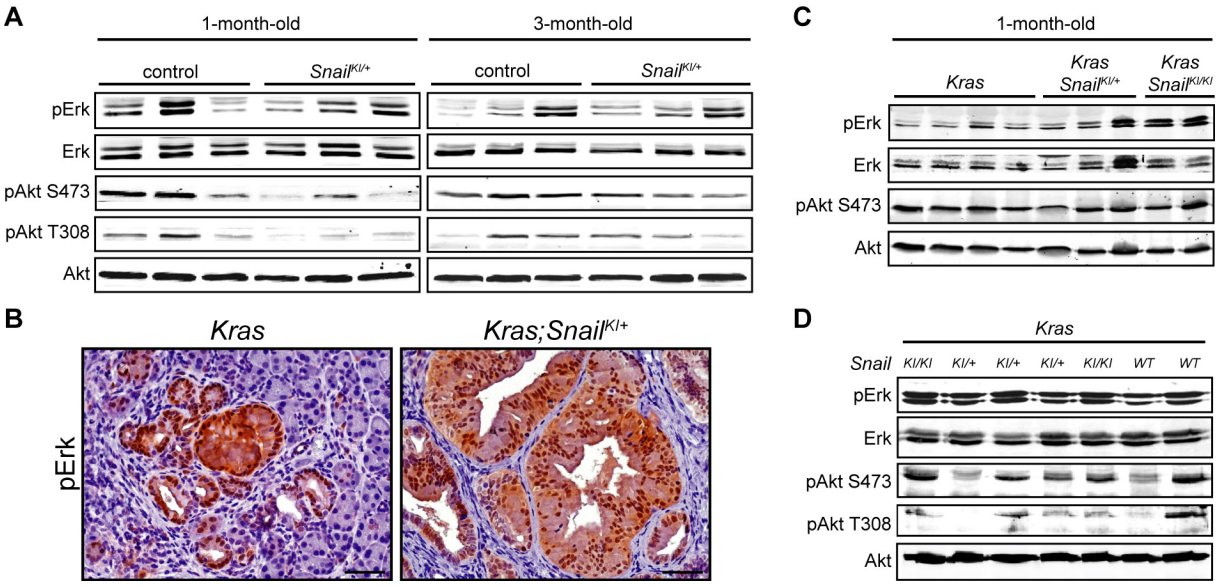

Figure 4-16: Influence of Snail on PI3K and MAPK signaling.
A) Western blot analysis of phosphorylated Erk (pErk) and total Erk (Erk) protein expression, as well as phosphorylated Akt (pAkt) at serine 473 (S473) and threonine 308 (T308) and total Akt (Akt) protein expression in pancreatic tissue of 1-month-old (left panel) and 3-month-old (right panel) *Snail*$^{KI/+}$ mice compared to control animals. **B)** Immunohistochemical staining for phosphorylated Erk (pErk) of pancreatic tissue from 3-month-old *Kras* and *Kras;Snail*$^{KI/+}$ mice. Scale bars represent 50 µm. **C)** Western blot analysis of phosphorylated Erk (pErk) and total Erk (Erk) protein expression as well as phosphorylated Akt (pAkt) at serine 473 (S473) and total Akt (Akt) protein expression in pancreatic tissue of 1-month-old mice of indicated genotypes. **D)** Western blot analysis of phosphorylated Erk (pErk) and total Erk (Erk) protein expression as well as phosphorylated Akt (pAkt) at serine 473 (S473) and threonine 308 (T308) and total Akt (Akt) protein expression in pancreatic tumor cells from mice of indicated genotypes.

Further, Akt and Erk phosphorylation were assessed in the $Kras^{G12D}$-dependent PDAC model. Immunohistochemical staining of phosphorylated Erk was positive in both cytoplasm and nucleus of neoplastic lesions in the pancreas of 3-month-old *Kras* and *Kras;Snail*$^{KI/+}$ mice and mostly negative in stromal and acinar cells (Figure 4-16B). Western blot analysis of 1-month-old *Kras* mice with few low-grade PanINs revealed weak Erk phosphorylation. *Kras;Snail*$^{KI/+}$ mice showed similar amounts of phosphorylated Erk as *Kras* animals. In same-aged *Kras;Snail*$^{KI/KI}$ mice, which already showed macroscopic tumor development and a high number of neoplastic lesions (data not shown), strong Erk phosphorylation was observed. Akt phosphorylation was not markedly altered among these groups (Figure 4-16C). Isolated pancreatic tumor cells from *Kras*, *Kras;Snail*$^{KI/+}$ and *Kras;Snail*$^{KI/KI}$ mice exhibited strong Erk phosphorylation, whereas Akt phosphorylation was variable without any clear genotypic tendency (Figure 4-16D).

These results indicate that Snail neither directly affects the PI3K nor the MAPK pathway to influence OIS and proliferation in the current setting.

4.13 Oncogene-induced senescence is overcome by Snail expression in a Trp53-independent manner

Senescence is associated with induction of Trp53 and its target cyclin-dependent kinase inhibitor 1A (Cdkn1a, hereafter called $p21^{CIP1}$, Collado and Serrano, 2010). As shown by immunohistochemistry, Trp53 and $p21^{CIP1}$ were frequently co-expressed in tumor cells of *Kras;Snail*$^{KI/+}$ mice (Figure 4-17A). To test whether the early bypass of senescence in *Kras;Snail*$^{KI/+}$ mice was Trp53-dependent, an *in vivo* approach using the established mutant gain-of-function Trp53 model (Olive *et al.*, 2004) was conducted. In the context of concomitant $Kras^{G12D}$ and Snail expression, pancreas-specific mutant $Trp53^{R172H}$ (hereafter called *p53*$^{mut/+}$) was expressed heterozygously in *Kras;Snail*$^{KI/+}$*;p53*$^{mut/+}$ animals. Longitudinally monitored mice developed invasive PDAC with the same morphological features as *Kras;Snail*$^{KI/+}$ mice (data not shown). The median survival of *Kras;Snail*$^{KI/+}$*;p53*$^{mut/+}$ mice was shortened to less than 3 months compared to more than 6 months in *Kras;Snail*$^{KI/+}$ animals (displayed in Figure 4-6C) and nearly 4 months in *Kras;p53*$^{mut/+}$ mice. Homozygous *R172H* mutation of *Trp53*, going along with simultaneous loss of wild type *Trp53* in *Kras;Snail*$^{KI/+}$*; p53*$^{mut/mut}$ animals, accelerated tumor progression with a median survival of 1 month compared to more than 2 months in *Kras;p53*$^{mut/mut}$ compound mutant mice (Figure 4-17B). Further, protein expression of Trp53 and its target $p21^{CIP1}$ were increased in pancreatic tumor cells isolated from *Kras* and *Kras;Snail*$^{KI/+}$ mice, which were treated 6 h with the topoisomerase inhibitor etoposide (Figure 4-17C). This indicates that the Trp53-dependent

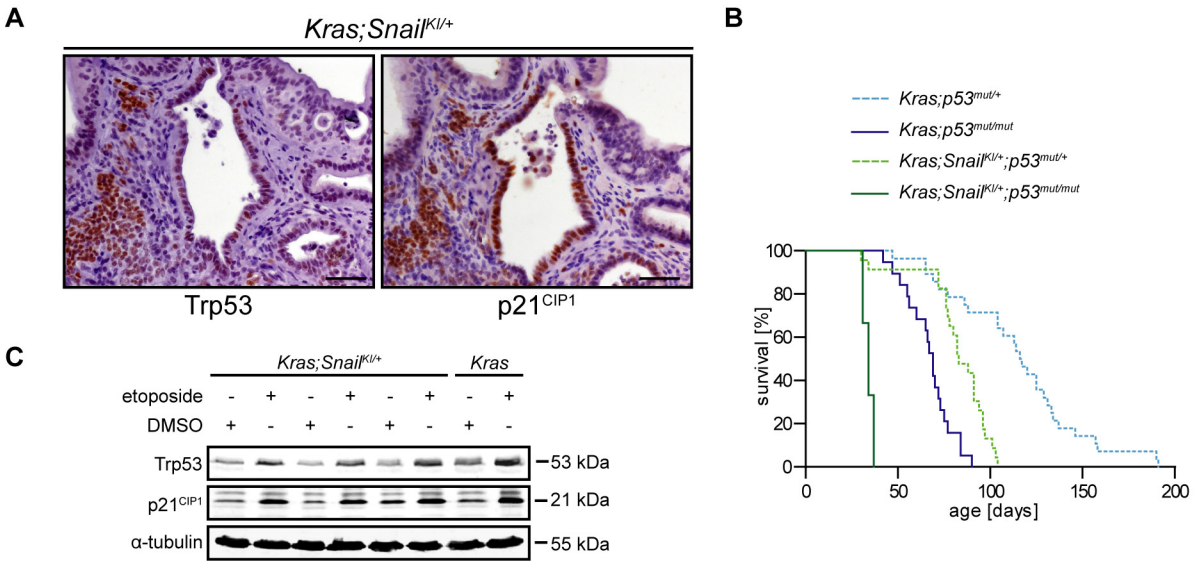

Figure 4-17: Snail induces Trp53-independent bypass of senescence.
A) Immunohistochemical Trp53 and p21^{CIP1} staining of PDAC tissue from 3-month-old *Kras;Snail$^{KI/+}$* mice. Scale bars represent 50 µm. **B)** Kaplan-Meier survival curves show a significantly decreased median survival of *Kras;Snail$^{KI/+}$;p53$^{mut/+}$* mice (n = 22; 83 d), compared to *Kras;p53$^{mut/+}$* animals (n = 28; 116 d; p < 0.0001; log rank test). Homozygous Trp53^{R172H} mutation in *Kras;Snail$^{KI/+}$;p53$^{mut/mut}$* mice (n = 3; 33 d) decreased the median survival when compared to *Kras;p53$^{mut/mut}$* mice (n = 19; 69 d; p < 0.0001; log rank test). **C)** Western blot analysis of Trp53, p21^{CIP1}, and α-tubulin (loading control) protein expression in pancreatic tumor cells after 6 h of treatment with 20 µM etoposide.

DNA damage response is intact in Snail-expressing mice. Because mutant Trp53 is not able to transcriptionally activate p21^{CIP1}, these data argue for active wild type Trp53 in PDAC as well as for Trp53-independent bypass of senescence in *Kras;Snail$^{KI/+}$* animals.

4.14 Role of the tumor suppressors p16^{INK4A} and p19^{ARF} in Snail-expressing mice

A further gene implicated in senescence and tumor suppression is the cell cycle regulator p16^{INK4A} (Collado and Serrano, 2010), which is frequently lost during pancreatic carcinogenesis. Together with p19^{ARF}, which is involved in Trp53 activation by inhibiting Mdm2, it is encoded by the *Cdkn2a* locus (Hezel *et al.*, 2006). In order to test whether loss of p16^{INK4A} or p19^{ARF} had any influence on *in vivo* pancreatic tumor evolution in Snail-expressing mice, *Kras;Snail$^{KI/+}$* mice were crossed with animals carrying a ubiquitously destabilized p16^{INK4A}, which results from a point mutation in the second exon of the *Cdkn2a* gene (Krimpenfort *et al.*, 2001, hereafter referred to as *Ink$^{*/+}$* mice). These *Kras;Snail$^{KI/+}$;Ink$^{*/+}$* mice developed invasive and metastatic PDAC with complete penetrance, and showed a median survival of nearly 6 months, which was not significantly shorter than in *Kras;Snail$^{KI/+}$* mice. Instead, conditional knock-out of both p16^{INK4A} and p19^{ARF} (Aguirre *et al.*, 2003) led to a significantly reduced median survival of less than 4 months in *Kras;Snail$^{KI/+}$;Cdkn2a$^{lox/+}$* mice

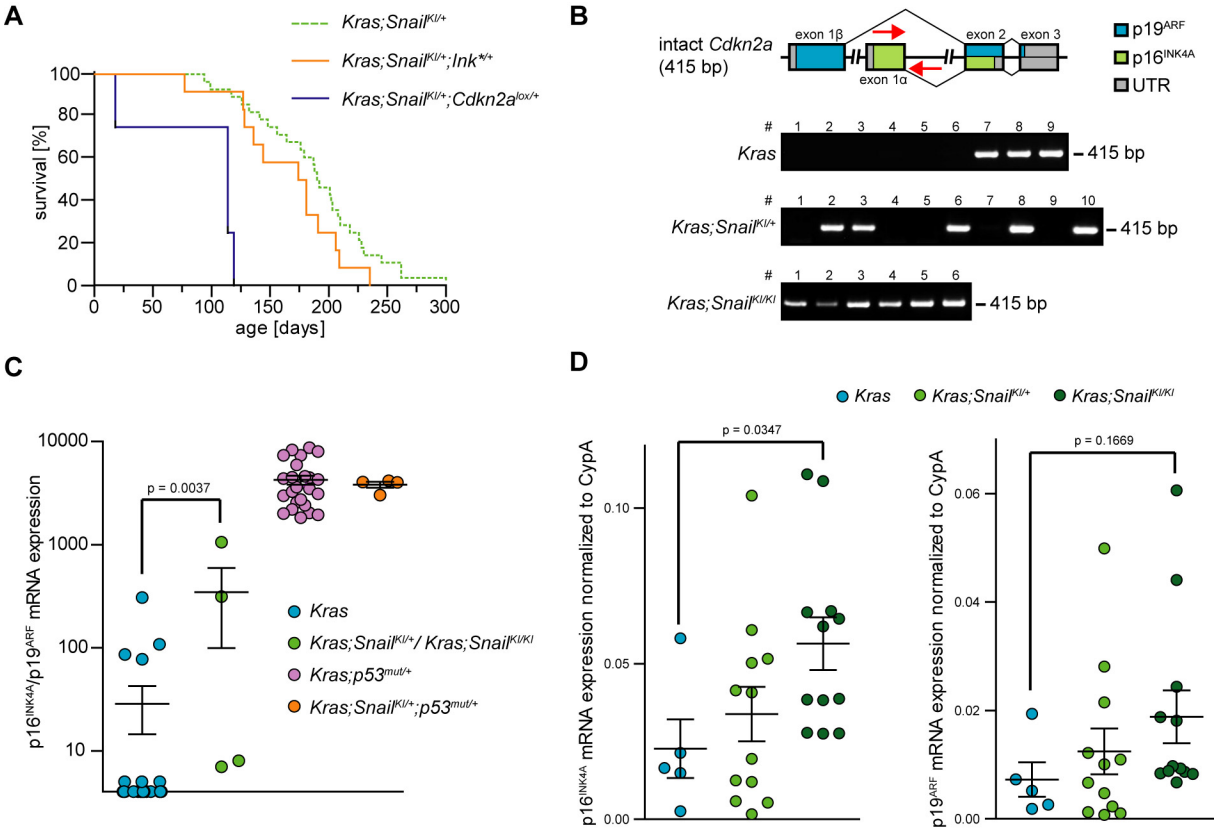

Figure 4-18: p16^{INK4A} and p19^{ARF} in Snail-expressing mice.
A) Kaplan-Meier survival curves do not show a significantly decreased median survival of *Kras;Snail$^{KI/+}$;Ink$^{*/+}$* mice (n = 13; 178 d), compared to *Kras;Snail$^{KI/+}$* animals (n = 28; 191 d; p = 0.1293, log rank test). Decreased median survival was observed in *Kras;Snail$^{KI/+}$;Cdkn2a$^{lox/+}$* mice when compared to *Kras;Snail$^{KI/+}$* animals (n = 4; 114 d; p < 0.0001, log rank test). **B)** DNA analysis of *Cdkn2a* locus integrity in cell lines isolated from pancreatic tumors of indicated genotypes. The non-related proteins p16^{INK4A} and p19^{ARF}, which are both encoded by the *Cdkn2a* locus are generated by alternative reading frames and alternative usage of exon 1. Scheme according to Krimpenfort *et al.*, 2001. **C)** p16^{INK4A}/p19^{ARF} mRNA expression microarray data (GeneChip mouse genome 430 2.0 array) from *Kras* PDAC cells (n = 23) were compared with *Kras;Snail$^{KI/+}$* and *Kras;Snail$^{KI/KI}$* cells (n = 4) as well as *Kras;p53$^{mut/+}$* (n = 25) and *Kras;Snail$^{KI/+}$; p53$^{mut/+}$* cells (n = 4). Data are mean ± SEM, indicated p-value by t test. **D)** Quantitative mRNA expression analysis of p16^{INK4A} (left panel) and p19^{ARF} (right panel). Total mRNA was prepared from pancreatic tissue of tumor-bearing *Kras* (n = 5) *Kras,Snail$^{KI/+}$* (n = 12), and *Kras;Snail$^{KI/KI}$* mice (n = 12). mRNA expression levels were normalized to CypA. Data are mean ± SEM, indicated p-values by t test.

(Figure 4-18A). This argues that here, loss of p19^{ARF} and thus Trp53 stabilization causes accelerated PDAC formation.

Further, integrity of the *Cdkn2a* locus was tested by PCR spanning a part of exon 1α, which encodes p16^{INK4A}. 67% of pancreatic tumor cell lines derived from *Kras* mice showed loss of the tested region. In contrast, this was the case in only 50% of *Kras;Snail$^{KI/+}$* and in 0% *Kras;Snail$^{KI/KI}$* cell lines, indicating lower pressure on loss of the *Cdkn2a* locus in tumor-developing Snail-expressing mice (Figure 4-18B).

Microarray-based mRNA expression data for the *Cdkn2a* locus of primary pancreatic tumor cells from *Kras;Snail$^{KI/+}$* and *Kras;Snail$^{KI/KI}$* mice was compared with *Kras* cells. As both p16^{INK4A} and p19^{ARF} mRNA expression levels are detected by the same probe, they cannot be distinguished using this approach. Whereas *Kras* cell lines showed low p16^{INK4A}/p19^{ARF} mRNA

expression levels (mean = 28.5), arguing for a loss of the *Cdkn2a* locus in these animals, some *Kras;Snail*$^{KI/+}$ and *Kras;Snail*$^{KI/KI}$ cell lines retained p16^{INK4A}/p19^{ARF} expression (mean = 346.5). Primary pancreatic tumor cells from mice with additional Trp53^{R172H} mutation retained p16^{INK4A}/p19^{ARF} positive irrespectively of Snail (*Kras;p53*$^{mut/+}$, mean = 4242; *Kras;Snail*$^{KI/+}$*; p53*$^{mut/+}$, mean = 3809; Figure 4-18C).

p16^{INK4A} mRNA expression levels in pancreatic tumor tissue of *Kras* animals (mean = 0.0227) resembled those in *Kras;Snail*$^{KI/+}$ mice (mean = 0.3381), whereas a significant increase was observed in *Kras;Snail*$^{KI/KI}$ mice (mean = 0.5647). Regarding p19^{ARF} mRNA expression, this difference was not that pronounced (*Kras*, mean = 0.0072; *Kras;Snail*$^{KI/+}$, mean = 0.1246; *Kras;Snail*$^{KI/KI}$, mean = 0.0188, Figure 4-18D).

Taken together, these data suppose that Snail might influence the pressure on loss of the *Cdkn2a* locus in the Kras^{G12D}-dependent mouse model of PDAC. This affects expression and tumor suppressive function of p16^{INK4A} and, to a lesser extend, p19^{ARF}.

4.15 The influence of Snail on retinoblastoma phosphorylation and E2F transcription factor activity

p16^{INK4A} is a cyclin-dependent kinase (CDK) inhibitor, which binds to CDK4 and 6 to inhibit complex formation with cyclin D (Bardeesy *et al.*, 2006). In case of an active cell cycle, the tumor suppressor retinoblastoma (Rb) is hyperphosphorylated by CDK/cyclin complexes.

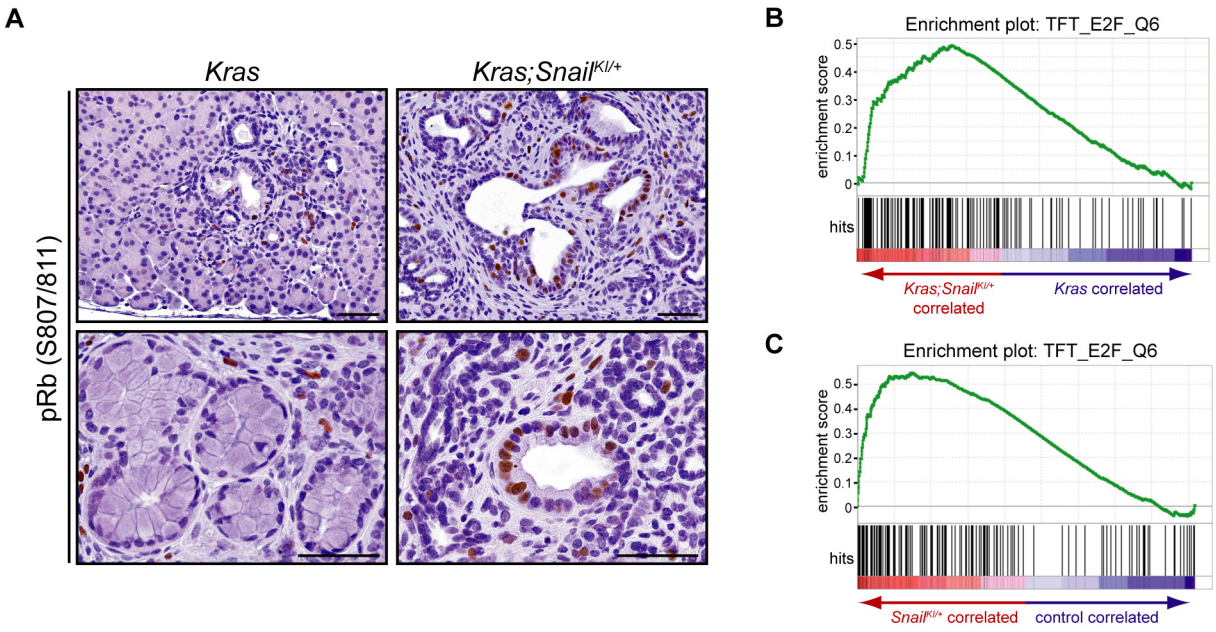

Figure 4-19: Snail induces Rb hyperphosphorylation and activates E2F.
A) Immunohistochemical staining for phosphorylated Rb at serine 807/811 (pRb S807/811) of pancreatic tissue from 1-month-old *Kras* and *Kras;Snail*$^{KI/+}$ mice. Scale bars represent 50 µm. **B)** and **C)** GSEA showing significant enrichment of transcription factor target (TFT) genes of E2F in pancreata of 1-month-old Snail-expressing mice. **B)** *Kras;Snail*$^{KI/+}$ (red, n = 2) vs. *Kras* pancreata (blue, n = 2). NES = 2.10; FDR q < 0.001; NOM p < 0.001. **C)** *Snail*$^{KI/+}$ (red, n = 2) vs. control pancreata (blue, n = 2). NES = 2.21; FDR q < 0.001; NOM p < 0.001.

This results in Rb inactivation and its dissociation from the E2F complex, thus leading to activation of the E2F transcription factors following expression of E2F target genes (Chen *et al.*, 2009). Immunohistochemical staining showed a much higher number of cells with hyperphosphorylated Rb in preneoplastic lesions and stroma of 1-month-old *Kras;Snail*$^{KI/+}$ mice than in same-aged *Kras* animals (Figure 4-19A). Further, GSEA revealed a significantly enriched expression of transcription factor target (TFT) genes of E2F in pancreata of 1-month-old *Kras;Snail*$^{KI/+}$ mice when compared to *Kras* animals (Figure 4-19B). This was also confirmed in *Snail*$^{KI/+}$ mice without Kras expression (Figure 4-19C), arguing for the inactivation of Rb by Snail in a p16^{INK4A}-dependent fashion, which results in E2F activity and sustained cell cycle activity in Snail-expressing mice.

4.16 Possible direct transcriptional targets of Snail: A microarray-based analysis

The data shown in this work strongly support that pancreatic Snail expression has to be very tightly regulated, as overexpression results in severe cellular changes like acinar dedifferentiation and ACC formation, bypass of senescence, derangement of cell cycle control, and dramatically accelerated PDAC development. Because Snail has mainly been shown as direct repressor by binding to E-boxes of certain promoters (Barrallo-Gimeno and Nieto, 2005), it is likely that this is also true for a number of genes in the used Snail knock-in model. To get an impression which genes were possibly negatively regulated by Snail, mRNA gene expression profiles of pancreatic tissue samples of 1-month-old, 3-month-old, as well as ACC or PDAC-bearing mice of different genotypes, were obtained. Genes that were downregulated at least 2-fold in both 1-month-old and 3-month-old *Snail*$^{KI/+}$ mice in comparison to same-aged control mice were determined in the first step. If these genes were also downregulated at least 2-fold in both 1-month-old and 3-month-old *Kras;Snail*$^{KI/+}$ mice in comparison to same-aged *Kras* animals, they were considered as possible targets of Snail. In the situation of fully developed PDAC, the samples from both *Kras* and *Kras;Snail*$^{KI/+}$ mice were comparable regarding these possible targets, thus the comparison of these tumors was not included in the analysis. Finally, 21 genes with continuous repression in Snail-expressing mice of different ages remained as putative targets of Snail (Figure 4-20A). Based on literature search, the 5 most interesting among them were chosen for further *in silico* promoter analysis.

With no lysine (K) 2 (Wnk2) is a serine/threonine kinase, which has been shown to act as a tumor suppressor in brain tumors (Jun *et al.*, 2009; Hong *et al.*, 2007). Further, Wnk2 inhibition *in vitro* leads to Mek and Erk1/2 activation thereby increasing cell proliferation

(Moniz *et al.*, 2007). Promoter analysis of *Wnk2* using ConTra (conserved transcription factor binding sites) v2 (Broos *et al.*, 2011), revealed the presence of a conserved 5'-CAGGTG E-box at position -55. Further E-boxes as putative Snail binding sites were detected at positions -861, -885 and -912 (all 5'-CAGGTG).

Another interesting possible target is the epidermal growth factor (Egf), which binds to the Egf receptor (Egfr), resulting in activation of several biological activities, like proliferation and inhibition of apoptosis. Aberrant Egf signaling is found in a number of tumors, including pancreatic cancer (Oliveira-Cunha *et al.*, 2011). In the *Egf* promoter, an atypical 5'-CTCAAG E-box was found at position -426.

Bone morphogenetic protein 3 (Bmp3) belongs to the transforming growth factor β (Tgfβ) superfamily, which is mainly investigated for its role during bone formation. Concerning oncologic functions, Bmp3 was shown to be methylated in both colorectal and pancreatic cancer (Loh *et al.*, 2008; Kisiel *et al.*, 2012). In the *Bmp3* promoter, a 5'-CAGCTG E-box at position -128 as well as a 5'-CAGGTG E-box at -1016 were identified.

Members of the crumbs family are relevant regulators of cell polarity and epithelial morphology (Hsu *et al.*, 2006). Crumbs homolog 1 (Crb1) was consistantly downregulated in Snail-expressing mice. Remarkably, direct binding and repression of Snail to crumbs homolog 3 (Crb3) was shown before (Whiteman *et al.*, 2008). Indeed, promoter analysis showed a 5'-CACCTG E-box at position -89 of the *Crb1* promoter.

The dual specificity phosphatases (Dusps) are a heterogenous family of phosphatases that have been shown to dephosphorylate many substrates like the MAPKs Erk, Jnk, and p38. (Patterson *et al.*, 2009). Since these genes are frequently altered in cancer, Dusp26 is an interesting candidate for closer investigation. Further, 2 5'-CACGTG E-boxes were found at positions -105 and -281 of the *Dusp26* promoter.

Because positive gene regulation by Snail could also be the case in this setting, the same experimental approach as described above was conducted to obtain a deeper insight into possibly upregulated genes by Snail. In the end, 25 genes with continuous overexpression in Snail knock-in mice remained (Figure 4-20B). Among them, Snail itself was present. Confirming previous studies showing Snail expression in human PDAC (Hotz *et al.*, 2007), Snail mRNA levels in *Kras* mice increased with advanced age and tumorigenesis. PDAC-bearing *Kras* animals and Snail knock-in mice expressed comparable amounts of Snail, underlining once more the physiology of the model used in this study.

Further, $p21^{CIP1}$ (indicated as Cdkn1a) is upregulated in most Snail-expressing animals. Interestingly, this senescence inducer and target of Trp53 was previously demonstrated to be repressed by Snail in an *in vitro* model of osteoblast differentiation (Takahashi *et al.*, 2004).

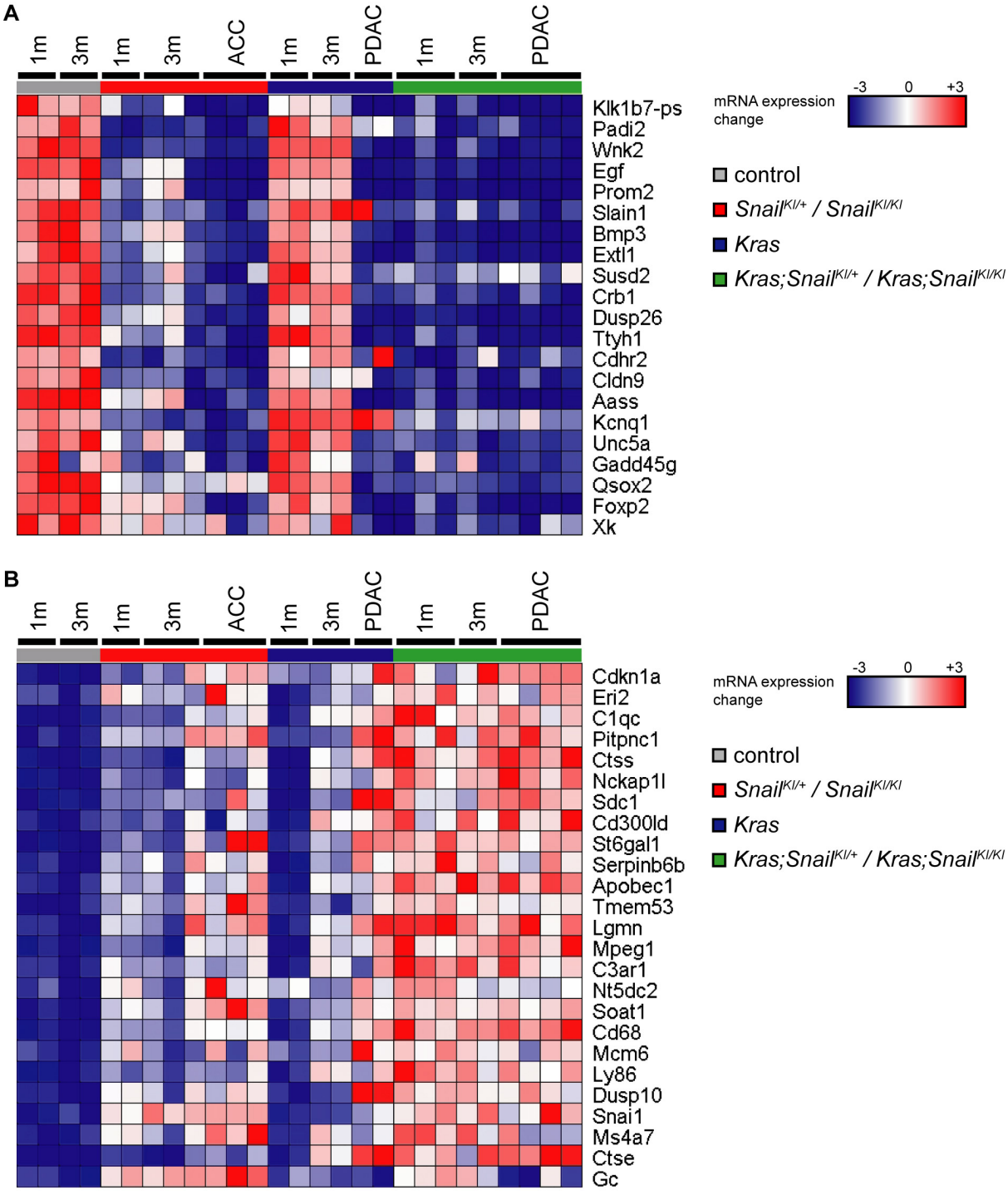

Figure 4-20: Genes with continuous regulation in Snail-expressing mice.
RNA was isolated from pancreatic tissue of the indicated genotypes, labeled, and hybridized onto GeneChip mouse gene 1.0 ST array. Heat map of **A)** continuously downregulated and **B)** upregulated genes in Snail-expressing mice, representing possible Snail targets.

As in this work it was shown that Snail-expressing mice bypass senescence and have increased proliferation rates, the increased $p21^{CIP1}$ mRNA levels in the used model seem not to be sufficient to effectively block entering of the cell cycle.

Although these data indicate an influence of Snail on the regulated genes mentioned above, their repression by direct binding of Snail to the found E-boxes has to be validated by chromatin immunoprecipitation (ChIP). Further, the contribution of the up- and downregulation of the mentioned genes to the phenotype of the mice, as well as their impact on ACC and PDAC development, have to be tested by *in vivo* experiments.

5 Discussion

Gaining insight into genetic alterations and molecular pathways that are responsible for initiation and progression of pancreatic cancer is an urgent need to develop methods for early and specific detection as well as successful therapeutic approaches – both of which do not exist. Nevertheless, the use of GEMs of pancreatic cancer has provided tremendous advances in our understanding of underlying molecular changes that orchestrate tumorigenesis.

The transcriptional repressor Snail has been extensively studied in regard to its role during EMT and embryonic development, in which it contributes to cell migration and invasion (Nieto, 2002; Barrallo-Gimeno and Nieto, 2009). As these 2 processes are important steps during tumorigenesis and metastasis, it is not astonishing that Snail is also expressed in several tumors including PDAC (Barrallo-Gimeno and Nieto, 2005; Hotz *et al.*, 2007). Importantly, we previously could show highly increased Snail expression in an *in vivo* selection model of highly metastatic pancreatic tumor cells (von Burstin *et al.*, 2009). These initial findings propose a role of Snail in pancreatic cancer initiation, progression, and metastasis, but the underlying molecular mechanisms are still poorly defined.

This study provides for the first time a GEM that allows us to investigate the molecular role of Snail in the pancreas or any other organ of interest *in vivo.* The findings presented here show that pancreas-specific Snail overexpression leads to dedifferentiation, induction of a stem cell signature and increased proliferation of acinar cells, resulting in exocrine insufficiency and development of acinar tumors. In the context of concomitant $Kras^{G12D}$ expression, Snail leads to accelerated PanIN progression due to bypass of senescence and increased proliferation, resulting in invasive and metastatic PDAC. Surprisingly, neither overt signs of EMT nor increased metastatic rates can be observed in this model.

5.1 Snail is no inducer of epithelial-mesenchymal transition and metastasis in pancreatic cancer

Most importantly, this study shows that pancreas-specific Snail expression in the context of activated $Kras^{G12D}$ leads to rapid development of invasive PDAC with complete penetrance and a drastically shortened median survival, indicating a relevant role of Snail in pancreatic tumorigenesis. According to this, Snail expression has been observed in several tumors (Yang *et al.*, 2007; Hardy *et al.*, 2007; Moody *et al.*, 2005; Yang *et al.*, 2009; Roy *et al.*, 2005; Heebøll *et al.*, 2009; Blechschmidt *et al.*, 2008) including PDAC (Hotz *et al.*, 2007). In breast and hepatocellular carcinoma, Snail has further been associated with poor prognosis and

tumor recurrence (Elloul *et al.*, 2005; Moody *et al.*, 2005; Miyoshi *et al.*, 2005). Snail has been intensively investigated regarding its role in EMT, which is a relevant element during cancer progression. In various *in vitro* and *in vivo* models of tumorigenesis, EMT has been shown to generally mark a bad outcome (Thiery *et al.*, 2009). Snail expression in cancerous tissue is often connected with induction of EMT, resulting in augmented invasion, metastasis, and thereby poor prognosis (Blanco *et al.*, 2002; Yang *et al.*, 2007; Cano *et al.*, 2000). In consideration of these facts, the differentiation grade and metastasis rates of pancreatic tumors of Snail-expressing mice were closely investigated in this study, considering EMT as a possible mechanism for accelerated Snail-dependent tumor development.

Interestingly, tumors in *Kras;Snail*$^{KI/+}$ mice as well as in *Kras;Snail*$^{KI/KI}$ mice with biallelic Snail expression strongly resemble those of *Kras* mice, being mostly well-differentiated or mixed. Also, independently of transgenic Snail expression, pancreatic tumor cells of both epithelial or mesenchymal morphology have been isolated. Further, microarray analyses show that Snail-expressing epithelial cells clearly cluster with morphologically similar cells isolated from *Kras* mice, whereas the mRNA expression profile is distinct from mesenchymal cells. Remarkably, Cdh1-levels in both tumor tissue and isolated tumor cells are not altered either, although Snail was previously shown to repress Cdh1 in many contexts (von Burstin *et al.*, 2009; Peinado *et al.*, 2004; Batlle *et al.*, 2000; Cano *et al.*, 2000). Being consistent with these data, the metastasis rates of *Kras* and *Kras;Snail*$^{KI/+}$ mice are comparable. The strong decrease of metastasis formation in *Kras;Snail*$^{KI/KI}$ mice can be explained by the high difference in age at comparable tumor stage. In contrast to *Kras;Snail*$^{KI/KI}$ animals with a very short timespan until cancer formation, tumors in *Kras* animals grow relatively slowly, increasing the likelihood that cells dissociate from the primary tumor to form distant metastases.

Apparently, in this experimental setting, EMT and Cdh1 expression rather depend on the cell morphology and other still unknown factors than on transgenic Snail expression levels. In some further tissues, Snail expression is not sufficient to cause overt EMT or only leads to incomplete EMT, as shown in murine cleft palates (Martínez-Álvarez *et al.*, 2004) and breast cancer cell lines exposed to hypoxia (Lundgren *et al.*, 2009). Also, in human PDAC samples, Snail expression was found without being significantly correlated with Cdh1 (Hotz *et al.*, 2007). It is likely that in these contexts, as well as in the model used in this work, further proteins that form a repressory complex with Snail during the initiation of EMT, are missing. For instance, Snail recruits HDAC1/2 and the corepressor mSin3A, which is crucial for EMT in several mammalian tumor cell lines (Peinado *et al.*, 2004; von Burstin *et al.*, 2009). Furthermore, Snail-mediated Cdh1 repression is dependent on polycomb repressive complex

2 (Prc2) in various cancer cells (Herranz *et al.*, 2008). It would be important to reveal which factors are potentially missing, to get further insight into the mechanisms behind Snail-regulated transcriptional repression and EMT in pancreatic cancer *in vivo*.

Although increased Snail levels in the $Kras^{G12D}$-dependent mouse model of PDAC neither induce any overt EMT nor increased metastasis rates, the median survival is severely decreased in Snail-expressing animals. Thus, a mechanism different from EMT must be responsible for the poor survival of these mice.

5.2 Snail expression in the pancreas leads to acinar dedifferentiation and thereby favors tumorigenesis

One possible hint for the underlying mechanism could be explained by the observation that overexpression of Snail in the pancreas without $Kras^{G12D}$ leads to dedifferentiation of acinar cells going along with downregulation of many adult pancreatic markers in a dose dependent manner. High differentiation of cells is generally associated with a low tumorigenic potential, whereas low differentiation favors tumor development and is further often correlated with poor prognosis (Ben-Porath *et al.*, 2008), which would be a potential reason for the accelerated tumor development in Snail-expressing mice.

To link the tumor-promoting function of Snail and the observed phenotype of dedifferentiated cells in the used setting, one has to understand how Snail contributes to embryonic development. During embryogenesis, sensitive regulation of Snail expression levels is crucial, as ectopic expression or knock-out of Snail lead to severe developmental defects (Del Barrio and Nieto, 2002; Carver *et al.*, 2001; Murray *et al.*, 2007). In mouse and *Drosophila melanogaster*, Snail is expressed extensively during early phases of embryogenesis, whereas later its expression is restricted and persists generally at very low levels (Alberga *et al.*, 1991; Nieto *et al.*, 1992). Importantly, Snail expression is present in the developing pancreas of sheep and mouse, in contrast to the differentiated pancreas, where Snail levels are markedly decreased (Cole *et al.*, 2009; Rukstalis *et al.*, 2006). Recently, it was demonstrated in differentiating myoblasts that ectopic Snail expression blocks their entry into differentiation. During growth phase of myoblasts, Snail directly binds to various differentiation-specific genes to repress them (Soleimani *et al.*, 2012). In another study about hair follicle morphogenesis, transgenic mice with sustained epidermal Snail expression are small and have a distorted differentiation of the epidermis (Jamora *et al.*, 2005). Also, in pancreatic endocrine cell lines, Snail impedes differentiation and is inversely correlated with hormone expression, which tags adult cells (Rukstalis *et al.*, 2006).

The data shown in this study strongly support these findings, proposing a substantial role of

Snail in development of the pancreatic exocrine department. Prolonged expression of Snail, as it is the case in *Snail*$^{KI/+}$ mice, hinders the cells from maintaining differentiation, converting them back into an embryonic-like state. This is likely due to direct or indirect repression of adult pancreatic markers like Ptf1a. In *Snail*$^{KI/KI}$ animals with biallelic Snail expression, this effect is even stronger, leading to a particularly reduced production of essential pancreatic digestion enzymes and dramatic growth retardation. The exocrine insufficiency is proofed and efficiently rescued by provision of pancreatic enzymes, which leads to significant weight gain of the mice.

Most likely, this dedifferentiation induced by Snail expression results in the development of acinar tumors. As the development of acinar cell carcinoma does not occur with complete penetrance, at least not in *Snail*$^{KI/+}$ mice, it seems that a certain Snail expression threshold is needed to fulfill tumor-favoring conditions, resulting in an increased incidence of tumor formation as well as accelerated tumor progression. Concomitant with this, Snail activation in human mammary epithelial cells increases the ability to form soft agar colonies as an *in vitro* measurement of tumorigenicity. Also, formation of mammospheres and tumor spheres was shown to be augmented, which both are associated with stemness (Mani *et al.*, 2008). In colonospheres of colorectal cancer cells, Snail is co-expressed with the stem cell marker CD44, and overexpression of Snail in colorectal cancer cells induces cell dedifferentiation (Hwang *et al.*, 2011). Presumably, remaining Snail expression in the adult pancreas facilitates tumor formation by inducing an undifferentiated, stem cell-like state as indicated by increased CD44 expression as well as by enrichment of stem cell signatures and increased proliferation.

An important point which has to be addressed to support this theory is whether Snail completely prevents the acinar cells from differentiation throughout embryonic and adult state or if the cells dedifferentiate more and more with increasing age. Also, it is still of interest, why classical stem cell markers like CD133, Nestin, or Oct3/4 are not affected by Snail expression. Here, additional investigations are required to reveal the mechanism how Snail contributes to the acquisition of stem cell-like properties.

In agreement with the data found in *Snail*$^{KI/+}$ mice, Snail expression in the Kras^{G12D}-driven PDAC model induces a developmental phenotype with increased proliferation and stem cell-like features, resulting in acceleration of Kras^{G12D}-dependent premalignant ductal lesion formation and rapid PDAC progression, although Snail alone is not sufficient to initiate PDAC. Embryonic pathways that normally act during cell differentiation such as Wnt-β-catenin, Notch, and Hedgehog signaling are frequently deregulated during PDAC (Morris *et al.*, 2010).

Taking this into account, the influence of developmentally related pathways on PDAC is indisputable. A connection between developmentally active genes and pancreatic cancer was further confirmed in a recent genome-wide association study of nearly 4000 pancreatic cancer cases (Li *et al.*, 2012). Snail is likely to be one of these numerous factors, which on the one hand orchestrate embryonic development of the pancreas and further organs and on the other hand participate in the network of pancreatic tumor initiation and progression, when pathologically activated.

5.3 Snail overcomes senescence and favors cellular stress by interfering with the G1/S checkpoint

Senescence is an important tumor suppressive mechanism, preventing transformed cells from uncontrolled proliferation (Reinhardt and Schumacher, 2012). Besides its role in initiation of pancreatic cancer, activated Kras was shown to trigger the so-called oncogene-induced senescence in premalignant lesions of pancreatic cancer and other tumors, preventing from progression to higher-graded lesions and tumor development (Collado and Serrano, 2010). Consistent with this, senescence is detected in PanIN lesions of 3-month-old *Kras* mice. In contrast, a bypass of senescence is observed in preneoplastic lesions of *Kras;Snail*$^{KI/+}$ animals. It was shown before that Snail knockdown induces senescence in prostate cancer cells (Emadi Baygi *et al.*, 2010), but generally, the interplay between Snail and senescence-associated factors is not well-defined.

Importantly, this work shows that senescence is bypassed by strongly augmented acinar proliferation. During development, proliferation is a pivotal process for embryonic growth, whereas in adults the cell cycle is arrested in most cells. By contrast, under pathological conditions like cancer, a high level of proliferation favors tumor growth, and generally leads to a bad outcome (Hanahan and Weinberg, 2011). The role of Snail in proliferation is controversial. Interestingly, Snail represses cyclin D2 and thereby impairs cell cycle progression in MDCK cells and mouse embryos (Vega *et al.*, 2004). Further, Snail depletion in the murine liver induces proliferation, which is accompanied by the upregulation of cell cycle-related proteins (Sekiya and Suzuki, 2011). Instead, hyperproliferation is exhibited by transgenic mice, which ectopically express Snail in the skin epidermis (Jamora *et al.*, 2005), and decreased proliferation is observed after Snail knockdown in murine squamous and spindle cell carcinoma cells as well as in human glioblastoma cell lines (Han *et al.*, 2011; Olmeda *et al.*, 2007). Apparently, the influence of Snail on proliferation and cell cycle is highly context- and tissue-specific, as the expression levels of possible Snail targets and co-factors vary strongly among different cellular contexts.

Aberrant activation of both the phosphoinositide 3-kinase (PI3K) and the mitogen-activated protein kinase (MAPK) pathway often result in increased proliferation and bypass of senescence (Vanhaesebroeck *et al.*, 2012; Pylayeva-Gupta *et al.*, 2011). Both pathways are active in Snail-expressing MDCK cells, where stimulation of Akt phosphorylation works at least in part through direct repression of the Akt-inhibitor PTEN (Vega *et al.*, 2004; Escrivà *et al.*, 2008). Also, in transgenic mice with epidermal Snail expression, PI3K and MAPK activation could be observed in the Snail-positive regions (Jamora *et al.*, 2005; Du *et al.*, 2010). Further, during TGFβ-induced EMT of lens epithelial cells and in several tumor cell lines, PI3K-signaling has been positioned downstream from Snail (Villagrasa *et al.*, 2011; Cho *et al.*, 2007). These findings implicate that increased proliferation and bypass of senescence could depend on Snail-directed PI3K and MAPK stimulation also in the used pancreatic *in vivo* model. However, the results of this work do not show any overt influence of Snail on neither PI3K nor MAPK activity, thus refuting this theory.

One of the cell cycle-regulating mechanisms is the G2/M checkpoint, preventing cells with genomic DNA damage in gap 2 phase (G2) from entering mitosis (M) (Malumbres and Barbacid, 2009). With increased rate of proliferation, more spontaneous chromosome breaks can occur, resulting in augmented DNA damage repair (DDR). Indeed, independently of activated $Kras^{G12D}$, Snail-expressing mice show significantly higher DNA damage rates, indicating a high Snail-induced cellular stress level. The cell-intrinsic response to genomic instability is characterized by induction of DDR pathways, which are often mediated through the tumor suppressor Trp53, finally leading to temporary cell cycle arrest, apoptosis, or senescence (Reinhardt and Schumacher, 2012). As Snail-expressing mice bypass senescence, it is important to evaluate whether Trp53 is still functional in the used mouse model. Pancreatic and other tumors frequently carry a *TP53* mutation, which inhibits its tumor suppressor function (Bardeesy and DePinho, 2002; Lüttges *et al.*, 2001; Rozenblum *et al.*, 1997). PanINs of *Kras* mice, in contrast to normal ducts, have been shown to be Trp53 positive and also exhibit expression of its target $p21^{CIP1}$, pointing out Trp53 functionality. In *Kras* animals carrying an additional $Trp53^{R172H}$ mutation, tumors develop after loss of the remaining Trp53 wild type allele, accompanied by accumulation of mutant $Trp53^{R172H}$ protein. Mutant $Trp53^{R172H}$ is not capable to transcriptionally activate $p21^{CIP1}$, leading to maintenance of Trp53 expression in PDAC and advanced PanIN lesions, whereas $p21^{CIP1}$ is lost (Morton *et al.*, 2010). Trp53 functionality is retained in $Kras;Snail^{KI/+}$ animals, as high-grade PanIN lesions and tumor cells of these mice express both Trp53 and $p21^{CIP1}$. Also, cells isolated from respective tumors exhibit expression of both proteins when stimulated with the topoisomerase inhibitor etoposide. Importantly, Trp53 functionality is proofed on genetic level,

since dominant-negative oncogenic Trp53^{R172H} in *Kras;Snail$^{KI/+}$;p53^{mut}* mice further significantly accelerates tumor development, which is even stronger in mice carrying a homozygous Trp53^{R172H} mutation. These data imply that the tumor suppressor Trp53 is still functional in Snail-expressing mice, and that the bypass of senescence most probably has a different origin.

Apoptosis is essential to remove damaged or redundant cells and often is disturbed in cancer (Hamacher *et al.*, 2008). In this work, young Snail-expressing mice have a significantly higher apoptosis rate than control cohorts, however, Snail is generally seen as a promoter of apoptotic resistance. In MDCK cells, Snail confers resistance to TGFβ-induced cell death and in the developing mouse embryo, an inverse correlation between Snail expression and cell death is observed (Vega *et al.*, 2004; Martínez-Álvarez *et al.*, 2004). Further, in human cancer cells, Snail expression promotes resistance to cell death induced by a topoisomerase inhibitor (Kajita *et al.*, 2004). These facts raise the question, why *Snail$^{KI/+}$* mice exhibit a contrary behavior. One can argue that the effect of Snail on apoptosis is highly dependent on the experimental context, as it is obviously true for Snail-induced proliferation. Because pancreas-specific Snail expression in the mouse model of pancreatic cancer promotes tumor evolution, Snail can be rather seen as an oncogene than an inducer of EMT in this context, and oncogene expression generally is able to induce apoptosis (Pylayeva-Gupta *et al.*, 2011; Strasser *et al.*, 2011). This might occur directly or indirectly, as it is likely that apoptosis, as increased DNA damage, is a side effect of Snail-induced cellular stress. However, the exact interplay between Snail, DNA damage response, and apoptosis still has to be elucidated not only in pancreatic cancer.

A key role in cell cycle regulation is played by cyclin-dependent kinases (CDKs) that need to form a complex with cyclins to be activated, resulting in entering of the cell cycle. In a healthy organism, progression through the cell cycle is strictly monitored by checkpoints that, once activated, induce cell cycle arrest. (Malumbres and Barbacid, 2009). One regulatory checkpoint is the G1/S restriction point, which controls the transition of cells through the gap 1 (G1) phase to enter the DNA synthesis phase (S). Here, p16^{INK4A}, a tumor suppressor which is often lost in PDAC (Hezel *et al.*, 2006) and appears to be a principal factor in senescence regulation (Romagosa *et al.*, 2011), plays a pivotal role. It is encoded by the *Cdkn2a* locus together with p19^{ARF}, a further tumor suppressor which inhibits Mdm2 and thereby is involved in Trp53 activation (Hezel *et al.*, 2006). The *Cdkn2a* locus is kept in all *Kras;Snail$^{KI/KI}$* mice, whereas in most of the *Kras* animals, it is lost most probably due to selective pressure. Further, microarray analysis show that PDAC cell lines isolated from *Kras;Snail$^{KI/+}$* mice partly exhibit p16^{INK4A}/p19^{ARF} expression, whereas in nearly all tested *Kras* cell lines, p16^{INK4A}/p19^{ARF}

is lost. Unfortunately, in this setting it is not possible to distinguish between $p16^{INK4A}$ and $p19^{ARF}$, because as the locus is shared, the same probe is used for detection of both mRNAs. qPCR analysis of PDAC tissue reveals a generally higher level of $p16^{INK4A}$ but not $p19^{ARF}$ mRNA in Snail-expressing mice. Basal levels in these mice can be explained by stromal expression, which is not existing in cell lines. Most importantly, in *Kras;Snail$^{KI/+}$;Ink$^{*/+}$* mice loss of $p16^{INK4A}$ does not accelerate PDAC evolution when compared with *Kras;Snail$^{KI/+}$* cohorts. In contrast, conditional knock-out of both $p16^{INK4A}$ and $p19^{ARF}$ in *Kras;Snail$^{KI/+}$; Cdkn2a$^{lox/+}$* mice results in rapid tumor formation and significant reduction of median survival. This leads to the conclusion that Snail induces proliferation by misregulation of the G1/S restriction point by interfering directly with $p16^{INK4A}$ or having an influence on $p16^{INK4A}$ downstream targets, whereas $p19^{ARF}$ is not affected and still functional. Although a direct influence of Snail on $p16^{INK4A}$ cannot be excluded in this model, an indirect interaction, like a reduced need for selective pressure on loss of $p16^{INK4A}$, is more presumable, as especially in heterozygous *Kras;Snail$^{KI/+}$* mice the integrity of the *Cdkn2a* locus as well as $p16^{INK4A}$ expression are not consistently present. Comparative genomic hybridization (CGH) arrays comparing *Kras* with *Kras;Snail$^{KI/+}$* animals will supply more detailed data about the *Cdkn2a* locus and the effect of Snail expression on genetic integrity in general.

$p16^{INK4A}$ and further suppressors prevent binding of cyclin-dependent kinases (CDK) 4 and 6 to cyclin D. During the active cell cycle, this CDK/cyclin complex phosphorylates and thereby inactivates the retinoblastoma (Rb) protein, leading to its dissociation from E2F transcription factors and finally to entry into S phase (Bardeesy *et al.*, 2006). Rb has been described as a crucial tumor suppressor and it is thought to be inactivated indirectly or directly in almost all human cancers. This is also true for PDAC, as deletion of Rb strongly accelerates $Kras^{G12D}$-dependent tumor formation by inhibiting senescence. In contrast, activating mutations of the Rb binding partners of the E2F family are rare events, still E2F transcription factors play a role during tumor formation, as mutations of the E2F1 gene reduce pituitary and thyroid tumor formation which characterize Rb mutant mice (Carrière *et al.*, 2011; Burkhart and Sage, 2008). It is no surprise that highly increased Rb phosphorylation is observed in preneoplastic lesions of young *Kras;Snail$^{KI/+}$* mice, suggesting a Snail-dependent uncontrolled entry into S phase. Rb inactivity and E2F activity are further supported by microarray data, which show a significant enrichment of E2F target genes in Snail-expressing mice independently of activated Kras. It is likely that Snail represses one or several of the numerous factors which function during regulation of the G1/S transition, leading to uncontrolled proliferation, but although this work highlights an important role of Snail during cell cycle progression control, the exact mechanism still has to be revealed.

Especially, cyclin expression levels and activity of CDK4/6, as linkers between $p16^{INK4A}$ and Rb during the G1/S restriction point, have to be tested to find out how and where Snail interacts with the cell cycle.

5.4 Outlook: Investigation of possible direct transcriptional targets of Snail and beyond

One question that has been raised through this study is, which are potential direct targets of Snail when expressed *in vivo* in the pancreas. As the well-known downstream target Cdh1 does not seem to be influenced by Snail in this experimental context, it is likely that Snail binds and affects different target genes thus leading to the phenotype described above. To get a gross imagination of possible Snail targets, microarray analysis of pancreatic tissue samples of differently-aged mice with various tumor stages was conducted to detect genes that are continuously regulated in Snail-expressing mice. Some of these genes have already been implicated in tumorigenesis or proliferation and therefore are now considered for further examination. Binding of Snail to their promoters will be tested in pancreatic tissue and cell lines by chromatin immunoprecipitation (ChIP). Also, chromatin immunoprecipitation sequencing (ChIP-seq) using pancreatic tissue of young $Snail^{KI/+}$ mice will broaden our knowledge by revealing new Snail binding sites. Further validation of herein identified genes and signatures will be of great interest.

In this work, Snail was conditionally overexpressed in all pancreatic cell types with help of the $Ptf1a^{Cre/+}$ mouse line. Also, by acinar cell-specific expression of Snail using the $Ela1\text{-}Cre^{ERT2}$ line, a comparable phenotype could be observed. But PDAC is further characterized by abundance of stroma, which is composed of extracellular matrix (ECM) proteins, stellate cells, fibroblasts, immune cells, neurons, and endothelial cells (Erkan *et al.*, 2012). It would be interesting to know if Snail overexpression alters the stromal reaction to influence tumor development. Conditional expression of Snail in different stromal cell types in the $Kras^{G12D}$-dependent mouse model can be achieved by combination of 2 different recombination systems, namely Flp-frt and Cre-loxP (unpublished data PD Dr. Dieter Saur).

As pancreas-specific expression of Snail causes several changes with impact on pancreatic differentiation and cancer development, it would also be important to know what happens if Snail is lost in different cell types of the pancreas as well as in the stroma. Application of the available conditional Snail knock-out mouse (Murray and Gridley, 2006 b) in combination with the $Kras^{G12D}$-dependent PDAC model therefore will be a crucial step.

Finally, it will be very useful to cross the newly developed Snail knock-in overexpression mouse into other GEMs of cancer and further diseases, as in this work it was demonstrated

that Snail undoubtedly is an important player of the molecular machinery of cancer and beyond. Thus, in the long term, this mouse model will serve as a tool to provide us with new therapeutic approaches for pancreatic cancer and other diseases.

6 Summary

Pancreatic ductal adenocarcinoma (PDAC) is a dismal disease with 5-year survival rates below 6% due to lack of successful therapeutic approaches. The transcription factor Snail plays a crucial role in epithelial-mesenchymal transition (EMT) and is overexpressed in PDAC, but so far, little is known about the functions of Snail in this kind of cancer.

In this work, the *in vivo* role of Snail in pancreatic differentiation, carcinogenesis, metastasis, and EMT was investigated in a new genetically engineered mouse model. Therefore, a latent *Snail* allele silenced by a lox-stop-lox (LSL) cassette as a knock-in at the murine *Rosa26* locus was generated (*LSL-Rosa26*$^{Snail/+}$). Expression of Snail in the pancreas was activated using a pancreas-specific Cre driver line (*Ptf1a*$^{Cre/+}$). Mice with pancreas-specific Snail expression from one *Rosa26* allele (*Snail*$^{KI/+}$) exhibited normal development but showed focal acinar dedifferentiation. Increasing gene dose by expressing Snail from both *Rosa26* alleles (*Snail*$^{KI/KI}$) resulted in dramatic growth retardation caused by exocrine dysfunction and acinar dedifferentiation. In both cases, expression of pancreatic differentiation markers was markedly reduced and development of metastatic acinar cell carcinoma was observed. Besides, increased CD44 levels and a stem cell signature was exhibited by *Snail*$^{KI/+}$ mice.

For investigation of Snail functions during pancreatic carcinogenesis, the *LSL-Rosa26*$^{Snail/+}$ line was crossed into the well-established Kras^{G12D}-dependent PDAC model to generate *Kras;Snail*$^{KI/+}$ animals, which developed invasive PDAC. Median survival was shortened to 6 months compared to 15 months in *Kras* mice. Biallelic Snail expression further reduced median survival to 2 months. Interestingly, PDAC from Snail-expressing mice showed a well-differentiated morphology without signs of EMT or increased metastasis. Instead, investigation of precursor lesions revealed acceleration of their formation and progression due to bypass of senescence and increased proliferation, which was accompanied by augmented DNA damage and apoptosis. Whereas the tumor suppressors Trp53 and p19^{ARF} were still functional and not influenced by Snail, activity of the cell cycle regulator p16^{INK4A} was at least partly bypassed, as pressure on its loss was reduced in Snail-expressing animals, and p16^{INK4A} inactivation in *Kras;Snail*$^{KI/+}$*;Ink*$^{*/+}$ mice did not decrease median survival. Further, high retinoblastoma protein phosphorylation as well as enrichment of E2F transcription factor targets in these mice indicated dysregulated cell cycle activity.

The results shown in this work provide important new insights into Snail gene function as tumor promoter for pancreatic cancer *in vivo*. Further investigation of the underlying mechanisms and determination of unknown Snail target genes will open potential novel therapeutic strategies for this fatal disease.

7 Zusammenfassung

Mit einer 5-Jahres Überlebensrate unter 6% ist das duktale Pankreaskarzinom (PDAC) eine der aggressivsten und tödlichsten Krebserkrankungen in der westlichen Welt. Der Transkriptionsfaktor Snail spielt eine entscheidende Rolle bei der Epithelial-mesenchymalen Transition (EMT) und ist im humanen PDAC stark überexprimiert.

In der vorliegende Arbeit wurde die Rolle von Snail im Pankreas für die Differenzierung, Karzinogenese, EMT und Metastasierung im endogenen genetisch definierten murinen Modell untersucht. Um Snail pankreasspezifisch zu exprimieren, wurde eine konditionale Knock-in Mauslinie generiert. Hierzu wurde eine Snail-Expressionskassette, deren Expression durch eine lox-Stop-lox (LSL) Kassette blockiert ist, in den *Rosa26*-Lokus inseriert (*LSL-Rosa26*$^{Snail/+}$). In dieser Linie wurde Snail durch pankreasspezifische Expression der Cre-Rekombinase unter der Kontrolle des *Ptf1a* Promotors (*Ptf1a*$^{Cre/+}$) aktiviert. Heterozygote Mäuse mit pankreasspezifischer Snail-Expression (*Snail*$^{KI/+}$) entwickelten sich regelgerecht, wiesen jedoch eine fokale Dedifferenzierung der Azini auf. Erhöhung der Snail-Gendosis durch Expression von beiden Allelen des *Rosa26*-Lokus führte zu einer dramatischen Wachstumsretardierung durch exokrine Dysfunktion und azinäre Dedifferenzierung. Beide Genotypen wiesen eine reduzierte Expression pankreatischer Differenzierungsmarker auf und entwickelten metastatische azinäre Pankreaskarzinome. Passend hierzu führt Snail zu einer erhöhten CD44-Expression und einer Stammzellsignatur im Pankreas.

Um die Rolle von Snail in der Karzinogenese des PDAC zu untersuchen, wurde die *LSL-Rosa26*$^{Snail/+}$ Linie in das etablierte Kras^{G12D}-abhängige PDAC-Modell eingekreuzt, um *Kras;Snail*$^{KI/+}$ Tiere zu generieren. Diese entwickelten invasive Tumore mit einer dramatischen Akzeleration der Karzinogenese und einer auf 6 Monate verkürzten mittleren Überlebenszeit, die in *Kras* Mäusen bei 15 Monaten liegt. Die biallelische Snail-Expression führte zu einer weiteren Akzeleration der PDAC-Entstehung mit einer mittleren Überlebenszeit von 2 Monaten. Interessanterweise wiesen alle PDACs eine gut differenzierte Morphologie ohne Anzeichen einer EMT oder erhöhter Metastasierungsrate auf. Anstatt EMT zu induzieren, führte Snail zu einer schnelleren Entstehung und Progression von Vorläuferläsionen des PDAC durch Blockade der Seneszenz sowie gesteigerte Proliferation. Zusätzlich wurde eine erhöhte zelluläre Antwort auf DNA-Schaden sowie höhere Apoptoseraten beobachtet. In diesem Modell waren die beiden Tumorsuppressoren Trp53 und p19^{ARF} funktionell intakt und nicht von Snail beeinflusst. Die Funktion des Zellzyklusregulators p16^{INK4A} hingegen wurde zumindest teilweise umgangen, denn es konnte ein verringerter Druck auf dessen Verlust nachgewiesen werden. Weiterhin führte die

genetische Inaktivierung von $p16^{INK4A}$ in *Kras;Snail*$^{KI/+}$*;Ink*$^{*/+}$ Tieren zu keiner signifikanten Änderung der mittleren Überlebenszeit. Fehlregulation des Zellzyklus konnte außerdem durch gesteigerte Phosphorylierung des Retinoblastom-Proteins und eine Anreicherung von E2F-Zielgenen in Snail-exprimierenden Mäusen nachgewiesen werden.

Die Erkenntnisse der vorliegenden Arbeit zeigen die Bedeutung von Snail als Tumorpromotor *in vivo*. Eine genaue Untersuchung der zugrunde liegenden Mechanismen sowie die Bestimmung von bisher unbekannten Snail-Zielgenen werden neue therapeutische Strategien für die Bekämpfung des duktalen Pankreaskarzinoms eröffnen.

8 References

Abraham SC, Wu T-T, Hruban RH, *et al.* (2002). Genetic and immunohistochemical analysis of pancreatic acinar cell carcinoma: frequent allelic loss on chromosome 11p and alterations in the APC/beta-catenin pathway. *The American Journal of Pathology* **160**: 953–62.

Aguirre AJ, Bardeesy N, Sinha M, *et al.* (2003). Activated Kras and Ink4a/Arf deficiency cooperate to produce metastatic pancreatic ductal adenocarcinoma. *Genes & Development* **17**: 3112–26.

Alberga A, Boulay J-L, Kempe E, *et al.* (1991). The snail gene required for mesoderm formation in Drosophila is expressed dynamically in derivatives of all three germ layers. *Development* **111**: 983–92.

Almoguera C, Shibata D, Forrester K, *et al.* (1988). Most human carcinomas of the exocrine pancreas contain mutant c-K-ras genes. *Cell* **53**: 549–54.

Ansieau S, Bastid J, Doreau A, *et al.* (2008). Induction of EMT by twist proteins as a collateral effect of tumor-promoting inactivation of premature senescence. *Cancer Cell* **14**: 79–89.

Bachelder RE, Yoon S-O, Franci C, *et al.* (2005). Glycogen synthase kinase-3 is an endogenous inhibitor of Snail transcription: implications for the epithelial-mesenchymal transition. *The Journal of Cell Biology* **168**: 29–33.

Bardeesy N, Aguirre AJ, Chu GC, *et al.* (2006). Both p16(Ink4a) and the p19(Arf)-p53 pathway constrain progression of pancreatic adenocarcinoma in the mouse. *Proceedings of the National Academy of Sciences* **103**: 5947–52.

Bardeesy N, and DePinho RA. (2002). Pancreatic cancer biology and genetics. *Nature Reviews Cancer* **2**: 897–909.

Barrallo-Gimeno A, and Nieto MA. (2009). Evolutionary history of the Snail/Scratch superfamily. *Trends in Genetics* **25**: 248–52.

Barrallo-Gimeno A, and Nieto MA. (2005). The Snail genes as inducers of cell movement and survival: implications in development and cancer. *Development* **132**: 3151–61.

Del Barrio MG, and Nieto MA. (2002). Overexpression of Snail family members highlights their ability to promote chick neural crest formation. *Development* **129**: 1583–93.

Batlle E, Sancho E, Francí C, *et al.* (2000). The transcription factor snail is a repressor of E-cadherin gene expression in epithelial tumour cells. *Nature Cell Biology* **2**: 84–9.

Ben-Porath I, Thomson MW, Carey VJ, *et al.* (2008). An embryonic stem cell-like gene expression signature in poorly differentiated aggressive human tumors. *Nature Genetics* **40**: 499–507.

Benjamini Y, and Hochberg Y. (1995). Controlling the false discovery rate: A practical and powerful approach to multiple testing. *Journal of the Royal Statistical Society* **57**: 289–300.

Blanco MJ, Moreno-Bueno G, Sarrio D, *et al.* (2002). Correlation of Snail expression with histological grade and lymph node status in breast carcinomas. *Oncogene* **21**: 3241–6.

Blechschmidt K, Sassen S, Schmalfeldt B, *et al.* (2008). The E-cadherin repressor Snail is associated with lower overall survival of ovarian cancer patients. *British Journal of Cancer* **98**: 489–95.

Boutet A, De Frutos CA, Maxwell PH, *et al.* (2006). Snail activation disrupts tissue homeostasis and induces fibrosis in the adult kidney. *The EMBO Journal* **25**: 5603–13.

Bradford MM. (1976). A rapid and sensitive method for the quantitation of microgram quantities of protein utilizing the principle of protein-dye binding. *Analytical Biochemistry* **72**: 248–54.

Brembeck FH, Schreiber FS, Deramaudt TB, *et al.* (2003). The mutant K-ras oncogene causes pancreatic periductal lymphocytic infiltration and gastric mucous neck cell hyperplasia in transgenic mice. *Cancer Research* **63**: 2005–9.

Broos S, Hulpiau P, Galle J, *et al.* (2011). ConTra v2: a tool to identify transcription factor binding sites across species, update 2011. *Nucleic Acids Research* **39**: W74–8.

Burkhart DL, and Sage J. (2008). Cellular mechanisms of tumour suppression by the retinoblastoma gene. *Nature Reviews Cancer* **8**: 671–82.

Burris III HA, Moore MJ, Andersen J, *et al.* (1997). Improvements in survival and clinical benefit with gemcitabine as first-line therapy for patients with advanced pancreas cancer: a randomized trial. *Journal of Clinical Oncology* **15**: 2403–13.

von Burstin J, Eser S, Paul MC, *et al.* (2009). E-cadherin regulates metastasis of pancreatic cancer in vivo and is suppressed by a SNAIL/HDAC1/HDAC2 repressor complex. *Gastroenterology* **137**: 361–71.

Cano A, Pérez-Moreno MA, Rodrigo I, *et al.* (2000). The transcription factor Snail controls epithelial-mesenchymal transitions by repressing E-cadherin expression. *Nature Cell Biology* **2**: 76–83.

Carrière C, Gore AJ, Norris AM, *et al.* (2011). Deletion of Rb accelerates pancreatic carcinogenesis by oncogenic Kras and impairs senescence in premalignant lesions. *Gastroenterology* **141**: 1091–101.

Carver EA, Jiang R, Lan Y, *et al.* (2001). The mouse Snail gene encodes a key regulator of the epithelial-mesenchymal transition. *Molecular and Cellular Biology* **21**: 8184–8.

Chames P, Kerfelec B, and Baty D. (2010). Therapeutic antibodies for the treatment of pancreatic cancer. *Stress* **10**: 1107–20.

Chen H-Z, Tsai S-Y, and Leone G. (2009). Emerging roles of E2Fs in cancer: an exit from cell cycle control. *Nature Reviews Cancer* **9**: 785–97.

Cheng J-C, Klausen C, and Leung PCK. (2010). Hydrogen peroxide mediates EGF-induced down-regulation of E-cadherin expression via p38 MAPK and snail in human ovarian cancer cells. *Molecular Endocrinology* **24**: 1569–80.

Cho HJ, Baek KE, Saika S, *et al.* (2007). Snail is required for transforming growth factor-beta-induced epithelial-mesenchymal transition by activating PI3 kinase/Akt signal pathway. *Biochemical and Biophysical Research Communications* **353**: 337–43.

Christofori G, and Semb H. (1999). The role of the cell-adhesion molecule E-cadherin as a tumour-suppressor gene. *Trends in Biochemical Sciences* **24**: 73–76.

Cicchini C, Filippini D, Coen S, *et al.* (2006). Snail controls differentiation of hepatocytes by repressing HNF4a expression. *Journal of Cellular Physiology* **238**: 230–238.

Ciruna B, and Rossant J. (2001). FGF signaling regulates mesoderm cell fate specification and morphogenetic movement at the primitive streak. *Developmental Cell* **1**: 37–49.

Cole L, Anderson M, Antin PB, *et al.* (2009). One process for pancreatic beta-cell coalescence into islets involves an epithelial-mesenchymal transition. *The Journal of Endocrinology* **203**: 19–31.

Collado M, and Serrano M. (2010). Senescence in tumours: evidence from mice and humans. *Nature Reviews Cancer* **10**: 51–7.

Costello E, Greenhalf W, and Neoptolemos JP. (2012). New biomarkers and targets in pancreatic cancer and their application to treatment. *Nature Reviews Gastroenterology & Hepatology* **9**: 435–44.

Cotter TG. (2009). Apoptosis and cancer: the genesis of a research field. *Nature Reviews Cancer* **9**: 501–7.

Cowden J, and Levine M. (2002). The Snail repressor positions Notch signaling in the Drosophila embryo. *Development* **129**: 1785–93.

De Craene B, Gilbert B, Stove C, *et al.* (2005).(a). The transcription factor snail induces tumor cell invasion through modulation of the epithelial cell differentiation program. *Cancer Research* **65**: 6237–44.

De Craene B, Van Roy F, and Berx G. (2005).(b). Unraveling signalling cascades for the Snail family of transcription factors. *Cellular Signalling* **17**: 535–47.

Dominguez D, Montserrat-Sentis B, Virgos-Soler A, *et al.* (2003). Phosphorylation regulates the subcellular location and activity of the Snail transcriptional repressor. *Molecular and Cellular Biology* **23**: 5078–89.

Du F, Nakamura Y, Tan T-L, *et al.* (2010). Expression of Snail in epidermal keratinocytes promotes cutaneous inflammation and hyperplasia conducive to tumor formation. *Cancer Research* **70**: 10080–9.

Elloul S, Elstrand MB, Nesland JM, *et al.* (2005). Snail, Slug, and Smad-interacting protein 1 as novel parameters of disease aggressiveness in metastatic ovarian and breast carcinoma. *Cancer* **103**: 1631–43.

Emadi Baygi M, Soheili ZS, Schmitz I, *et al.* (2010). Snail regulates cell survival and inhibits cellular senescence in human metastatic prostate cancer cell lines. *Cell Biology and Toxicology* **26**: 553–67.

Erkan M, Hausmann S, Michalski CW, *et al.* (2012). The role of stroma in pancreatic cancer: diagnostic and therapeutic implications. *Nature Reviews Gastroenterology & Hepatology* **9**: 454–67.

Escrivà M, Peiró S, Herranz N, *et al.* (2008). Repression of PTEN phosphatase by Snail1 transcriptional factor during gamma radiation-induced apoptosis. *Molecular and Cellular Biology* **28**: 1528–40.

Fujita N, Jaye DL, Kajita M, *et al.* (2003). MTA3, a Mi-2/NuRD complex subunit, regulates an invasive growth pathway in breast cancer. *Cell* **113**: 207–19.

Gal A, Sjöblom T, Fedorova L, *et al.* (2008). Sustained TGF beta exposure suppresses Smad and non-Smad signalling in mammary epithelial cells, leading to EMT and inhibition of growth arrest and apoptosis. *Oncogene* **27**: 1218–30.

Gannon M, Herrera P-L, and Wright CVE. (2000). Mosaic Cre-mediated recombination in pancreas using the pdx-1 enhancer/promoter. *Genesis* **26**: 143–4.

Gentleman RC, Carey VJ, Bates DM, *et al.* (2004). Bioconductor: open software development for computational biology and bioinformatics. *Genome Biology* **5**: R80.

Glavic A, Silva F, Aybar MJ, *et al.* (2004). Interplay between Notch signaling and the homeoprotein Xiro1 is required for neural crest induction in Xenopus embryos. *Development* **131**: 347–59.

Grau Y, Carteret C, and Simpson P. (1984). Mutations and chromosomal rearrangements affecting the expression of Snail, a gene involved in embryonic patterning in Drosophila melanogaster. *Genetics* **108**: 347–60.

Gregory PA, Bert AG, Paterson EL, *et al.* (2008). The miR-200 family and miR-205 regulate epithelial to mesenchymal transition by targeting ZEB1 and SIP1. *Nature Cell Biology* **10**: 593–601.

Grimes HL, Chan TO, Zweidler-McKay PA, *et al.* (1996). The Gfi-1 proto-oncoprotein contains a novel transcriptional repressor domain, SNAG, and inhibits G1 arrest induced by interleukin-2 withdrawal. *Molecular and Cellular Biology* **16**: 6263–72.

Grippo PJ, Nowlin PS, Demeure MJ, *et al.* (2003). Preinvasive pancreatic neoplasia of ductal phenotype induced by acinar cell targeting of mutant Kras in transgenic mice. *Cancer Research* **63**: 2016–9.

Gupta S, and El-Rayes BF. (2008). Small molecule tyrosine kinase inhibitors in pancreatic cancer. *Biologics: Targets & Therapy* **2**: 707–15.

Guz Y, Montminy MR, Stein R, *et al.* (1995). Expression of murine STF-1, a putative insulin gene transcription factor, in beta cells of pancreas, duodenal epithelium and pancreatic exocrine and endocrine progenitors during ontogeny. *Development* **121**: 11–8.

Hamacher R, Schmid RM, Saur D, *et al.* (2008). Apoptotic pathways in pancreatic ductal adenocarcinoma. *Molecular Cancer* **7**: 64.

Han S-P, Kim J-H, Han M-E, *et al.* (2011). SNAI1 is involved in the proliferation and migration of glioblastoma cells. *Cellular and Molecular Neurobiology* **31**: 489–96.

Hanahan D, and Weinberg RA. (2011). Hallmarks of cancer: The next generation. *Cell* **144**: 646–74.

Hardy RG, Vicente-Dueñas C, González-Herrero I, *et al.* (2007). Snail family transcription factors are implicated in thyroid carcinogenesis. *The American Journal of Pathology* **171**: 1037–46.

Heebøll S, Borre M, Ottosen PD, *et al.* (2009). Snail1 is over-expressed in prostate cancer. *Acta Pathologica, Microbiologica, et Immunologica Scandinavica* **117**: 196–204.

Herranz N, Pasini D, Díaz VM, *et al.* (2008). Polycomb complex 2 is required for E-cadherin repression by the Snail1 transcription factor. *Molecular and Cellular Biology* **28**: 4772–81.

Hezel AF, Kimmelman AC, Stanger BZ, *et al.* (2006). Genetics and biology of pancreatic ductal adenocarcinoma. *Genes & Development* **20**: 1218–49.

Hingorani SR, Petricoin EF, Maitra A, *et al.* (2003). Preinvasive and invasive ductal pancreatic cancer and its early detection in the mouse. *Cancer Cell* **4**: 437–50.

Hingorani SR, Wang L, Multani AS, *et al.* (2005). Trp53R172H and KrasG12D cooperate to promote chromosomal instability and widely metastatic pancreatic ductal adenocarcinoma in mice. *Cancer Cell* **7**: 469–83.

Hong C, Moorefield KS, Jun P, *et al.* (2007). Epigenome scans and cancer genome sequencing converge on WNK2, a kinase-independent suppressor of cell growth. *Proceedings of the National Academy of Sciences* **104**: 10974–9.

Hoorens A, Lemoine NR, McLellan E, *et al.* (1993). Pancreatic acinar cell carcinoma. An analysis of cell lineage markers, p53 expression, and Ki-ras mutation. *The American Journal of Pathology* **143**: 685–98.

Hotz B, Arndt M, Dullat S, *et al.* (2007). Epithelial to mesenchymal transition: expression of the regulators snail, slug, and twist in pancreatic cancer. *Clinical Cancer Research* **13**: 4769–76.

Hruban RH, Adsay NV, Albores–Saavedra J, *et al.* (2001). Pancreatic intraepithelial neoplasia - A new nomenclature and classification system for pancreatic duct lesions. *The American Journal of Surgical Pathology* **25**: 579–86.

Hruban RH, Goggins M, Parsons J, *et al.* (2000). Progression model for pancreatic cancer. *Clinical Cancer Research* **6**: 2969–72.

Hsu Y-C, Willoughby JJ, Christensen AK, *et al.* (2006). Mosaic Eyes is a novel component of the Crumbs complex and negatively regulates photoreceptor apical size. *Development* **133**: 4849–59.

Hughes SH, Greenhouse JJ, Petropoulos CJ, *et al.* (1987). Adaptor plasmids simplify the insertion of foreign DNA into helper-independent retroviral vectors. *Journal of Virology* **61**: 3004–12.

Hwang W-L, Yang M-H, Tsai M-L, *et al.* (2011). SNAIL regulates interleukin-8 expression, stem cell-like activity, and tumorigenicity of human colorectal carcinoma cells. *Gastroenterology* **141**: 279–91, 291.e1–5.

Ikenouchi J, Matsuda M, Furuse M, *et al.* (2003). Regulation of tight junctions during the epithelium-mesenchyme transition: direct repression of the gene expression of claudins/occludin by Snail. *Journal of Cell Science* **116**: 1959–67.

Inukai T, Inoue A, Kurosawa H, *et al.* (1999). SLUG, a ces-1-related zinc finger transcription factor gene with antiapoptotic activity, is a downstream target of the E2A-HLF oncoprotein. *Molecular Cell* **4**: 343–52.

Isaac A, Cohn MJ, Ashby P, *et al.* (2000). FGF and genes encoding transcription factors in early limb specification. *Mechanisms of Development* **93**: 41–8.

Jackson EL, Willis N, Mercer K, *et al.* (2001). Analysis of lung tumor initiation and progression using conditional expression of oncogenic K-ras. *Genes & Development* **15**: 3243–8.

Jamora C, Lee P, Kocieniewski P, *et al.* (2005). A signaling pathway involving TGF-beta2 and Snail in hair follicle morphogenesis. *PLoS Biology* **3**: e11.

Jiang R, Copeland N, Gilbert D, *et al.* (1997). Genomic organization and chromosomal localization of the mouse snail gene. *Mammalian Genome* **8**: 686–8.

Jun P, Hong C, Lal A, *et al.* (2009). Epigenetic silencing of the kinase tumor suppressor WNK2 is tumor-type and tumor-grade specific. *Neuro-Oncology* **11**: 414–22.

Kajita M, Mcclinic KN, and Wade PA. (2004). Aberrant expression of the transcription factors Snail and Slug alters the response to genotoxic stress. *Molecular and Cellular Biology* **24**: 7559–66.

Kajiyama H, Shibata K, Terauchi M, *et al.* (2007). Chemoresistance to paclitaxel induces epithelial-mesenchymal transition and enhances metastatic potential for epithelial ovarian carcinoma cells. *International Journal of Oncology* **31**: 277–83.

Kalluri R, and Weinberg RA. (2009). The basics of epithelial-mesenchymal transition. *The Journal of Clinical Investigation* **119**: 1420–8.

Kataoka H, Murayama T, Yokode M, *et al.* (2000). A novel Snail-related transcription factor Smuc regulates basic helix-loop-helix transcription factor activities via specific E-box motifs. *Nucleic Acids Research* **28**: 626–33.

Kawaguchi Y, Cooper B, Gannon M, *et al.* (2002). The role of the transcriptional regulator Ptf1a in converting intestinal to pancreatic progenitors. *Nature Genetics* **32**: 128–34.

Kisiel JB, Yab TC, Taylor WR, *et al.* (2012). Stool DNA testing for the detection of pancreatic cancer: assessment of methylation marker candidates. *Cancer* **118**: 2623–31.

Klimstra DS, Heffess CS, Oertel JE, *et al.* (1992). Acinar cell carcinoma of the pancreas. A clinicopathologic study of 28 cases. *The American Journal of Surgical Pathology* **16**: 815–37.

Klimstra DS. (2007). Nonductal neoplasms of the pancreas. *Modern Pathology* **20**: S94–112.

Knutson KL, Lu H, Stone B, *et al.* (2006). Immunoediting of cancers may lead to epithelial to mesenchymal transition. *Journal of Immunology* **177**: 1526–33.

Krapp A, Knofler M, Ledermann B, *et al.* (1998). The bHLH protein PTF1-p48 is essential for the formation of the exocrine and the correct spatial organization of the endocrine pancreas. *Genes & Development* **12**: 3752–63.

Krimpenfort P, Quon KC, Mooi WJ, *et al.* (2001). Loss of p16Ink4a confers susceptibility to metastatic melanoma in mice. *Nature* **413**: 83–6.

Laemmli UK. (1970). Cleavage of structural proteins during the assembly of the head of bacteriophage T4. *Nature* **227**: 680–5.

Leach SD. (2004). Mouse models of pancreatic cancer: the fur is finally flying! *Cancer Cell* **5**: 7–11.

Li D, Duell EJ, Yu K, *et al.* (2012). Pathway analysis of genome-wide association study data highlights pancreatic development genes as susceptibility factors for pancreatic cancer. *Carcinogenesis* **33**: 1384–90.

Liu G, McDonnell TJ, Montes de Oca Luna R, *et al.* (2000). High metastatic potential in mice inheriting a targeted p53 missense mutation. *Proceedings of the National Academy of Sciences* **97**: 4174–9.

Loh K, Chia JA, Greco S, *et al.* (2008). Bone morphogenic protein 3 inactivation is an early and frequent event in colorectal cancer development. *Genes, Chromosomes & Cancer* **47**: 449–60.

Lu Z, Ghosh S, Wang Z, *et al.* (2003). Downregulation of caveolin-1 function by EGF leads to the loss of E-cadherin, increased transcriptional activity of beta-catenin, and enhanced tumor cell invasion. *Cancer Cell* **4**: 499–515.

Lundgren K, Nordenskjöld B, and Landberg G. (2009). Hypoxia, Snail and incomplete epithelial-mesenchymal transition in breast cancer. *British Journal of Cancer* **101**: 1769–81.

Lüttges J, Galehdari H, Bröcker V, *et al.* (2001). Allelic loss is often the first hit in the biallelic inactivation of the p53 and DPC4 genes during pancreatic carcinogenesis. *The American Journal of Pathology* **158**: 1677–83.

Maitra A, Adsay NV, Argani P, *et al.* (2003). Multicomponent analysis of the pancreatic adenocarcinoma progression model using a pancreatic intraepithelial neoplasia tissue microarray. *Modern Pathology* **16**: 902–12.

Maitra A, and Hruban RH. (2008). Pancreatic cancer. *Annual Review of Pathology* **3**: 157–88.

Malumbres M, and Barbacid M. (2009). Cell cycle, CDKs and cancer: a changing paradigm. *Nature Reviews Cancer* **9**: 153–66.

Malumbres M, and Barbacid M. (2003). RAS oncogenes: the first 30 years. *Nature Reviews Cancer* **3**: 459–65.

Mani SA, Guo W, Liao M-J, *et al.* (2008). The epithelial-mesenchymal transition generates cells with properties of stem cells. *Cell* **133**: 704–15.

Martínez-Álvarez C, Blanco MJ, Pérez R, *et al.* (2004). Snail family members and cell survival in physiological and pathological cleft palates. *Developmental Biology* **265**: 207–18.

Mauhin V, Lutz Y, Dennefeld C, *et al.* (1993). Definition of the DNA-binding site repertoire for the Drosophila transcription factor Snail. *Nucleic Acids Research* **21**: 3951–7.

Mazur PK, Einwächter H, Lee M, *et al.* (2010). Notch2 is required for progression of pancreatic intraepithelial neoplasia and development of pancreatic ductal adenocarcinoma. *Proceedings of the National Academy of Sciences* **107**: 13438–43.

Miyoshi A, Kitajima Y, Kido S, *et al.* (2005). Snail accelerates cancer invasion by upregulating MMP expression and is associated with poor prognosis of hepatocellular carcinoma. *British journal of cancer* **92**: 252–8.

Moniz S, Veríssimo F, Matos P, *et al.* (2007). Protein kinase WNK2 inhibits cell proliferation by negatively modulating the activation of MEK1/ERK1/2. *Oncogene* **26**: 6071–81.

Montero JA, Gañan Y, Macias D, *et al.* (2001). Role of FGFs in the control of programmed cell death during limb development. *Development* **128**: 2075–84.

Moody SE, Perez D, Pan T, *et al.* (2005). The transcriptional repressor Snail promotes mammary tumor recurrence. *Cancer Cell* **8**: 197–209.

Morris JP, Wang SC, and Hebrok M. (2010). KRAS, Hedgehog, Wnt and the twisted developmental biology of pancreatic ductal adenocarcinoma. *Nature Reviews Cancer* **10**: 683–695.

Morton JP, Timpson P, Karim SA, *et al.* (2010). Mutant p53 drives metastasis and overcomes growth arrest/senescence in pancreatic cancer. *Proceedings of the National Academy of Sciences* **107**: 246–51.

Mukhopadhyay A, Deplancke B, Walhout AJM, *et al.* (2008). Chromatin immunoprecipitation (ChIP) coupled to detection by quantitative real-time PCR to study transcription factor binding to DNA in Caenorhabditis elegans. *Nature Protocols* **3**: 698–709.

Mullis K, Faloona F, Scharf S, *et al.* (1986). Specific enzymatic amplification of DNA in vitro: the polymerase chain reaction. *Cold Spring Harbor Symposia on Quantitative Biology* **51 Pt 1**: 263–73.

Murphy KM, Brune KA, Griffin C, *et al.* (2002). Evaluation of candidate genes MAP2K4, MADH4, ACVR1B, and BRCA2 in familial pancreatic cancer: deleterious BRCA2 Mutations in 17%. *Cancer Research* **62**: 3789–93.

Murray SA, and Gridley T. (2006).(a). Snail family genes are required for left-right asymmetry determination, but not neural crest formation, in mice. *Proceedings of the National Academy of Sciences* **103**: 10300–4.

Murray SA, and Gridley T. (2006).(b). Snail1 gene function during early embryo patterning in mice. *Cell Cycle* **5**: 2566–70.

Murray SA, Oram KF, and Gridley T. (2007). Multiple functions of Snail family genes during palate development in mice. *Development* **134**: 1789–97.

Nakhai H, Sel S, Favor J, *et al.* (2007). Ptf1a is essential for the differentiation of GABAergic and glycinergic amacrine cells and horizontal cells in the mouse retina. *Development* **134**: 1151–60.

Nieto MA, Bennett MF, Sargent MG, *et al.* (1992). Cloning and developmental expression of Sna, a murine homologue of the Drosophila snail gene. *Development* **116**: 227–37.

Nieto MA. (2002). The snail superfamily of zinc-finger transcription factors. *Nature Reviews Molecular Cell Biology* **3**: 155–66.

Nüsslein-Volhard C, Wieschaus E, and Kluding H. (1984). Mutations affecting the pattern of the larval cuticle in Drosophila melanogaster. *Wilhelm Roux's Archives of Developmental Biology* **193**: 267–82.

Offield MF, Jetton TL, Labosky PA, *et al.* (1996). PDX-1 is required for pancreatic outgrowth and differentiation of the rostral duodenum. *Development* **122**: 983–95.

Ohlsson H, Karlsson K, and Edlund T. (1993). IPF1, a homeodomain-containing transactivator of the insulin gene. *The EMBO Journal* **12**: 4251–9.

Olive KP, Tuveson DA, Ruhe ZC, *et al.* (2004). Mutant p53 gain of function in two mouse models of Li-Fraumeni syndrome. *Cell* **119**: 847–60.

Oliveira-Cunha M, Newman WG, and Siriwardena AK. (2011). Epidermal growth factor receptor in pancreatic cancer. *Cancers* **3**: 1513–26.

Olmeda D, Jordá M, Peinado H, *et al.* (2007). Snail silencing effectively suppresses tumour growth and invasiveness. *Oncogene* **26**: 1862–74.

Orban PC, Chui D, and Marth JD. (1992). Tissue- and site-specific DNA recombination in transgenic mice. *Proceedings of the National Academy of Sciences* **89**: 6861–5.

Ornitz D, Hammer R, Messing A, *et al.* (1987). Pancreatic neoplasia induced by SV40 T-antigen expression in acinar cells of transgenic mice. *Science* **238**: 188–93.

Park S-M, Gaur AB, Lengyel E, *et al.* (2008). The miR-200 family determines the epithelial phenotype of cancer cells by targeting the E-cadherin repressors ZEB1 and ZEB2. *Genes & Development* **22**: 894–907.

Patterson KI, Brummer T, Brien PMO, *et al.* (2009). Dual-specificity phosphatases: critical regulators with diverse cellular targets. *Biochemical Journal* **418**: 475–89.

Peinado H, Ballestar E, Esteller M, *et al.* (2004). Snail mediates E-cadherin repression by the recruitment of the Sin3A/histone deacetylase 1 (HDAC1)/HDAC2 complex. *Molecular and Cellular Biology* **24**: 306–19.

Peinado H, Olmeda D, and Cano A. (2007). Snail, Zeb and bHLH factors in tumour progression: an alliance against the epithelial phenotype? *Nature Reviews Cancer* **7**: 415–28.

Peinado H, Quintanilla M, and Cano A. (2003). Transforming growth factor beta-1 induces snail transcription factor in epithelial cell lines: mechanisms for epithelial mesenchymal transitions. *The Journal of Biological Chemistry* **278**: 21113–23.

Peiró S, Escrivà M, Puig I, *et al.* (2006). Snail1 transcriptional repressor binds to its own promoter and controls its expression. *Nucleic Acids Research* **34**: 2077–84.

Pellegata NS, Sessa F, Renault B, *et al.* (1994). K-ras and p53 gene mutations in pancreatic cancer: Ductal and nonductal tumors progress through different genetic lesions. *Cancer Research* **54**: 1556–60.

Pfaffl MW. (2001). A new mathematical model for relative quantification in real-time RT-PCR. *Nucleic Acids Research* **29**: e45.

Pylayeva-Gupta Y, Grabocka E, and Bar-Sagi D. (2011). RAS oncogenes: weaving a tumorigenic web. *Nature Reviews Cancer* **11**: 761–74.

Quaife CJ, Pinkert CA, Ornitz DM, *et al.* (1987). Pancreatic neoplasia induced by ras expression in acinar cells of transgenic mice. *Cell* **48**: 1023–34.

Rangarajan A, and Weinberg RA. (2003). Comparative biology of mouse versus human cells: modelling human cancer in mice. *Nature Reviews Cancer* **3**: 952–9.

Reinhardt HC, and Schumacher B. (2012). The p53 network: cellular and systemic DNA damage responses in aging and cancer. *Trends in Genetics* **28**: 128–36.

Richter A, Niedergethmann M, Sturm JW, *et al.* (2003). Long-term results of partial pancreaticoduodenectomy for ductal adenocarcinoma of the pancreatic head: 25-year experience. *World Journal of Surgery* **27**: 324–9.

Rigaud G, Moore PS, Zamboni G, *et al.* (2000). Allelotype of pancreatic acinar cell carcinoma. *International Journal of Cancer* **88**: 772–7.

Ringnér M. (2008). What is principal component analysis? *Nature Biotechnology* **26**: 303–4.

Romagosa C, Simonetti S, López-Vicente L, *et al.* (2011). p16(Ink4a) overexpression in cancer: a tumor suppressor gene associated with senescence and high-grade tumors. *Oncogene*: 2087–2097.

Roy HK, Smyrk TC, Koetsier J, *et al.* (2005). The transcriptional repressor Snail Is overexpressed in human colon cancer. *Digestive Diseases and Sciences* **50**: 42–46.

Rozen S, and Skaletsky H. (2000). Primer3 on the WWW for general users and for biologist programmers. *Methods in Molecular Biology* **132**: 365–86.

Rozenblum E, Schutte M, Goggins M, *et al.* (1997). Tumor-suppressive pathways in pancreatic carcinoma. *Cancer Research* **57**: 1731–4.

Rukstalis JM, Ubeda M, Johnson M V, *et al.* (2006). Transcription factor snail modulates hormone expression in established endocrine pancreatic cell lines. *Endocrinology* **147**: 2997–3006.

Safran H, Steinhoff M, Mangray S, *et al.* (2001). Overexpression of the HER-2/neu oncogene in pancreatic adenocarcinoma. *American Journal of Clinical Oncology* **24**: 496–9.

Sandgren EP, Quaife CJ, Paulovich AG, *et al.* (1991). Pancreatic tumor pathogenesis reflects the causative genetic lesion. *Proceedings of the National Academy of Sciences* **88**: 93–7.

Schneider G, Siveke JT, Eckel F, *et al.* (2005). Pancreatic cancer: Basic and clinical aspects. *Gastroenterology* **128**: 1606–25.

Seidler B, Schmidt A, Mayr U, *et al.* (2008). A Cre-loxP-based mouse model for conditional somatic gene expression and knockdown in vivo by using avian retroviral vectors. *Proceedings of the National Academy of Sciences* **105**: 10137–42.

Sekiya S, and Suzuki A. (2011). Glycogen synthase kinase 3 β-dependent Snail degradation directs hepatocyte proliferation in normal liver regeneration. *Proceedings of the National Academy of Sciences* **108**: 11175–80.

Siegel PM, and Massagué J. (2003). Cytostatic and apoptotic actions of TGF-beta in homeostasis and cancer. *Nature Reviews Cancer* **3**: 807–21.

Siegel R, Ward E, Brawley O, *et al.* (2011). Cancer statistics, 2011. *CA: A Cancer Journal for Clinicians* **61**: 212–36.

Simpson P. (1983). Maternal-zygotic gene Interactions during formation of the dorsoventral pattern in drosophila embryos. *Genetics* **105**: 615–32.

Smith DE, Del Amo FF, and Gridley T. (1992). Isolation of Sna, a mouse gene homologous to the Drosophila genes snail and escargot: its expression pattern suggests multiple roles during postimplantation development. *Development* **116**: 1033–9.

Soleimani VD, Yin H, Jahani-Asl A, *et al.* (2012). Snail regulates MyoD binding-site occupancy to direct enhancer switching and differentiation-specific transcription in myogenesis. *Molecular Cell* **47**: 1–12.

Soriano P. (1999). Generalized lacZ expression with the ROSA26 Cre reporter strain. *Nature Genetics* **21**: 70–1.

Southern EM. (1975). Detection of specific sequences among DNA fragments separated by gel electrophoresis. *Journal of Molecular Biology* **98**: 503–17.

Spagnoli FM, Cicchini C, Tripodi M, *et al.* (2000). Inhibition of MMH (Met murine hepatocyte) cell differentiation by TGF(beta) is abrogated by pre-treatment with the heritable differentiation effector FGF1. *Journal of Cell Science* **113 (Pt 20**: 3639–47.

Stanger BZ, Stiles B, Lauwers GY, *et al.* (2005). Pten constrains centroacinar cell expansion and malignant transformation in the pancreas. *Cancer Cell* **8**: 185–95.

Strasser A, Cory S, and Adams JM. (2011). Deciphering the rules of programmed cell death to improve therapy of cancer and other diseases. *The EMBO Journal* **30**: 3667–83.

Strizzi L, Bianco C, Normanno N, *et al.* (2004). Epithelial mesenchymal transition is a characteristic of hyperplasias and tumors in mammary gland from MMTV-Cripto-1 transgenic mice. *Journal of Cellular Physiology* **201**: 266–76.

Subramanian A, Tamayo P, Mootha VK, *et al.* (2005). Gene set enrichment analysis: a knowledge-based approach for interpreting genome-wide expression profiles. *Proceedings of the National Academy of Sciences* **102**: 15545–50.

Takahashi E, Funato N, Higashihori N, *et al.* (2004). Snail regulates p21(WAF/CIP1) expression in cooperation with E2A and Twist. *Biochemical and Biophysical Research Communications* **325**: 1136–44.

Tan C, Costello P, Sanghera J, *et al.* (2001). Inhibition of integrin linked kinase (ILK) suppresses b-catenin-Lef/Tcf-dependent transcription and expression of the E-cadherin repressor, snail, in APC -/- human colon carcinoma cells. *Oncogene* **20**: 133–140.

Thayer SP, Di Magliano MP, Heiser PW, *et al.* (2003). Hedgehog is an early and late mediator of pancreatic cancer tumorigenesis. *Nature* **425**: 851–6.

Thiery JP, Acloque H, Huang RYJ, *et al.* (2009). Epithelial-mesenchymal transitions in development and disease. *Cell* **139**: 871–90.

Towbin H, Staehelin T, and Gordon J. (1979). Electrophoretic transfer of proteins from polyacrylamide gels to nitrocellulose sheets: procedure and some applications. *Proceedings of the National Academy of Sciences* **76**: 4350–4.

Twigg SRF, and Wilkie AOM. (1999). Characterisation of the human snail gene and exclusion as a major disease gene in craniosynostosis. *Human Genetics* **105**: 320–6.

Valdés F, Alvarez AM, Locascio A, *et al.* (2002). The epithelial mesenchymal transition confers resistance to the apoptotic effects of transforming growth factor beta in fetal rat hepatocytes. *Molecular Cancer Research* **1**: 68–78.

Vanhaesebroeck B, Stephens L, and Hawkins P. (2012). PI3K signalling: the path to discovery and understanding. *Nature reviews. Molecular cell biology* **13**: 195–203.

Vega S, Morales A V, Ocaña OH, *et al.* (2004). Snail blocks the cell cycle and confers resistance to cell death. *Genes & Development* **18**: 1131–43.

Villagrasa P, Díaz VM, Viñas-Castells R, *et al.* (2011). Akt2 interacts with Snail1 in the E-

cadherin promoter. *Oncogene* **1**: 4022–33.

Viñas-Castells R, Beltran M, Valls G, *et al.* (2010). The hypoxia-controlled FBXL14 ubiquitin ligase targets SNAIL1 for proteasome degradation. *The Journal of Biological Chemistry* **285**: 3794–805.

De Vries A, Flores ER, Miranda B, *et al.* (2002). Targeted point mutations of p53 lead to dominant-negative inhibition of wild-type p53 function. *Proceedings of the National Academy of Sciences* **99**: 2948–53.

Wagner M, Greten FR, Weber CK, *et al.* (2001). A murine tumor progression model for pancreatic cancer recapitulating the genetic alterations of the human disease. *Genes & Development* **15**: 286–93.

Whiteman EL, Liu CJ, Fearon ER, *et al.* (2008). The transcription factor snail represses Crumbs3 expression and disrupts apico-basal polarity complexes. *Oncogene* **27**: 3875–9.

Wilentz RE, Iacobuzio-Donahue CA, Argani P, *et al.* (2000). Loss of expression of Dpc4 in pancreatic intraepithelial neoplasia: Evidence that DPC4 inactivation occurs late in neoplastic progression. *Cancer Research* **60**: 2002–6.

Wong DJ, Liu H, Ridky T, *et al.* (2008). Module map of stem cell genes guides creation of epithelial cancer stem cells. *Cell Stem Cell* **2**: 333–44.

Yang AD, Fan F, Camp ER, *et al.* (2006). Chronic oxaliplatin resistance induces epithelial-to-mesenchymal transition in colorectal cancer cell lines. *Clinical Cancer Research* **12**: 4147–53.

Yang M-H, Chang S-Y, Chiou S-H, *et al.* (2007). Overexpression of NBS1 induces epithelial-mesenchymal transition and co-expression of NBS1 and Snail predicts metastasis of head and neck cancer. *Oncogene* **26**: 1459–67.

Yang M-H, Chen C-L, Chau G-Y, *et al.* (2009). Comprehensive analysis of the independent effect of twist and snail in promoting metastasis of hepatocellular carcinoma. *Hepatology* **50**: 1464–74.

Yang Z, Rayala S, Nguyen D, *et al.* (2005). Pak1 phosphorylation of snail, a master regulator of epithelial-to-mesenchyme transition, modulates snail's subcellular localization and functions. *Cancer Research* **65**: 3179–84.

Yook JI, Li X-Y, Ota I, *et al.* (2005). Wnt-dependent regulation of the E-cadherin repressor snail. *The Journal of Biological Chemistry* **280**: 11740–8.

Yuan TL, and Cantley LC. (2008). PI3K pathway alterations in cancer: variations on a theme. *Oncogene* **27**: 5497–510.

Zhou BP, Deng J, Xia W, *et al.* (2004). Dual regulation of Snail by GSK-3beta-mediated phosphorylation in control of epithelial-mesenchymal transition. *Nature Cell Biology* **6**: 931–40.

9 Acknowledgements

I would like to give my sincere thanks to everybody who supported me during the time of my PhD research in any way.

First of all, I thank Prof. Roland M. Schmid for giving me the opportunity to do my PhD research in his department, the II. Medizinische Klinik at Klinikum rechts der Isar.
Further, I would like to thank Prof. Michael Schemann for taking over the exam chair.
I am very grateful to Prof. Angelika Schnieke for being my external PhD supervisor. Also, I want to thank her for scientific input and great interest in my work.

Above all, I am very thankful to PD Dr. Dieter Saur for giving me the excellent opportunity to do my PhD thesis in his group. By offering me such an interesting and promising project and by supporting me and my research in any possible way, he contributed substantially to the successful outcome of my work.

For microarray processing and subsequent analysis, I am very thankful to Silvia Weidner and to Olivia Prazeres da Costa from the Expression Core Facility. Many thanks go to Dr. Anne Gohlke for providing cell lines and associated microarray data. I also thank Philipp Eser for analysis of microarray data.

I give many thanks to all members of the Saur and Schneider group for the great working atmosphere and many helpful discussions throughout the years.
Especially Dr. Sandra Baumann, Dr. Anne Gohlke, PD Dr. Günter Schneider, Barbara Seidler, Dr. Benjamin Walter, Sören Weidemann, and Dr. Matthias Wirth made significant contributions to the success of this work by continually sharing their methodical experiences and scientific knowledge with me.

I further thank Ursula Götz, Juliana Götzfried, Miriam Schiller, and Tatiana Schmid for excellent technical support. Also, I want to give thanks to the animal keepers for always taking good care of my mice.

For critical reading of the manuscript, I would like to thank Dr. Rainer Hamacher, Annika Henrich, Tatiana Schmid, and Dr. Benjamin Walter.

Finally and most importantly, this dissertation would not have been possible without the constant help and support of my family and friends.